Numerical simulation of reaction fronts in dissipative media

A thesis submitted by

Rajeev Prakash Bhanot

B.Sc, UDelhi. B.Ed, IGNOU, India., M.Sc, USQ

For the award of the degree of

Doctor of Philosophy

2017

Dedication

This thesis work is dedicated to my wife, Vandana, who has been a constant source of support and encouragement during the challenges of research studies and life. I am truly thankful for having you in my life.
This work is also dedicated to my parents, my dad Late Mr Puran Prakash Bhanot and my mum Late Mrs Bimla Rani Bhanot both of them passed away in the examination period of this thesis, who have always loved me unconditionally and their good examples have taught me to work hard for the things that I aspire to achieve.

Abstract

Fronts of reaction in certain systems (such as so-called solid flames and detonation fronts) can be simulated by a single-equation phenomenological model of Strunin (1999, 2009). This is a high- order nonlinear partial differential equation describing the shape of the front as a function of spatial coordinates and time. The equation is of active-dissipative type, with 6th-order spatial derivative. For one-dimensional case, the equation was previously solved using the Galerkin method, but only one numerical experiment with limited information on the dynamics was obtained. For two-dimensional case only two numerical experiments were reported so far, in which a low-accuracy finite difference scheme was used. In this thesis, we use a more recent and sophisticated method, namely the one-dimensional integrated radial basis function networks (1D-IRBFN). The method had been developed by Tran-Cong and May-Duy (2001, 2003) and successfully applied to several problems such as structural analysis, viscoelastic flows and fluid-structure interaction. In contrast to commonly used approaches, where a function of interest is differentiated to give approximate derivatives, leading to a reduction in convergence rate for derivatives (and this reduction increases with derivative order, which magnifies errors), the 1D-IRBFN method uses the integral formulation. It utilizes spectral approximants to represent highest-order derivatives under consideration. They are then integrated analytically to yield approximate expressions for lower-order derivatives and the function itself.

In this thesis the following main results are obtained. A numerical program implementing the 1D-IRBFN method is developed in Matlab to solve the equation of interest. The program is tested by (a) constructing a forced version of the equation, which allows analytical solution, and verifying the numerical solution against the analytical solution; (b) reproducing one-dimensional spinning waves obtained from the model previously. A modified version of the program is successfully applied to similar high-order equations modelling auto-pulses in fluid flows with elastic walls.

We obtained numerically and analyzed a far richer variety of one-dimensional dynamics of the reaction fronts. Two kinds of boundary conditions were used: homogeneous conditions on the edges of the domain, and periodic conditions corresponding to periodicity of the front on a cylinder. The dependence of the dynamics on the size of the domain is explored showing how larger space accommodates multiple spinning waves. We determined the critical domain size (bifurcation point) at which non-trivial settled regimes become possible. We found a regime where the front is shaped as a pair of kinks separated by a rel-

atively short distance. Interestingly, the pair moves in a stable joint formation far from the boundaries. A similar regime for three connected kinks is obtained. We demonstrated that the initial condition determines the direction of motion of the kinks, but not their size and velocity. This is typical for active-dissipative systems. The settled character of these regimes is demonstrated. We also applied the 1D-IRBFN method to two-dimensional topology corresponding to a solid cylinder. Stable spinning wave solutions are obtained for this case.

Keywords

Active dissipative systems, reaction-diffusion systems, nonlinear partial differential equation, nonlinear excitation, finite difference, spinning waves, 1D-RBFN (one dimentional radial basis function network) method.

Publications by the candidate

The following publications were produced during the period of candidature:

- D.V. Strunin, D. Ngo-Cong and R.P. Bhanot (2015) Using 1D-IRBFN method for solving high-order nonlinear differential equations arising in models of active-dissipative systems. In: 1st Pan-American Congress on Computational Mechanics, (PANACM 2015) in conjunction with the XI Argentine Congress on Computational Mechanics (MECOM 2015), 27-29 April 2015, Buenos Aires, Argentina, pp. 1103-1110.

- R.P. Bhanot and D.V. Strunin, Dynamics of curved reaction fronts under a single-equation model, submitted to the *ANZIAM Journal (E)* [EMAC2015].

- F. Ahmed, D.V. Strunin, M.G. Mohammed, and R.P. Bhanot, Numerical solution for the fluid flow between active elastic walls, the journal *ANZIAM Journal (E)* [EMAC2015]. Vol. 57 (2016) pp. C221-C234.

- R.P. Bhanot, D.V. Strunin and D. Ngo-Cong. Numerical simulation of spinning reaction fronts using integrated radial basis function networks, submitted to the journal *IMA Journal of Applied Mathematics*.

Certification of thesis

This thesis is entirely the work of **Rajeev Prakash Bhanot** except where otherwise acknowledged. The work is original and has not previously been submitted for any other award, except where acknowledged.
Student and supervisors signatures of endorsement are held at USQ.

Rajeev Prakash Bhanot

Candidate

ENDORSEMENT

A/Prof. Dmitry V. Strunin

Principal Supervisor

Prof. Thanh Tran-Cong

Co-Supervisor

Dr. Duc Ngo-Cong

Co-Supervisor

Acknowledgments

The research reported in this thesis was carried out at the Computational Engineering and Science Research Centre (CESRC), USQ.

It is my great pleasure to take this opportunity to express my sincere gratitude to several people who directly or indirectly played a key role in the successful completion of this work. Their persistent support and encouragement was a considerable helping to me in many ways.

First and foremost I would like to express my sincere appreciation to my supervisor, Associate Professor Dmitry Strunin for his guidance, inspiration, suggestions, criticism and financial support in the form of casual academic work, that he has provided throughout the course of my research and studies. Without his continuous and very active support, this thesis would not have been completed.

Over the years I have gained from Assoc Prof Dmitry invaluable experience in conducting cutting edge research with the highest standards of exposition and rigor. Our discussions on various subjects helped me to shape my opinion on many different aspects of my research area. His kindness and patience are greatly appreciated.

I would like to thank my co-supervisor Dr. Duc Ngo-Cong and Prof.Thanh Tran-Cong for their active support during my PhD study journey.

I would like to thank to Ms. Katrina Hall, Mrs. Juanita Ryan, and Mrs. Rebecca Darr for their kind support.

I would like to express my special appreciation to my parents for their love and continued support. The deepest thanks are expressed to my wife Vandana and my son Rajvan for their endless confidence, encouragement, and patience I should not forget my relatives as well as my friends here in Australia and there in India.

Finally, my warmest regards go to the University of Southern Queensland (Toowoomba) for supporting me financially by offering the scholarship for the completion of the PhD. USQ's financial support is gratefully acknowledged.

Rajeev Prakash Bhanot

2017

Contents

List of Figures

List of Tables

Acronyms & Abbreviations

NEP	Nonlinearly excited phase
ODE	Ordinary differential equation
PDE	Partial differential equation
RBF	Radial basis function
MQ	Multiquartic function
RBFN	Radial basis function network
IRBFN	Integrated/Indirect radial basis function network
CGLE	Complex Ginzburg-Landau equation
GNPD	Generalized nonlinear phase diffusion

Chapter 1

Introduction

1.1 Overview and motivation

Active or, excitable media often exhibit oscillatory behaviour. In this chapter we mainly follow Strunin (1999, 2009) to present the background of this project. In many situations, this behaviour can be described by a single partial differential equation for the phase of oscillations. Of crucial importance is the question of whether a regular motion, or chaotic motion of the phase is eventually settled, in other words what pattern is eventually formed. The pattern formation depends on how it is born from the equilibrium state. Does it occur via linear or nonlinear mechanism? While the linear mechanism has been studied extensively (Sivashinsky, 1977; Kuramoto and Tsuzuki, 1976; Kuramoto, 1984*a*; Tribelsky and Velarde, 1996; Tanaka, 2004), for example, in the Kuramoto-Sivashinsky equation, the *nonlinear* mechanism remains virtually unexplored. We emphasize that the subject of our work is the *phase* of the oscillations rather than the oscillations themselves. As for the latter, their excitation mechanisms — both linear and nonlinear — have been widely studied.

Recently, it was found that *nonlinearly* excited phase dynamics are quite typical for a range of systems of chemical, biological and physical origin. Biochemical systems comprise a particularly large group of such systems. Among those are cellular slime molds and oscillating yeast cells under glycolysis (Tanaka and Kuramoto, 2003). The focus of our present research is combustion systems. An example of such systems is the Self-propagating High-temperature Synthesis in solid flames, used to manufacture advanced materials (Merzhanov et al., 1992; Merzhanov, 1996; Merzhanov, 1997; Merzhanov and Rumanov, 1999; Merzhanov, 2004). For example, porous multiphase/heterogeneous calcium phosphate HCaP, NiTi-TiC and TiB-Ti are used for bone tissue engineering and drug delivery systems (Ayers et al., 2005). Another example involving combustion is the fronts of detonation. They have apparent significance for military and mining applications.

Indeed, the *nonlinear* mechanism, which is the focus of this study, is very important and needs consideration. Thus, this study aims to describe pattern formation in combustion fronts in detail, especially the spinning waves. To simulate

such waves, Strunin (1999) designed the following phenomenological equation, which is in the focus of the present research, is

$$\partial_t u = -A(\partial_x u)^2 \partial_x^2 u + B(\partial_x u)^4 + C\partial_x^6 u, \tag{1.1}$$

where $A > 0$, B and $C > 0$ are constants.

The nonlinear term in the equation above represents the excitation that can be treated as an anti-diffusion expressed by $(-\partial_x^2 u)$ with the positive coefficient, $(\partial_x u)^2$. The dissipation is represented by the last term $\partial_x^6 u$. Equation (1.1) generates wide variety of regular and irregular dynamics (Strunin, 1999; Strunin and Suslov, 2005). We will refer to (1.1) as the NEP (Nonlinearly excited phase) equation or model. Some models of arterial blood flows are structurally similar to this equation (Strunin, 2009*a*). Our plan in this thesis is to study this equation in 1-D and 2-D cases for combustion systems. We aim to accurately describe characteristics of regular and irregular dynamics and specify the conditions leading to different patterns.

1.2 The phenomenon and observations

Apart from the solid flames, detonation is another example of a system where the spinning reaction fronts occur. A description of basic features of this phenomenon can be found in the book of Landau and Lifshits (1987). A more detailed review is given in the monograph of Zel'dovich and Kompaneets (1960). A qualitative study of the spinning detonation was conducted by Zel'dovich and other authors in 1940s. In the spinning regime, the reaction front propagates being substantially distorted. The front assumes the form of one or more localized kinks moving along spirals through the tube. Since the reaction products adjacent to the kinks are at very high temperature the kinks is sometimes referred to as hot spot.

As stressed in (Landau and Lifshits, 1987) the regime occurs when the combustion is close to its limit. This means that the combustion process is suppressed by heat loss through the walls of the tube. This factor cannot be eliminated even if the tube is placed in vacuum as the loss still exists due to radiation. Along quasi-plane sections of the spinning wave Fig. 1.1-1.2 the combustion is damped so that the kink (or kinks when there are several of them) is the only area where the reaction occurs. The heat loss has that dramatic affect on the reaction for the following reasons. Chemical characteristics of the reacting mixture are such that the propagation of the plane front with constant velocity is unstable. The front can only move by hops, but at the moment when a hop happens the temperature sharply increases. Accordingly, the heat loss also increases, tending to suppress the combustion.

The hot spot 'survives' because of self-sustained favourable combustion conditions near the kink, where unburned gas is embraced by the hot and compressed burned gas from two sides. This is the limiting situation realized at large degree of instability. If the instability degree is increased further even the hot spots will be extinguished by the heat loss. The height and width of the fissures are much smaller than the perimeter of the tube (Zel'dovich and Kompaneets, 1960).

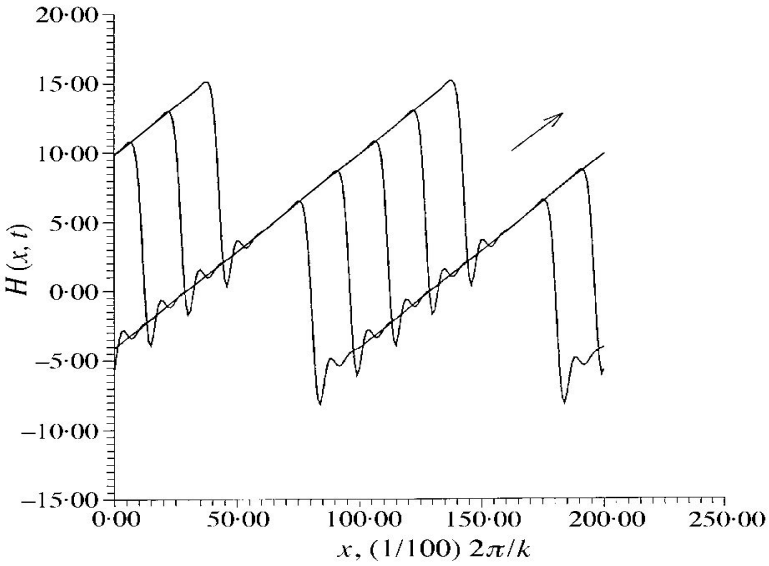

Figure 1.1: A running spinning wave solution of Eq.(1.1) evolved from a random initial condition (Strunin, 1999).

Figure 1.2: A post-combustion trace left by the spinning solid flame on a hollow cylinder.

Similar spinning waves are observed in the solid flames near the combustion limit. In (Merzhanov et al., 1973) experimentally discovered that the unstable front converts into one or more hot spots travelling along spiral trajectories over the surface of a cylindrical sample. The mechanism of the spinning solid flame is analogous to the spinning detonation. As the temperature in the hot spots is much higher than elsewhere in the system, the hot spots often look like bright points.

For this reason Dvoyankin (1982) called the regime multiple-point. We stress the component 'point' in this term which highlights the localized character of the kinks. Later, the term was used by different authors in a number of papers. The work of Dvoryankin et al. also reported disordered motion of the hot spots. Strunin et al. (1994) experimentally showed that this motion is chaotic and calculated fractal dimensionality of the associated strange attractor. To explain the difference between existing theories and the model proposed below we review the literature on the non-stationary solid flames in the next section.

1.2.1 Modelling of the spinning reaction fronts

Makhviladze and Novozhilov (1971) , Shkadinsky et al. (1971) and Matkowsky and Sivashinsky (1978) showed that at a certain critical value of a control parameter (called Zel'dovich number) the plane uniformly propagating front loses stability. This is a type of a reaction-diffusion instability induced by fast diffusion of the activator (heat).

In order to describe the nonlinear dynamics of the distorted front Volpert et al. (1982), Margolis (1991), Matkowsky and Volpert (1992) and others applied bifurcation theory. Within this approach, the plane uniformly moving front is supposed weakly unstable so that the degree of instability (deviation ΔZ of the Zel'dovich number from the instability threshold) serves as a small parameter. In these works, non-stationary solutions to the reaction-diffusion activator-inhibitor equations (the reaction products play the role of inhibitor) are obtained as small corrections of order of ΔZ to the uniformly moving plane front solution. Aldushin et al. (1981) constructed a phenomenological equation which also assumed the instability degree to be small. Those approaches generally lead to the Ginzburg-Landau type equations for the front deviation h about the moving (unstable) plane front position.

The solutions to the equations turn out to be small-amplitude quasi-harmonical waves travelling in the direction transversal to the average motion. The spinning motion here is a corollary of the specific way of losing stability by the plane front. It transpires that any unstable mode appears as travelling wave. Most vividly, this is expressed in the phenomenological model by Aldushin et al. (1981):

$$\frac{\partial^2 h}{\partial t^2} + w^2 h = 2\lambda \left[\frac{\partial h}{\partial t} - \mu \left(\frac{\partial h}{\partial t} \right)^3 + \nu \frac{\partial^3 h}{\partial t \partial x^2} \right], \tag{1.2}$$

$$w^2 = \lambda^2 + \eta^2; \lambda, \mu, \nu > 0.$$

The linear part of the above equation expresses self-excited oscillations with the frequency η and increment λ of the front elements and their coupling through the heat conductivity. Combination of these two factors already results in the travelling wave. The only function of the nonlinear term is to stop the growth of the wave in amplitude. Meanwhile, in the reported experiments the spinning waves had distinct unharmonical, kink-like shape. The same is true for the spinning detonation. The divergence between the experiments and the models can be explained by strong instability that is the large value of ΔZ. This assertion is in line with the numerical experiments of Ivleva et al. (1980) who studied the combustion (that is reaction-diffusion) equations. They made no weak instability assumption and obtained the kink-shaped fronts.

The reason why experimentalists usually deal with strong rather than weak instability is seemingly that on the dark background the localized luminous hot spots are easy to observe, whereas it is not so for the harmonical small-amplitude distortions of the evenly bright front. There is no doubt that the bifurcation method works well in the weak instability limit and gives convincing evidence of the existence of spinning waves. Given this and the presented considerations, Strunin (1999) distinguished two sorts of spinning waves: weak and strong. The Strunin model (1999) relates to the latter case. The mechanism of the strong spinning waves resembles the way of propagation of a normal steady combustion front: the hot spot heats the fresh mixture ahead of itself and thereby excites the reaction there.

In other words the wave runs exceptionally due to the transmission of signal from one element of the front to another. The self-motions of the elements are prohibited because of the damping role of the heat loss. Qualitative considerations of the spinning wave which rested on the analogy between the wave and the steady front were made by Iveleva et al. (1980). Later, the idea about the strong spinning waves was explicitly formulated by Novozhilov (1992) who used the above analogy together with the localized character of the hot spots. However, this model does not describe the head-on collision of the hot spots and other complicated regimes. Strunin (1995) attempted to design a phenomenological equation that could serve as a tool for studying such regimes.The semiempirical equation of a nonstationary front was suggested. It reproduces the spinning combustion regimes as a particular solution.

Strunin (1995) suggested the evolution equation for H in the form

$$\partial_t H = \alpha \int_{-\infty}^{\infty} |k| dk \int_L \exp(ik(x-z)) H(z,t) dz + \partial_x^2 H(\beta - \gamma(\partial_x H)^2) + (\partial_x H)^2, \tag{1.3}$$

where $H(x,t)$ be the position of the temprature front (a narrow zone with large temprature gradient) and $\alpha, \beta, \gamma > 0$. Equation (1.3) invoves only dimensionless values, integration with respect to z is performed over the domain of existence of the front.The nonlinear quadratic term expresses predominant displacement of the front along x, towards a fresh mixture warmed up by the products of the reaction.The cubic term decreases dissipation or, in effect, increases the pumping in the region facing the warmed up fresh mixture.Thus it expresses more intense

combustion in hot spots. An analysis shows that Eq. (1.3) has a spin combution solution only when this term has a special form. Because dissipation is determined by the second order derivative the term must include the first order derivative. The equation was solved numerically and few results were presented, although the presented solution were mathematically correct, but they were unstable.

On the contrary, the later model of Strunin (1999) is stable. It is also important that, unlike the previous one, it contains a purely dissipative linear part which addresses the condition that the system is near the combustion limit. After the hot-spot passage the reaction front returns into its previous physical state of immobility. The state of the front should not be confused with the state of the mixture described by concentrations of the activator and inhibitor. The mixture undergoes an irreversible transition from the initial state, cold fresh compound, to the final state, hot reaction products. It is important that the state of the front that is described by the model.

1.2.2 Strunin model of strong spinning fronts

In this section we follow the paper (Strunin, 1999). Consider the one-dimensional case when the front propagates through a thin strip rolled up into a cylinder. Let $H = H(x,t)$ denote the dimensionless distance from the end of the cylinder the front has passed by the moment t. Here x is the dimensionless coordinate along the cylinder perimeter. Thus H is a periodic function in x with some period L. The author intended to design a simplest partial differential equation for H to capture the qualitative features of the spinning wave discussed in the previous section. The model must comply with the fact that the front moves forward so that the value H increases with time (on average).

To avoid infinitely large terms in the equation and to express the interactions between the neighbouring front elements, it is required that H does not appear alone, but only under differentiation operators. The basic consideration underlying the model is that the uniform state $H =$ contant is linearly stable. It expresses the fact that the combustion is near the limit. The spatially uniform front section is the place where the reaction is damped and thus unable to resume spontaneously. Therefore the linear part of the model must be purely dissipative. This requirement can be met by the equation

$$\frac{\partial H}{\partial t} = (-1)^{m+1}\frac{\partial^{2m} H}{\partial x^{2m}}, m = 1, 2\ldots . \tag{1.4}$$

Eq. (1.4) leads to the spatially uniform motionless front as a final state of the system. This state is equivalent to the absence of the reaction because H does not increase as time passes. Instead of (1.4) one can take a sum of such terms with some coefficients before them and, after the model is built, look into question of suitable magnitudes of the coefficients. Taking into account that the main purpose is to build the simplest model we confine ourself for now to only one dissipative term. The order m will be determined later from the energy balance. The rest of the equation must be nonlinear. The deeper the cavity formed by the hot products the better the conditions for the reaction, that is, for the "survival"

of the cavity. Such a tendency can be described by the diffusion-type term with non-positive nonlinear coefficient

$$-\left(\frac{\partial H}{\partial x}\right)^2 \frac{\partial^2 H}{\partial x^2}. \tag{1.5}$$

This term controls the distortion of the front due to the reaction. However, the dissipation and nonlinearity are not sufficient for the model because they do not balance each other. In addition, it is not less important that they do not make the front move through the mixture on average. This is seen after placing both of above terms to the right-hand side of Eq. (1.4) and integrating over the period L: we get zero. Consequently, H does not increase on average, that is, the model still contains no mechanism adequately allowing for consumption of the fresh mixture due to the reaction. In order to express the consumption and provide the balance between pumping and dissipation another nonlinear term needs to be introduced, and it should be positive. The simplest form of such a term with H appearing under the differentiation operator is

$$\left(\frac{\partial H}{\partial x}\right)^{2n}, \quad n = 1, 2... . \tag{1.6}$$

From all of above we obtain

$$\frac{\partial H}{\partial t} = (-1)^{m+1}\frac{\partial^{2m} H}{\partial x^{2m}} - \left(\frac{\partial H}{\partial x}\right)^2 \frac{\partial^2 H}{\partial x^2} + \left(\frac{\partial H}{\partial x}\right)^{2n}. \tag{1.7}$$

The balance between the terms is achieved if the pumping has smaller order of nonlinearity than the so called "transition" term, which is the last

$$2n > 3. \tag{1.8}$$

The transition term carries no pumping function but transfers the energy to small scales. Small-scale disturbances must dissipate, so we require

$$2m > 2n. \tag{1.9}$$

Subtract (1.9) from (1.8), the simplest variant satisfying is $n = 2, m = 3$ leading to the equation,

$$\frac{\partial H}{\partial t} = \frac{\partial^6 H}{\partial x^6} - \left(\frac{\partial H}{\partial x}\right)^2 \frac{\partial^2 H}{\partial x^2} + \left(\frac{\partial H}{\partial x}\right)^4, \tag{1.10}$$

which Strunin referred to in (2009) as the NEP (nonlinearly excited phase) equation.

1.3 Our research

In our research we analyse the model. (1.10), which we re-write using u in place of H through out our work. As we mentioned, the model describes two kinds of the fronts of reaction: (a) detonation front, which is a shock wave in a gas accompanied by combustion reaction and (b) solid flame, which is a combustion front propagating through a solid-phase compound,

$$\partial_t u = -A(\partial_x u)^2 \partial_x^2 u + B(\partial_x u)^4 + C\partial_x^6 u\,. \tag{1.11}$$

Under the term front we imply a conditional border assumed to be a line, between cold fresh mixture and hot reaction products. Rigorously speaking, the border is not a line but some strip with finite thickness, within which the temperature undergoes a considerable variation. This thickness is known to an accuracy of order of magnitude so that the frontal line can only be a rough representation of the actual front. The model was shown (Strunin, 1999) to give, as a particular solution, autosolitary waves similar to the experimentally found spinning regimes.

The autosoliton is a well-known type of wave which has been found in many physical, chemical and biological systems and described in detail in review articles (Kerner and Osipov, 1989) and (Cross and Hohenberg, 1993). The term autosoliton is used by some authors to distinguish this concept from solitons in conservative systems. In contrast to the solitons, the autosolitons occur in active systems with dissipation. Note here that combustion front is a typical example of such a system due to the key role of reaction and thermoconductivity. Appearing as a result of the balance between pumping and dissipation, the autosolitons have a unique amplitude and width governed by the dynamical system.

Such waves are stable with respect to small disturbances but may decay if violated too strongly. These properties correlate well with the observations of the spinning waves and are used as a basis of the model. Consequently, it was worth making an attempt to give them a unified description within a single model. Furthermore, the solid flame is a complicated phenomenon which includes many physical and chemical factors such as mechanical deformations, melting, complex chemical reactions, etc. However, the spinning waves are experimentally observed in many of them. Given this, using a phenomenological approach looked reasonable. Strunin used the phenomenological approach because the situation in question is characterized by a large degree of instability of the plane front so that regular small parameter method would not work. Like all phenomenological models, the one proposed does not claim a precise description of the phenomenon and is focused on its qualitative side.

1.4 Aims of this project

The key aims and research questions of the project are:

(a) Develop Matlab numerical codes for solving the Strunin model in one and two dimensions using the Integrated Radial Basis Function Network (IRBFN) col-

location method; verify accuracy and stability of the code using standard methods and also by exploring modified versions of the equation which allow analytical solutions.

(b) Investigate comprehensively different dynamic regimes in 1D (one spatial dimension): the shapes of settled solutions, their evoltion in time and space and the dependence on the size of available domain under different boundary and initial conditions. Special attention will be given to steady and unsteady spinning regimes with more then one spinning heads. We will explore the co-directed and counter-directed moving heads and their interactions.

(c) Simulate the two dimensional regimes with x and y spatial dimensions.

1.5 Focus and scope of the thesis

This study aims to accurately describe pattern formation in reaction fronts modelled by Eq. (1.1). This research may help predict the pattern type – regular or chaotic – of material properties caused by the dynamics. Although this equation contains only three terms in its right hand side, preliminary results indicate that it can generate complicated regimes, both regular and irregular. At present there are only few examples of numerical solutions of this equation in 1D (Strunin, 1999) and a series of numerical experiments in 2D (Strunin and Suslov, 2005; Strunin and Mohammed, 2015), but they were based on finite difference method compared to which the 1D-IRBFN method of the current thesis presents an advanced numerical approach. We will be especially interested to simulate multiple head spinning regimes. We will also explore forced Strunin equation to investigate its numerical and exact solutions.

1.6 Outline of the thesis

The thesis is organized as follows:

Chapter 2: As a background we describe basic concepts of spinning reaction waves and discuss the work which has been done previously for linear and nonlinear excited phase equations.

Chapter 3: We elaborate the numerical method 1D-IRBFN used in our research work. Its convergence and efficiency is supported by examples.

Chapter 4: We derive a forced Strunin equation and present selected exact solutions. These solutions are used to verify the numerical code. This is done by comparing the exact and numerical solutions.

Chapter 5: We solved the Strunin model in 1D with homogeneous boundary conditions; the solutions are presented and discussed.

Chapter 6: We solved the model in 1D with periodic boundary conditions ; the solutions are presented and discussed.

Chapter 7: We solved the model in 2D with homogeneous boundary conditions; the solutions are presented and discussed.

Chapter 8: We conclude the thesis and discuss future directions.

Chapter 2

Literature Review

2.1 Introduction

This chapter will start with a brief review of dynamics of reaction waves. Then, we will give review of literature on the dynamical equations with different types of excitation.

2.2 Simulation and application of reaction waves

The following model presents a single-equation simulation tool for the reaction waves (Strunin, 1999),

$$\partial_t u = -A(\partial_x u)^2 \partial_x^2 u + B(\partial_x u)^4 + C\partial_x^6 u\,, \tag{2.1}$$

where A, B, $C > 0$. In practical terms, this model is relevant to the so called superadiabatic waves, detonation waves and instabilities in certain type of reaction-diffusion systems (Strunin, 2009). We will discuss dynamical mechanism behind Eq. (2.1) in the next chapters in detail.

Despite a short form, the equation generates rich variety of dynamical regimes, the most spectacular of which is the spinning wave shown in Figures 1.1 and 1.2. The superadiabatic waves of combustion is clean technology used for waste processing (Institute of Problems of Chemical Physics, Russian Academy of Sciences, www.icp.ac.ru/ eng/developments/; (Slimane et al., 2002), (Rozenberg et al., 2005). The usage of superadiabatic combustion waves for waste treatment is underpinned by fundamental research initially conducted by chemical physicists looking for ways to use super- hot (hot-spot) combustion regimes for processing low-calorie stock into electrical energy. The low-calorie composition is the key factor in this process because it the conditions when the combustion is confined within a relatively small fragment of space, which allows to achieve high levels of temperature. They considerably exceed the temperature that would take place should the composition burn in a normal regime under thermally insulating (adiabatic) conditions. This technology proves suitable for processing low-quality

combustible fossil, biofuel as well as industrial and municipal waste. The superadiabatic combustion also takes place in Self-propagating High-temperature Synthesis of materials, for example porous multiphase/heterogeneous calcium phosphate (HCaP), NiTi, NiTi-TiC and TiB-Ti.

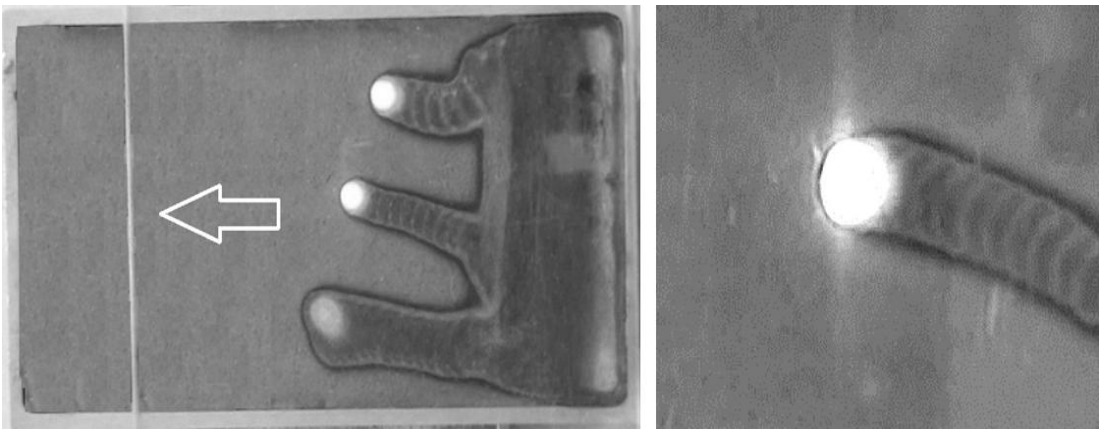

Figure 2.1: The propagating infiltration combustion on a plane substrate (Kostin et al., 2015).

Fig. 2.1 displays a similar 2D cellular structure of infiltration combustion. The solutions of 2D version of Eq. (2.1), obtained by Strunin and Mohammed (2015), give similar patterns.

2.3 Background

Recently an increased attention has been drawn to the research of the structure of the combustion fronts in heterogeneous reactive compositions. Regardless of the effect of initial perturbations, the combustion process can be accompanied by the spontaneous formation of regular structures, the symmetry of which differ from the symmetry of initial conditions. For systems in which the reactive gas is blown through the reaction products in the direction of the propagating front, it was shown (Aldhushin and Ivleva, 2013) that, if the permeability of the combustion products exceeds that of the initial charge, the combustion process may become unstable, accompanied by the formation of a finger-shaped front. These processes were experimentally studied in (Aldhushin and Braverman, 2010) for the propagation of a smoldering wave in a slit-like channel filled with sawdust. In this work, the focus was on examining the effect of scale factors on the loss of stability of the combustion of highly porous media.The structuring of the combustion front in metal powders subject to natural gas infiltration was theoretically and experimentally investigated in (Kostin et al., 2015; Kostin et al., 2014; Kostin et al., 2012). The authors analysed the infiltration combustion of porous media and the dynamics of initiation and propagation of cellular wave structures. They studied the dependence of the number and shape of cells on the governing thermophysical, macrokinetic, and infiltration parameters of the heterogeneous medium,

on the geometric characteristics and dimensions of the porous composition, on the parameters of gas exchange with the environment, heat loss, etc. The studies showed that the planar front may break into individual cells of self-sustaining exothermic chemical reaction. It was shown that the cells move through the condensed material layer in the pulsation mode, leaving behind a band of condensed combustion products with periodic structure. (Kostin et al., 2015) determined the boundaries of existence of the steady and unsteady modes of the infiltration front. The focus was on establishing the macrokinetic laws of combustion propagation in the parametric domain, where a planar combustion front is unstable and cellular pulsating combustion waves arise and propagate. From a practical point of view, analysis of the combustion of the system enabled the determination of optimal conditions of the infiltration combustion of porous media for obtaining synthesis products.

These regimes are successfully simulated by Eq. (2.1). The equation is based on phenomenological principles – it is designed to simulate the main dynamical features of the process (Strunin, 1999) while ignoring details. As is clear, waste or SHS systems can be extremely complex in composition, which renders their detailed description prohibitively difficult. The phenomenological methods have been used in many areas of mathematical modelling. For example, (Das and Puri, 2003) proposed a phenomenological description of the long-term cluster evolution in granular gases (Aranson and Tsimring, 2006). For the spinning combustion waves, the first attempt to construct a model based on phenomenological principles was undertaken by Aldushin et al. (1981). However, as we explain below, our model (2.1) far better addresses the actual experimental observation. The spinning waves occur in the so-called solid flames, where the products of combustion are solids. Merzhanov et al. (1973) reported the experiments where a solid flame breaks down into a set of hot spots travelling along spiral trajectories on the surface of a cylindrical specimen. Because a hot spot is much hotter than the surrounding area and even hotter than the adiabatic temperature (from here the term super-adiabatic), the hot spot appears to the eye as a luminous patch.

If there are more than one hot spot, the regime is referred to as multiple-point. The very word "point" highlights the localised character of combustion. Many papers that followed used the same terminology. Dvoryankin et al. (1982) also reported a different regime, when a number of hot spots performed a seemingly disordered motion. In an experimental work of Strunin et al. (1994) this motion was shown to be chaotic, and fractal dimensionality of the respective strange attractor was determined. Makhviladze and Novozhilov (1971), Shkadinsky et al. (1971) and Matkowsky and Sivashinsky (1978) showed that at a certain critical value of the control parameter called Zel'dovich number, Z, the plane uniformly propagating combustion front loses stability. In order to describe the nonlinear dynamics of the unstable front Volpert et al. (1982), Margolis (1991), Matkowsky and Volpert (1992) and others used bifurcation theory. Within this approach, the plane uniformly moving front is supposed weakly unstable so that the distance from the instability threshold (the deviation ΔZ from the critical value Z_c) can be used as a small parameter. In these works, non-stationary solutions to the

reaction-diffusion activator-inhibitor equations are obtained as small corrections of order ΔZ to the uniformly moving plane front solution. The phenomenological model of Aldushin et al. (1981) too implied that the instability is weak. Both approaches led to the Ginzburg-Landau type equations for the front deviation about the (moving) average front position. The solutions turned out to be small-amplitude quasi-harmonic waves travelling in the direction transversal to the average motion.

The superposition of the average motion and this transversal propagation resulted in the spinning wave on the cylinder. Meanwhile, in the experiments the spinning waves had a distinct non-sinusoidal, kink-like shape. The discrepancy between the experiments and the models can be explained by strong instability that is large value of ΔZ . This proposition agrees with the numerical experiments of Ivleva et al. (1980) who studied the combustion (reaction-diffusion activator-inhibitor) equations. The reason why the experimentalists usually deal with strong rather than weak instability is the easiness of observation: the luminous hot spots are clearly visible, whereas small (sinusoidal) distortions of a weakly unstable front are a much less prominent with respect to the neighbouring sections. Undoubtedly, the bifurcation method works well in the weak instability limit. Given this, we distinguish two types of the spinning waves: weak and strong. Our model (2.1) describes the strong waves – the ones reported by the experimentalists. The mechanism of the strong spinning waves resembles the way of propagation of the usual plane combustion front: the hot spot heats the fresh mixture in front of itself and thereby excites the reaction. It is important that the linear part of the model (2.1) is purely dissipative. Consequently, after the hot spot (steep slope section) passes a location x, the state of the front at this location returns to rest, and this state is stable. The state of the front should not be confused with the state of the reacting mixture, that is the activator and inhibitor. They undergo the irreversible transition from the initial state – cold and unreacted – to the final state – hot and reacted.

The kink-like wave shown in Fig. 1.1 transforms into a single-kink shape when the period of the solution tends to infinity. In terms of the derivative, $F = \partial_x H$, the kink becomes a kind of soliton called auto-soliton. The auto-soliton is a type of wave encountered in many physical, chemical and biological systems (Kerner and Osipov, 1989; Cross and Hohenberg, 1993). The prefix auto- distinguishes the concept from usual solitons in conservative systems. While the solitons result from the balance between nonlinearity and dispersion, the auto-solitons result from the balance between energy release and dissipation. The combustion front is a typical example of the active-dissipative system, where the energy is released by reactions and the dissipation is facilitated by thermoconductivity. The auto-soliton in a given system possesses a unique size and unique velocity as dictated by the balance. The auto-soliton is resistant to small perturbations but decays if impacted by a sufficiently strong external factor. These properties agree with the experiments and have been used as the basis of the model (2.1). Another motivation for constructing the model of this form is suitability for dynamically similar phenomena in different systems while disregarding details. The combus-

tion may involve many reactions and reacting components, be complicated by mechanical deformations, melting etc. However, the front localisation is typical to all super-adiabatic waves.

Considering this, the phenomenological model is our simulation instrument of choice. We remark that the auto-solitons or, by another terminology, localised states are known from many different systems, for example chiral bubbles in liquid crystals, current filaments in gas discharge, localised states in fluid surface waves, oscillons in granular media, isolated states in thermal convection.

2.3.1 Mathematical novelty

As we mentioned earlier, Eq. (2.1) governs the evolution of the distance, u, passed by the reaction front through the combustible medium. In a sense, the distance u plays the role of phase as it always increases with time. Hence the equation can be called phase equation. It is noteworthy that in the context of reaction-diffusion systems the generalised phase equations (Kuramoto, 1984) literally describe the phase of oscillations. The lowest-order forms of the phase equation are based on the 2nd-order dissipation; their classical examples are the diffusion equation

$$\partial_t u = \nabla^2 u \tag{2.2}$$

and the nonlinear diffusion equation transformable into the Burgers equation. Both equations are dissipative, with no excitation. Their solutions tend to smear over space, and thus reduce the phase differences. However, under certain circumstances, the phase differences amplify. This occurs when the parameter values of the system are such that the coeffcient in front of $\nabla^2 u$ becomes negative so that the diffusion turns into anti-diffusion. In order to prevent blow-up and maintain balance, a higher-order dissipative effect must be included into consideration. This was done by Kuramoto and Suzuki (1976) in the context of reaction-diffusion systems and Sivashinsky (1977) in the context of unstable combustion waves in gases,

$$\partial_t u = -\nabla^2 u - \nabla^4 u + (\nabla u)^2. \tag{2.3}$$

In Eq. (2.3) the excitation is represented by the linear anti-diffusion,$-\nabla^2 u$, and the dissipation by $(-\nabla^4 u)$. Later on, a sixth order model was derived by Nikolaevskiy (1989) for seismic waves,

$$\partial_t u = a\nabla^2 u + \nabla^4 u + \nabla^6 u + (\nabla u)^2, \tag{2.4}$$

$a > 0$.

Similarly to the Kuramoto-Sivashinsky Eq. (2.3), the Nikolaevskiy Eq. (2.4) involves linear excitation, represented by $\nabla^4 u$. Recently (Strunin, 2009) rigorously derived the nonlinear excited phase equation in the context of reaction-diffusion systems with nonlocal coupling (Tanaka and Kuramoto, 2003); Tanaka, 2004). The nonlinear character of excitation manifests the qualitative difference between Eq. (2.2), Eq. (2.3) and Eq. (2.4).

2.4 Complex Ginzburg-Landau equation (CGLE) and the phase equation

Strunin (2009b) showed that Eq. (2.1) is a particular case of a more general equation called the generalized nonlinear phase diffusion (GNPD) equation. In turn, the GNPD equation is derived from the Complex Ginzburg-Landau (CGL) equation. The GNPD equation directly applies to the reaction-diffusion systems, but is also phenomenologically connected to the propagation of reaction fronts, which interests us in our present research.

The general form of the phase equation is

$$\begin{aligned}\partial_t u = {} & a_1\nabla^2 u + a_2(\nabla u)^2 + \\ & b_1\nabla^4 u + b_2\nabla^3 u\nabla u + b_3(\nabla^2 u)^2 + b_4\nabla^2 u(\nabla u)^2 + b_5(\nabla u)^4 + \\ & g_1\nabla^6 u + g_2\nabla^5 u\nabla u + g_3\nabla^4 u\nabla^2 u + g_4(\nabla^3 u)^2 + g_5\nabla^4 u(\nabla u)^2 + \\ & g_6(\nabla^2 u)^3 + g_7\nabla^3 u\nabla^2 u\nabla u + g_8\nabla^3 u(\nabla u)^3 + g_9(\nabla^2 u)^2(\nabla u)^2 + \\ & g_{10}\nabla^2 u(\nabla u)^4 + g_{11}(\nabla u)^6 + \\ & e_1\nabla^8 u + \cdots .\end{aligned} \tag{2.5}$$

where a_n, b_n, g_n, e_n, ... are constant coefficients. The operator $\nabla^2 \sim (1/L)^2$ plays the role of a small parameter: where L is the large characteristic spatial scale of variations of u. Thus, the phase u varies slowly in space.

As frequently noted e.g., (Mohammed, 2015) the cubic complex Ginzburg-Landau equation (CGLE) is one of the widely-studied nonlinear equations representing dissipative systems. It describes on a qualitative and a quantitative level a large variety of phenomena. In fact, many properties of nonequibirium systems are encountered in this equation and many difficult problems, such as the existence and interaction of defects and coherent structures, or the appearance of chaos, may profitably be addressed in the simple framework provided by this equation (Cross and Hohenberg, 1993). Also, the equation describes the dynamics of excitations in nerve membranes, pattern formation in two-dimensional chemical reactors where an autocatalytic reaction takes place (Kuramoto, 1984*a*), some structures in fluid flows (Newell and Whitehead, 1969) and many other physical processes (Rabinovich et al., 2000). In the context of chemical systems the CGLE was introduced by Kuramoto and Tsuzuki (1976). A number of reviews and original works have appeared during the last two decades, showing the generality of the CGLE in many physical situations at all scales, see for example (Newell et al., 1993; Dangelmayr and Kramer, 1998; Pismen, 1999).

The equation has the form

$$\partial_t A = A + (1 + ib)\Delta A - (1 + ic)|A|^2 A, \tag{2.6}$$

where A is a complex function of (scaled) time t and space x (often in reduced dimension $D = 1$ or 2) and the real parameters b and c characterise linear and

nonlinear dispersion. Detailed introductions into the concepts underlying the equation can be found in (Manneville, 1990; Aranson and Kramer, 2002).

The equation was first derived by Newell and Whitehead (1969) when modelling the onset of instability in fluid convection problems. In these situations, at some critical value μ_c of a control parameter μ that can be tuned experimentally, a spatially homogeneous steady state loses stability to oscillations whose frequency ω_0 and wavelength can be understood in terms of a linearised equation. Newell and Whitehead found that when nonlinear effects are included, these oscillations are modulated over long time and space scales by a quantity A that plays a role of a complex order parameter (García-Morales and Krischer, 2012). In fluid dynamics, CGLE emerges generically, as shown by Stewartson and Stuart in 1971 in the context of plane Poiseuille flow (Stewartson and Stuart, 1971).

Specific importance of this equation in the present research is related to the fact that the general behaviour of the nonlinear oscillators in the vicinity of the Hopf bifurcation point is governed by the CGLE.

2.5 Nonlinearly excited phase equation in reaction-diffusion systems

2.5.1 Linear excitation in the phase equation

The simplest truncation of the GNPD equation is the classical second-order linear diffusion.

$$\partial_t u = a_1 \nabla^2 u \,. \tag{2.7}$$

If $a_1 > 0$ then Eq. (4.6) becomes a linear diffusion equation. With the next term taken into account, one gets the Burgers equation. The Burgers equation can be also called the nonlinear diffusion equation. These forms of the phase equation are dissipative and excitation-free.

A more complex form involving linear excitation was introduced by Kuramoto and co-authors (Kuramoto and Tsuzuki, 1976; Kuramoto, 1984*b*) in the context of reaction-diffusion systems. This equation has the following form,

$$\partial_t u = -\varepsilon \nabla^2 u - \nabla^4 u + (\nabla u)^2 \,. \tag{2.8}$$

where $\varepsilon > 0$. Their theory is based on a generalised time-dependent Ginzburg-Landau equation for a complex field A and is linked to the persistent propagation of concentration waves. A mathematically equivalent equation was independently derived by Sivashinsky (1977) in the context of weak thermal diffusive instabilities in a laminar flame front. The Kuramoto-Sivashinsky (KS) equation has the form

$$\partial_t u = -\nabla^2 u - \nabla^4 u + a_1 (\nabla u)^2 . \tag{2.9}$$

In (2.9), as we have already mentioned, the excitation is represented by the linear anti-diffusion term, $(-\nabla^2 u)$, and the dissipation by the term $(-\nabla^4 u)$. The role of the nonlinear term $a_1(\nabla u)^2$ is to provide the bridge between those two.

Topologically, the nonlinear term creates segments of relatively sharp variation of u. As a result, the KS equation provides a dynamical balance between "energy" gain and loss. Figure (2.2) shows an example of solution of the KS equation.

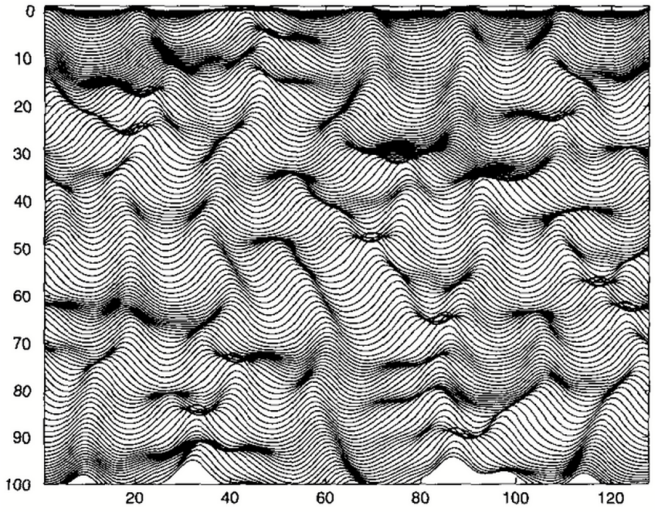

Figure 2.2: Solution of the KS equation in the (x, t) plane. $L = 64$, $n = 128$, with a time interval $\Delta t = 1$ between two successive snapshots (Manneville, 2010).

Nikolaevskii (1989) derived a particular case of the GNPD equation in connection to seismic waves in fluid-saturated solids,

$$\partial_t u = a\nabla^2 u + b_1\nabla^4 u + \nabla^6 u + a_2(\nabla u)^2.$$

Like the KS equation the Nikolaevskii equation has linear excitation (represented by the 4th-order term $(b_1\nabla^4 u)$, $b_1 > 0$). The nonlinear term $a_2(\nabla u)^2$ limits the growth by transferring the energy to higher modes, where a damping force, $\nabla^6 u$, prevails.

Spatiotemporal chaos generated by this equation was explored by Tribelsky and Velarde (1996). The KS and Nikolaevskii equations have been extensively studied, see for example (Kudryashov, 1990; Hyman and Nicolaenko, 1986; Tanaka, 2005).

As we have already mentioned that Eq (1.1) was derived from the CGLE relevant to reaction-diffusion systems. These are the systems of the type considered by Kuramoto (1995) where non-local coupling plays important role,

$$\begin{aligned} \partial_t X &= f(X) + kg(S), \\ \tau\partial_t S &= -S + D\nabla^2 S + h(X)\,, \end{aligned} \tag{2.10}$$

where the n-dimensional real vector field f represents a local limit cycle oscillator with dynamical variable X. When $k = 0$ the first equation represents a field of continuously distributed oscillators without collective coupling. The production term $h(X)$ depends on the local value of X. The dynamics are also affected by the local concentration of S via the term $kg(S)$. In the second equation, the parameter τ is introduced to explicitly express the characteristic time scale for S, anticipating a limiting case in which τ is vanishingly small. The system above has no direct coupling among the oscillators, however, the diffusive chemical represented by S provides an indirect coupling.

Tanaka and Kuramoto (2003) derived the GL equation with nonlocal coupling as a reduced form of a universal class of reaction-diffusion systems near the Hopf bifurcation point and in the presence of another small parameter μ which, when changing from $\mu < 0$ to $\mu > 0$, brings about oscillatory instability (μ is included in the system (2.11)-(2.12) implicitly, not directly). They reduced the reaction diffusion system

$$\partial_t X = f(X) + \delta\nabla^2 X + kg(S) \tag{2.11}$$

$$\tau\partial_t S = -S + D\nabla^2 S + h(X), \tag{2.12}$$

to a non-local universal equation of the Ginzburg Landau type for the amplitude of oscillations,

$$\begin{aligned}\partial_t A = A - (1 + ic_2)|A|^2 A + (\delta_1 + i\delta_2)\nabla^2 A \\ +K(1 + ic_1)\int dr' G(\mathbf{r} - \mathbf{r}')[A(\mathbf{r}', t) - A(\mathbf{r}, t)],\end{aligned} \tag{2.13}$$

where c_1, c_2, δ_1, δ_2 and K are real constants and G is a coupling function. They commented that the GL equation involves six independent parameters c_1, c_2, K, θ, δ_1, and δ_2. Here the parameter $\theta = \omega_0\tau$ is proportional to the basic frequency of oscillations, ω_0, and characteristic time τ.

Tanaka (2004) found evidence that the nonlocal CGLE describing certain class of reaction-diffusion systems exhibits turbulence that is equivalent to turbulence under the Nikolaevskii equation. He confirmed numerically that these chaotic states are structurally stable. In addition, he demonstrated that the Nikolaevskii equation can be obtained from the CGLE via a phase reduction procedure. He also described situation when the CGLE does not reduce exactly to the Nikolaevskii equation.Tanaka (2006) also presented numerical results which demonstrated that at points where the reaction-diffusion systems do not reduce to the Nikolaevskii equation the spatiotemporal chaos is structurally stable.

All the works mentioned above explore systems where the phase dynamics are excited by linear mechanism. Our research focuses on an essentially different mechanism of excitation – nonlinear.

2.5.2 Nonlinear excitation in the phase equation

Although the nonlinearly excited phase dynamics are essential in many applications, very limited studies have been done in this area.

Strunin (1999) phenomenologically constructed the nonlinearly excited phase (NEP) equation (1.1), modelling two types of reaction front – the solid flame front and detonation wave – under the conditions close to the combustion limit (where the combustion is on the brink of decay). He considered the simplest geometry when the front propagates through a hollow cylinder as illustrated by Figure 2.3. The equation is formulated in terms of the position H of the combustion front on the cylinder as the line separating cold fresh mixture from hot reaction products (the original variable H in his paper has been changed to u in order to ensure consistency). The distance u (H in his paper) traveled by the front is in a sense similar to the phase in the context of systems of oscillators. Indeed, the distance u always increases like the phase. However, this occurs not uniformly but with oscillations around some uniformly moving average position. It was demonstrated that the equation can generate single-kink and multiple-kink (multiple solitons in terms of $\partial_x u$) spinning regimes. The model contains the nonlinear excitation

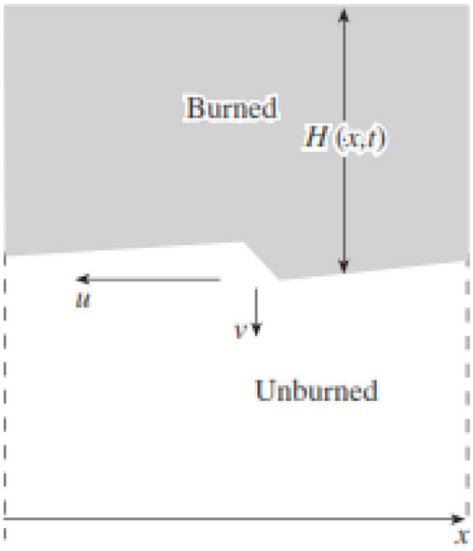

Figure 2.3: Schematic presentation of the reaction front (Strunin, 1999).

term $-b\partial_x^2 u(\partial_x u)^2$ with $b > 0$, linear dissipation term $a\partial_x^6 u$ with $a > 0$ and nonlinear term $c(\partial_x u)^4$ transferring energy from the excitation to dissipation. The equation was solved in 1D numerically, using Galerkin method, under periodic conditions in space. A settled regime was obtained, in which a kink-shaped wave was moving along a spiral trajectory on the surface of a cylinder, see Figure (2.4). An important feature of the wave is that it is not just the correct shape – a kink – that is reproduced but also the dynamic mechanism behind it. In laboratory experiments, the spinning combustion occurs when the reacting chemical composition is diluted with some neutral substance. As a consequence, it becomes difficult for the combustion process to maintain itself — it actually occurs on the

brink of collapse. For the 1D topology Strunin (1999) did not investigate whether, apart from the periodic waves, there may also realise irregular regimes. Perhaps, those are possible at large diameters of the cylinder, when there is enough space for a number of kinks to co-exist and interact with each other in a complicated way. For the 2D topology, that is with an extra dimension available, there is a strong anticipation that chaotic dynamics may form and self-sustain provided the size of the space domain is sufficiently large.

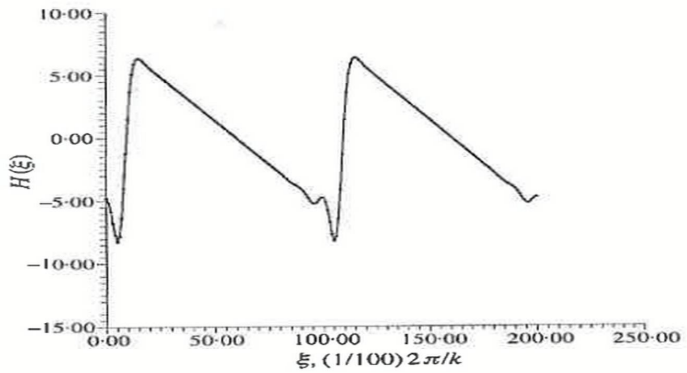

Figure 2.4: The settled solution at $k = 0.12$. Two periods are shown (Strunin, 1999).

2.6 Scaling and hierarchy for the phase equations

Table (2.1) shows the magnitude order of the coefficients of the phase equation (4.6) leading to different truncations and scalings. It also shows the signs of the coefficients, were important.

Denoting the characteristic scale of the phase variations by $U > 0$ and the length scale by $L > 0$, we can evaluate the balancing equation terms in absolute value: For the KS equation (2.9), the balance $\varepsilon U/L^2 \sim U^2/L^2 \sim U/L^4$ gives

$$U \sim \varepsilon, \qquad L \sim \frac{1}{\sqrt{\varepsilon}}. \tag{2.14}$$

Table 2.1: Hierarchy of truncations of the GNPD equations (4.6) (Strunin, 2009*b*)

a_1	a_2	b_1	b_2	b_3	b_4	b_5	g_1	truncation
+1	1	1	1	1	1	1	1	diffusion Eq
excitation: $-\varepsilon$	1	-1	1	1	1	1	1	KS Eq
$+\varepsilon^2$	1	excitation: ε	1	1	1	1	+1	Nikolaevskii Eq
o(ε^6)	o(ε^5)	o(ε^3)	o(ε^2)	o(ε^2)	excitation: -ε	1	+1	Eq (1.1)

The time scale is determined from $U/T \sim \varepsilon U/L^2$,

$$T \sim L^2/\varepsilon \sim 1/\varepsilon^2. \tag{2.15}$$

Hence, from (2.14) and (2.15) we have the scaling relations

$$u = \varepsilon u_1(r_1, t_1), \qquad r_1 = \sqrt{\varepsilon} r, \qquad t_1 = \varepsilon^2 t. \tag{2.16}$$

For the Nikolaevskii equation, the scaling is different: The balance

$$\varepsilon^2 U/L^2 \sim \varepsilon U/L^4 \sim U/L^6 \sim U^2/L^2 \tag{2.17}$$

gives

$$U \sim \varepsilon^2, \qquad L \sim 1/\sqrt{\varepsilon} \tag{2.18}$$

and, using $U/T \sim \varepsilon^2 U/L^2 \sim \varepsilon^5$,

$$T \sim U/\varepsilon^5 \sim 1/\varepsilon^3. \tag{2.19}$$

Thus, the scaling relations are

$$u = \varepsilon^2 u_1(r_1, t_1), \qquad r_1 = \sqrt{\varepsilon} r, \qquad t_1 = \varepsilon^3 t. \tag{2.20}$$

For the NEP equation (1.1),

$$\nabla^2 u(\nabla u)^2 \sim U^3/L^4, (\nabla u)^4 \sim U^4/L^4, \nabla^6 u \sim U/L^6. \tag{2.21}$$

therefore, the balance is

$$\varepsilon U^3/L^4 \sim U^4/L^4 \sim U/L^6\,, \tag{2.22}$$

from where the scales of the dissipative structures,

$$U \sim \varepsilon, \quad L \sim (1/\varepsilon)^{3/2}. \tag{2.23}$$

So, from $u/T \sim u^4/L^4 \sim \varepsilon^{10}$,

$$T \sim 1/\varepsilon^9.$$

Therefore, the scaling is

$$u = \varepsilon u_1(r_1, t_1), \qquad r_1 = \varepsilon^{3/2} r, \qquad t_1 = \varepsilon^9 t. \tag{2.24}$$

2.7 Chapter summary

We discussed the main concepts of dynamical systems such as the different structures of the combustion fronts, especially spinning waves. This is followed by the literature review for the phase equation with both linear and nonlinear excitation.

Chapter 3

Research methodology

A research methodology is a description on how the research will be conducted.The research methodology provides a detailed description of the approaches taken in carrying out the research and the performance evaluation.

3.1 The methodology

There are many problems arises from physical and other sciences, which can be converted to ODEs and PDEs through the process of mathematical modelling. As a result numerous numerical methods have been developed for finding the solutions of ODEs and PDEs, such as finite difference method (FDM), finite element method (FEM), finite volume method (FEM) and others. The method termed as radial basis function method has emerged as an effective tool for solving differential equations. Radial-basis-function networks (RBFNs) have become one of the main fields of research in numerical analysis (Haykin, 1999). (Mai-Duy and Tran-Cong, 2001) proved the effectiveness of IRBF proposed by them. In this approach highest order derivative in differential equation are approximated by radial basis functions and further the lower order derivatives and function itself are then obtained by integration. In this method they choses multiquadric (MQ) function as the basis function. It has been proved that RBFNs have the property of universal approximation, i.e. an arbitrary continuous function can be approximated to a prescribed degree of accuracy by increasing the number of hidden neurons (Park and Sandberg, 1991). Madych and Nelson (1988, 1990) showed that the RBF interpolation scheme using multiquadrics (MQ) can offer exponential convergence rates/spectral accuracy.

The application of MQ-RBFNs for the numerical solution of differential equations has received a great deal of attention over the past 20 years (see, for example, (Kansa, 1990; Fasshauer, 2007), Mai-Duy and Tran-Cong, (2001). These global methods had considerable success in solving a variety of scientific and engineering problems governed by differential equations. It should also be noted that the performance of the RBF scheme is strongly affected by the RBF width.To date, there is a lack of mathematical theory for finding appropriate values of the RBF width. In practice, the RBF width is chosen either by empirical approaches or by

optimization techniques. The latter are expensive, especially for non-linear problems. Generally, the RBF scheme is more accurate, but less stable with increasing RBF-width.

Recently, an alternative approach based on integration to construct the RBF expressions for the interpolation of functions and the solution of differential equations was proposed (Mai-Duy and Tran-Cong, 2001, 2003). It was found that the indirect/integration-based RBFN approach (IRBFN) outperforms the direct/differentiation-based RBFN approach (DRBFN) regarding accuracy and convergence rate over a wide range of the RBF width. The improvement is attributable to the fact that integration is a smoothing operation and is more numerically stable.

It has been found that among RBFNs the multiquadric functions yield more accurate result (Haykin,1999) then others. The IRBFN ability to capture sharp gradients and the resultant sparse system matrix will enable us to effectively investigate Eq. (2.1). To solve Eq. (2.1) numerically in one dimension and two dimensions, we will develop computational program based on the 1D-IRBFN method developed by Mai-Duy and Tran-Cong (2001) and will also use a modified IRBFN method proposed by Mai-Duy and Tran-Cong in future work. We ran the numerical experiments on desktop computers provided by the School of Agricultural, Computational and Environmental Sciences Toowoomba campus. Necessary software, such as Matlab, was also provided by the School.

3.1.1 One-Dimensional IRBFNs collocation method

In this section, we extend the 1D-IRBFN method (Mai-Duy and Tanner, 2007) to compute function derivatives up to 6th-order. The domain of interest is discretised using a uniform Cartesian grid, i.e. an array of straight lines that run parallel to the x and y-axes. The dependent variable u and its derivatives on each grid line are approximated using an IRBFN interpolation scheme. Consider an x-grid line with n grid points. The variation of u along this line is sought in the IRBF form. The highest-order derivative (order p) of the ODE's or PDE's is decomposed into RBFs. Then the RBF networks are successively integrated to obtain the lower-order derivatives and the function itself. Consider a univariate function $u(x)$.

The basic idea of the integral RBF form (Mai-Duy and Tran-Cong, 2001) is to decompose a pth-order derivative of the function u into RBFs

$$\frac{d^p u}{dx^p} = \sum_{i=1}^{n} w_i I_i^p(x), \tag{3.1}$$

where $[w_i]_{i=1}^n$ is the set of network weights, and $[I_i^p(x)]_{i=1}^n$ is the set of RBFs. Lower-order derivatives and the function itself are then obtained through further integration,

$$\frac{d^{p-1} u}{dx^{p-1}} = \sum_{i=1}^{n} w_i I_i^{p-1}(x) + c_1, \tag{3.2}$$

$$\frac{d^{p-2}u}{dx^{p-2}} = \sum_{i=1}^{n} w_i I_i^{p-2}(x) + c_1 x + c_2, \tag{3.3}$$

and so on...

$$\frac{du}{dx} = \sum_{i=1}^{n} w_i I_i^{1}(x) + c_1 \frac{x^{p-2}}{(p-2)!} + c_2 \frac{x^{p-3}}{(p-3)!} + \cdots + c_{p-2} x + c_{p-1}, \tag{3.4}$$

$$u = \sum_{i=1}^{n} w_i I_i^{0}(x) + c_1 \frac{x^{p-1}}{(p-1)!} + c_2 \frac{x^{p-2}}{(p-2)!} + \cdots + c_{p-1} x + c_p. \tag{3.5}$$

Where $I_i^{p-1}(x) = \int I_i^p(x)dx$,$I_i^{p-2}(x) = \int (I_i^{p-1}(x))dx$,.....$I_i^o(x) = \int I_i^1(x)dx$ and $c_1, c_2, ..., c_p$ are the constants of integration, number of constants generated by continuous integration is always equal to highest order present in the differential equation. Unlike conventional differential schemes, the starting point of the integral scheme can vary in use, depending on the particular application under consideration.The scheme is said to be of order p, denoted by IRBFN-p, if the pth-order derivative is taken as the starting point. The evaluation of (3.1)-(3.5) at a set of collocation points $[x]_{j=1}^{n}$ leads to

$$\widehat{\frac{d^p u}{dx^p}} = \widehat{\mathbf{I}}_p^p \widehat{\alpha}, \tag{3.6}$$

$$\widehat{\frac{d^{p-1} u}{dx^{p-1}}} = \widehat{\mathbf{I}_p^{p-1}} \widehat{\alpha}, \tag{3.7}$$

$$\cdots\cdots\cdots$$

$$\widehat{\frac{du}{dx}} = \widehat{\mathbf{I}}_p^1 \widehat{\alpha}, \tag{3.8}$$

$$\widehat{u} = \widehat{\mathbf{I}}_p^0 \widehat{\alpha}. \tag{3.9}$$

where the subscript [.] and superscript (.) are used to denote the order of the IRBFN scheme and the order of a derivative function, respectively; by putting back the value of $\widehat{\alpha}$ in (3.6)-(3.9) we have

$$\widehat{\frac{d^p u}{dx^p}} = \widehat{\mathbf{I}}_p^p \widehat{\mathbf{I}}_p^{0\,-1} \widehat{u} = D_{px} u, \tag{3.10}$$

$$\widehat{\frac{d^{p-1} u}{dx^{p-1}}} = \widehat{\mathbf{I}_p^{p-1}} \widehat{\mathbf{I}}_p^{0\,-1} \widehat{u} = D_{(p-1)x} u, \tag{3.11}$$

$$\cdots\cdots\cdots$$

$$\widehat{\frac{du}{dx}} = \widehat{\mathbf{I}}_p^1 \widehat{\mathbf{I}}_p^{0\,-1} \widehat{u} = D_{1x} u, \tag{3.12}$$

and

$$u = D_0 u, \tag{3.13}$$

$$\widehat{\mathbf{I}}_p^p = \begin{bmatrix} I_1^p(x_1) & I_2^p(x_1) & \dots & I_n^p(x_1) & 0 & 0 & \dots & 0 & 0 \\ I_1^p(x_2) & I_2^p(x_2) & \dots & I_n^p(x_2) & 0 & 0 & \dots & 0 & 0 \\ \dots & & & & & & & & \\ I_1^p(x_n) & I_2^p(x_n) & \dots & I_n^p(x_n) & 0 & 0 & \dots & 0 & 0 \end{bmatrix},$$

$$\widehat{\mathbf{I}_p^{p-1}} = \begin{bmatrix} I_1^{p-1}(x_1) & I_2^{p-1}(x_1) & \dots & I_n^{p-1}(x_1) & 1 & 0 & \dots & 0 & 0 \\ I_1^{p-1}(x_2) & I_2^{p-1}(x_2) & \dots & I_n^{p-1}(x_2) & 1 & 0 & \dots & 0 & 0 \\ \dots & & & & & & & & \\ I_1^{p-1}(x_n) & I_2^{p-1}(x_n) & \dots & I_n^{p-1}(x_n) & 1 & 0 & \dots & 0 & 0 \end{bmatrix},$$

$$\dots\dots\dots$$

$$\widehat{\mathbf{I}}_p^0 = \begin{bmatrix} I_1^0(x_1) & I_2^0(x_1) & \dots & I_n^0(x_1) & \frac{x_1^{p-1}}{(p-1)!} & \frac{x_1^{p-2}}{(p-2)!} & \dots & x_1 & 1 \\ I_1^0(x_2) & I_2^0(x_2) & \dots & I_n^0(x_2) & \frac{x_2^{p-1}}{(p-1)!} & \frac{x_2^{p-2}}{(p-2)!} & \dots & x_2 & 1 \\ \dots & & & & & & & & \\ I_1^0(x_n) & I_2^0(x_n) & \dots & I_n^0(x_n) & \frac{x_n^{p-1}}{(p-1)!} & \frac{x_n^{p-2}}{(p-2)!} & \dots & x_n & 1 \end{bmatrix},$$

$\hat{\alpha} = (w_1, w_2, w_3 \dots\dots\dots w_n, c_1, c_2, \dots\dots c_p)^T$ or $\hat{\alpha} = \begin{pmatrix} \hat{w} \\ \hat{c} \end{pmatrix}$ and let us denote $\mathbf{H}_0 = \widehat{\mathbf{I}_{[6]}^{(0)}}, \mathbf{H}_1 = \widehat{\mathbf{I}_{[6]}^{(1)}}, \mathbf{H}_2 = \widehat{\mathbf{I}_{[6]}^{(2)}}$ and $\mathbf{H}_p = \widehat{\mathbf{I}_{[p]}^{(p)}}$. The use of integrated basis functions is expected to avoid the problem of reduction of convergence rate caused by differentiation. Numerical studies have shown that the integral collocation approach is more accurate than the differential approach (Mai-Duy, Tran-Cong, 2001). There are integration constants generated during integration process and they have been found to be extremely useful for handling the multiple boundary conditions.

3.1.2 Solving ODEs with one spatial dimension using 1D-IRBFN method

By considering a 1D boundary value problem having pth order ODE

$$F(u, \frac{du}{dx}, \frac{d^2u}{dx^2}, \dots\dots, \frac{d^pu}{dx^p}) = b(x), \ r \leq x \leq s, \tag{3.14}$$

where F and b are prescribed functions, together with boundary conditions for $u, du/dx$, ..., and $d^{p/2-1}u/dx^{p/2-1}$ at $x = r$ and $x = s$. The continuous domain of interest is replaced by a set of n discrete points with $x_1 = r$ and $x_n = s$. The integral scheme of order p (IRBFN-p) is employed here to approximate the field variable and its derivatives in the ODE and the boundary conditions.Owing to the presence of p integration constants in the integral formulation, one can add p extra equations to the discrete system.These extra equations can be utilized to represent the ODE and the values of the derivative boundary conditions at both ends of the domain.The governing equation (3.14) and the boundary conditions can be transformed into the following matrix form

$$A\alpha = f, \tag{3.15}$$

where A is the system matrix of size $(n+p)$ by $(n+p)$ defined as

$$A = \begin{bmatrix} F(\widehat{I^0_{p(1,:)}}, \widehat{I^1_{p(1,:)}}, \widehat{I^2_{p(1,:)}}, ...\widehat{I^p_{p(1,:)}}) \\ F(\widehat{I^0_{p(2,:)}}, \widehat{I^1_{p(2,:)}}, \widehat{I^2_{p(2,:)}}, ...\widehat{I^p_{p(2,:)}}) \\ ..... \\ F(\widehat{I^0_{p(n,:)}}, \widehat{I^1_{p(n,:)}}, \widehat{I^2_{p(n,:)}}, ...\widehat{I^p_{p(n,:)}}) \\ \widehat{I^0_{p([1,n],:)}} \\ \widehat{I^1_{p([1,n],:)}} \\ ..... \\ \widehat{I^{(p/2-1)}_{p([1,n],:)}} \end{bmatrix},$$

$\alpha = (w_1, w_2, w_3.....w_n, c_1, c_2, ...c_p)^T$, and
$f = (b_1, b_2, b_3.....b_n, u_r, u_s, \frac{du_r}{dx}, \frac{du_s}{dx}, ...\frac{d^{p/2-1}u_r}{dx}, \frac{d^{p/2-1}u_s}{dx})^T$.
By solving (3.15) we get $\alpha = A^{-1}f$, using α one is able to obtain values of u and its derivative at the grid points.

3.1.3 Solving PDEs with two spatial dimensions using 1D-IRBFN method

The domain of interest is discretized using a Cartesian grid, i.e. an array of straight lines that run parallel to the x and y axis. Let N_x and N_y be the numbers of grid lines in the x and y directions, respectively. The dependent variable u and its derivatives are approximated using a 1D-IRBF interpolation scheme. It should be indicated that the 1D interpolation scheme uses only N_x or N_y nodes (instead of N_x by N_y nodes) to construct the approximations for a given point, resulting in considerable economy.

Eq.(3.9) can be expressed as

$$\hat{u} = \hat{\mathbf{I}}^0_p \begin{pmatrix} \hat{w} \\ \hat{c} \end{pmatrix} = \mathbf{H}_0 \begin{pmatrix} \hat{w} \\ \hat{c} \end{pmatrix}, \tag{3.16}$$

where $\mathbf{H}_0$ is an n by $(n+p)$ matrix, $\hat{u} = (u^{(1)}, u^{(2)}, u^{(3)}, ...u^{(n)})$, $\hat{w} = (w^{(1)}, w^{(2)}, w^{(3)}, ...w^{(n)})$ and $\hat{c} = (c_{(1)}, c_{(2)}, c_{(3)}, ...c_{(p)})$.

Neumann boundary conditions at both ends of a grid line can be imposed by adding two following equations to (3.16),

$$\hat{f} = \begin{pmatrix} \frac{\partial u}{\partial x}(x^{(1)}) \\ \frac{\partial u}{\partial x}(x^{(n)}) \end{pmatrix} = \widehat{\mathbf{K}} \begin{pmatrix} \hat{w} \\ \hat{c} \end{pmatrix} \tag{3.17}$$

where

$$\widehat{\mathbf{K}} = \begin{bmatrix} I^{(1)}_1(x_1) & I^{(1)}_2(x_1) & \dots & I^{(1)}_n(x_1) & \frac{x_1^{p-2}}{(p-2)!} & \frac{x_1^{p-3}}{(p-3)!} & \dots & 1 & 0 \\ I^{(1)}_1(x_n) & I^{(1)}_2(x_n) & \dots & I^{(1)}_n(x_n) & \frac{x_n^{p-2}}{(p-2)!} & \frac{x_n^{p-3}}{(p-3)!} & \dots & 1 & 0 \end{bmatrix}.$$

The RBF coefficients including p integration constants can be transformed into the meaningful nodal variable values through the following relation

$$\begin{pmatrix} \hat{u} \\ \hat{f} \end{pmatrix} = \begin{bmatrix} \mathbf{H}_0 \\ \widehat{\mathbf{K}} \end{bmatrix} \begin{pmatrix} \hat{w} \\ \hat{c} \end{pmatrix} = \hat{\mathbf{C}} \begin{pmatrix} \hat{w} \\ \hat{c} \end{pmatrix}, \tag{3.18}$$

or

$$\begin{pmatrix} \hat{w} \\ \hat{c} \end{pmatrix} = \widehat{\mathbf{C}}^{-1} \begin{pmatrix} \hat{u} \\ \hat{f} \end{pmatrix}, \tag{3.19}$$

where $\widehat{C}$ is a non-square conversion matrix of dimension $(n+2)$ by $(n+p)$ whose inverse can be found using the singular value decomposition (SVD) technique. By substituting Eq. (3.16) into Eqs. (3.6)-(3.9), the values of derivatives of u with respect to (w.r.t.) x at the boundary and interior points on the x-grid line are obtained as

$$\widehat{\frac{\partial^p u}{\partial x^p}} = \mathbf{H_0} \begin{pmatrix} \hat{w} \\ \hat{c} \end{pmatrix}, \tag{3.20}$$

$$\widehat{\frac{\partial^p u}{\partial x^p}} = \mathbf{H}_0 \widehat{\mathbf{C}}^{-1} \begin{pmatrix} \hat{u} \\ \hat{f} \end{pmatrix}, \tag{3.21}$$

$$\widehat{\frac{\partial^p u}{\partial x^p}} = \hat{D}_{px}\hat{u} + \hat{k}_{px}, \tag{3.22}$$

$$\widehat{\frac{\partial^{p-1} u}{\partial x^{p-1}}} = \hat{D}_{(p-1)x}\hat{u} + \hat{k}_{(p-1)x}, \tag{3.23}$$

$$\cdots\cdots\cdots$$

$$\widehat{\frac{\partial^2 u}{\partial x^2}} = \hat{D}_{2x}\hat{u} + \hat{k}_{2x}, \tag{3.24}$$

$$\widehat{\frac{\partial u}{\partial x}} = \hat{D}_{1x}\hat{u} + \hat{k}_{1x}, \tag{3.25}$$

where $\hat{D}_{1x}, \hat{D}_{2x}, \hat{D}_{(p-1)x}$ and $\hat{D}_{px}$, are known matrices of dimension n by n: and $\hat{k}_{1x}, \hat{k}_{2x}, \hat{k}_{(p-1)x}$ and $\hat{k}_{px}$ are known vectors of length n. Similarly, the values of derivatives of u w.r.t. y at the boundary and interior points on the y grid line are given by

$$\widehat{\frac{\partial^p u}{\partial y^p}} = \hat{D}_{py}\hat{u} + \hat{k}_{py}, \tag{3.26}$$

$$\widehat{\frac{\partial^{p-1} u}{\partial y^{p-1}}} = \hat{D}_{(p-1)y}\hat{u} + \hat{k}_{(p-1)y}, \tag{3.27}$$

$$\cdots$$

$$\widehat{\frac{\partial^2 u}{\partial y^2}} = \hat{D}_{2y}\hat{u} + \hat{k}_{2y}, \tag{3.28}$$

$$\widehat{\frac{\partial u}{\partial y}} = \hat{D}_{1y}\hat{u} + \hat{k}_{1y}, \tag{3.29}$$

where $\hat{D}_{1y}, \hat{D}_{2y}, \hat{D}_{(p-1)y}$ and $\hat{D}_{py}$, are known matrices of dimension n by n: and $\hat{k}_{1y}, \hat{k}_{2y}, \hat{k}_{(p-1)y}$ and $\hat{k}_{py}$ are known vectors of length n.

3.1.4 Multiquadric (MQ) function

Generally it has been accepted that the multiquadric based schemes tend to result in highly accurate results as compared to other RBFNs. The present 1D-RBFN method implemented with MQ function which is

$$MQ = \sqrt{(x - c_i)^2 + a_i^2}, \tag{3.30}$$

where c_i and a_i are the centre and the width of the MQ function, respectively and the MQ widths are calculated by $a_i = \beta d_i$. The β is a factor and d_i is the distance between the ith centre and its closest neighbour. Throughout our research we consider β=1.

3.1.5 Relative error

As no analytical solutions of equation (2.1) are known we will modify the equation by adding a forcing term $F(x,t)$, to allow analytical solution to exist,

$$\partial_t u = -A(\partial_x u)^2 \partial_x^2 u + B(\partial_x u)^4 + C\partial_x^6 u + F(x,t). \tag{3.31}$$

The error between the 1D-IRBFN solution $u(x,t)$ and the exact solution $u_e(x,t)$ is determined as

$$N_e = \sqrt{\frac{\sum_{i=1}^{n}[u_e(x_i,t) - u(x_i,t)]^2}{\sum_{i=1}^{n} u_e^2(x_i)}}, \tag{3.32}$$

where $u(x_i,t)$ and $u_e(x_i,t)$ are the calculated and exact solution at the point i, respectively an n is number of collocation/grid points or nodes. The error reduces with refining grid size. Smaller N_e ensures that the approximation is more accurate. After verifying the 1D-IRBFN method by solving Eq. (3.31), we apply the method to solve Eq. (2.1). Eq. (2.1) is solved on different grid sizes (e.g., n=11, 21, 31, 41...., n is number of grid points). The influence of grid size on the numerical solution is studied to obtain the converged solution. We will use the exact solution to measure the error.

3.2 Numerical examples and convergence of the IRBFN method

To verify the convergence behavior of the 1D-IRBFN method over FDM we have solved two simple problems, one in 1D and the other in 2D case. The IRBFs are implemented with the multiquadric (MQ) function (3.30) for each stencil, the set of nodal points is taken to be the set of MQ centres. We assess the performance of the 1D-IRBFN method through a measure: (i) the relative discrete L_2 error defined by Eq. (3.32). The 1D-IRBFN method is validated through the solution of our test problems; the result proves satisfactory.

Example 1.

Consider the following second-order ODE

$$\frac{d^2u}{dx^2} + \frac{du}{dx} + u = -\exp(-5x)[9979\sin(100x) + 900\cos(100x)]. \tag{3.33}$$

The exact solution to this boundary value problem is chosen to be

$$u_{(e)}(x) = \sin(100x)\exp(-5x),$$

which is highly oscillatory and $0 \leq x \leq 1$.

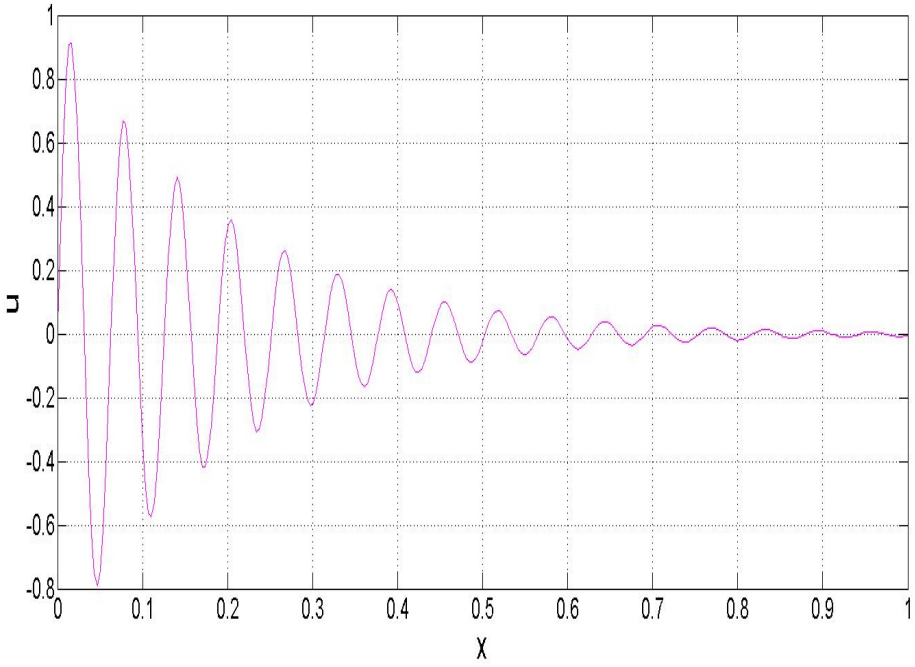

Figure 3.1: Exact solution of Eq. (3.33).

Dirichlet boundary conditions are adopted: $u = 0$ is prescribed at $x = 0$ and $x = 1$. There are two ways to improve accuracy: (i) the grid is refined (d

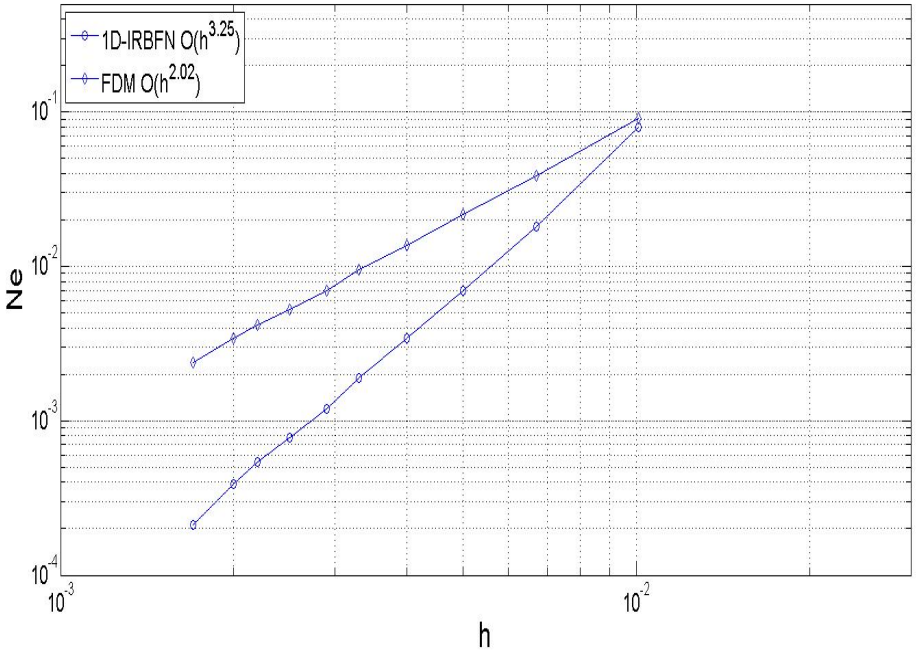

Figure 3.2: Convergence study for the 1D-IRBFN and FDM (central difference) of Eq.(3.33).

adaptivity) and (ii) the MQ width is increased (β adaptivity). The β adaptivity is out of scope of this present research as we consider $\beta = 1$ throughout our research studies.

Table 3.1: Example 1: 1D second-order problem subject to the Dirichlet boundary conditions; comparison of relative error norm (N_e) between the finite-difference method and 1D-IRBFN method ($\beta = 1$).

Grid	h	1D-IRBFN	FDM
100	0.0101	7.9300E-2	9.0700E-2
150	0.0067	1.8100E-2	3.8900E-2
200	0.0050	6.9000E-3	2.1600E-2
250	0.0040	3.4000E-3	1.3700E-2
300	0.0033	1.9000E-3	9.5000E-3
350	0.0029	1.2000E-3	6.9000E-3
450	0.0022	5.3833E-4	4.2000E-3
600	0.0017	2.1303E-4	2.4000E-3

Calculations are conducted on sets of uniformly distributed points, from 100 to 600. Results concerning the solution accuracy, the relative errors by the finite difference (FD) method with central difference scheme and the IRBF method

are presented in Table 3.1 and Fig. 3.2.The convergence behaviour of the FDM and 1D-IRBFN are O($h^{2.02}$) and O($h^{3.25}$) respectively. Numerical results show that in terms of accuracy, the 1D-IRBFN scheme converges faster and is much more accurate than the FDM. In an average sense, the FDM and IRBF solutions converge, respectively. At a grid of 600, the error N_e is 2.4×10^{-3} for FDs and 2.1303×10^{-4} for the IRBFs.The computer codes were written using MATLAB and run on a Dell X-based PC (Intel 3 GHz). Given a grid size, the CPU time by the 1D-IRBFN method is greater than that by the FDM. However, for a prescribed accuracy, the FDM requires much more grid nodes than the 1D-IRBFN method. In this regard (accuracy), the 1D-IRBFN method is more efficient than the FDM.

Example 2.

Consider the two-dimensional Poisson equation defined on a square domain

$$\frac{\partial^2 u}{\partial x^2} + \frac{\partial^2 u}{\partial y^2} = -2(\pi)^2 \sin(\pi x) \sin(\pi y). \tag{3.34}$$

The square domain for the problem is $0 \leq x, y \leq 1$ and it is subject to Dirichlet boundary conditions. The Dirichlet boundary conditions are imposed along all four edges.

The problem has the following exact solution

$$u_E = \sin(\pi x) \sin(\pi y), \tag{3.35}$$

from which the boundary values of u can be derived.

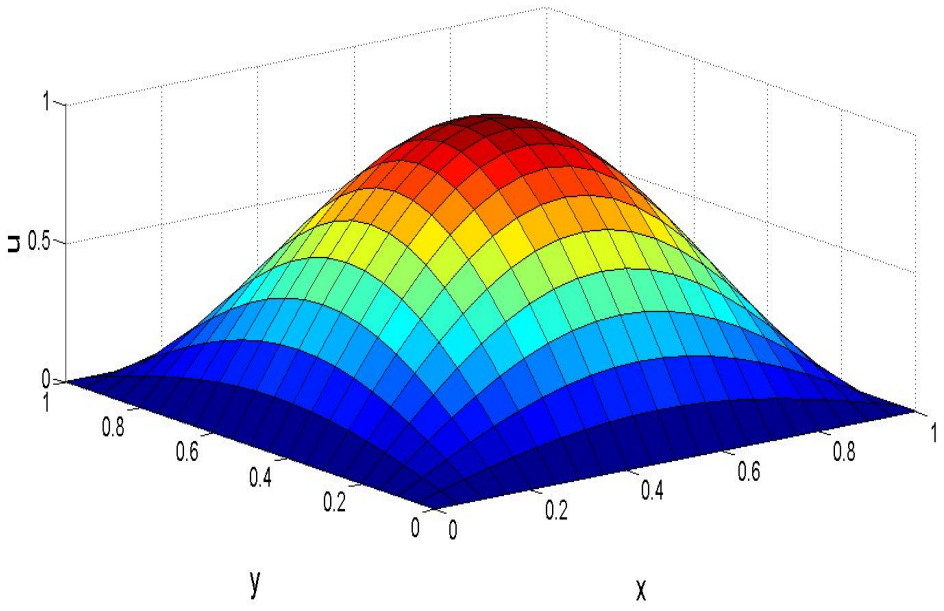

Figure 3.3: Exact solution of Eq. (3.34).

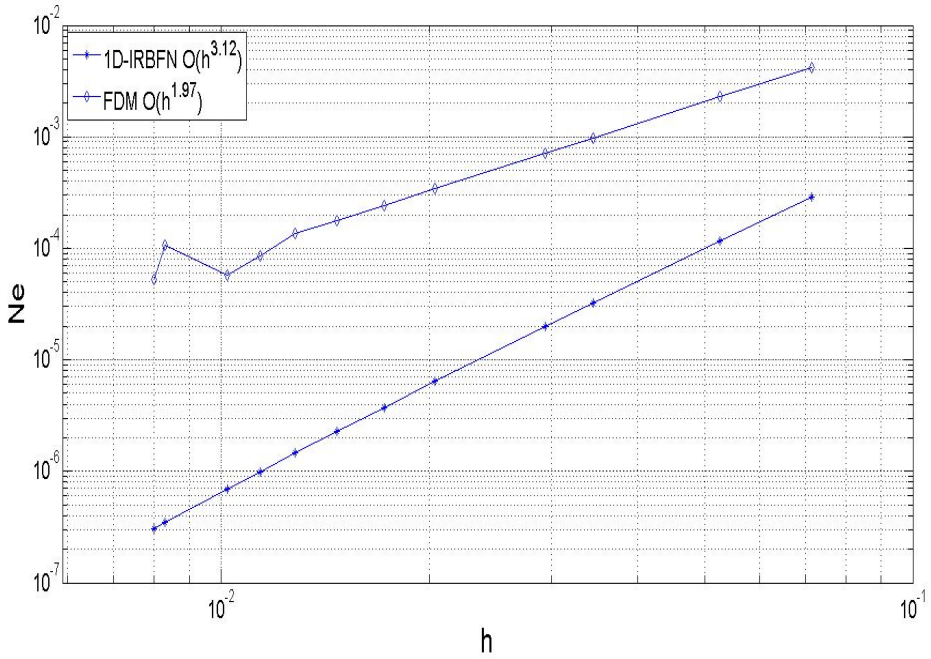

Figure 3.4: Poisson equation in a square domain subject to Dirichlet boundary conditions: Convergence study for 1D-IRBFN and FDM (central difference).

The grid convergence study for the IRBFN and FDM methods is presented in Fig. 3.4. Table 3.2 describes the relative error norms N_e of both the methods.The convergence behaviour of the FDM and 1D-IRBFN are O($h^{1.97}$) and O($h^{3.12}$) respectively. Numerical results show that in terms of accuracy, the 1D-IRBFN scheme converges faster and is much more accurate than the FDM. Thus the grid size can be refined to obtain more accurate solutions as shown in Fig. 3.4.

Table 3.2: Example 2: Poisson equation in a square domain subject to the Dirichlet boundary conditions. Comparison of relative error norm (N_e) between the finite-difference method and 1D-IRBFN method ($\beta = 1$) and h is the grid size (distance between consecutive grid nodes).

Grid	h	1D-IRBFN	FDM
15 x 15	0.0714	2.8892E-4	4.2000E-3
20 x 20	0.0526	1.1577E-4	2.3000E-3
30 x 30	0.0345	3.2171E-5	9.7854E-4
35 x 35	0.0294	1.9770E-5	7.1178E-4
50 x 50	0.0204	6.3722E-6	3.4200E-4
59 x 59	0.0172	3.7400E-6	2.4400E-4
89 x 89	0.0114	9.8300E-7	1.0620E-4
126 x 126	0.0080	3.0663E-7	5.2640E-5

3.3 Innovation and possible outcomes

3.3.1 Innovation

In the present research work a 6th-order nonlinear partial differential equation of Strunin (1999, 2009) will be solved by the 1D-IRBFN method, to simulate the dynamics of reaction fronts such as solid flames and fronts of detonation.Untill now Strunin (1999) has computed the dynamics to limited extent in the one-dimensional case whereas Mohammed and Strunin (2015), have computed the dynamics of two-dimensional case using finite differences but in a different physical context. In both cases, the range of studied dynamical regimes were limited, for example Strunin (1999) presented only one settled regime showing spinning waves, and Mohammed and Strunin (2015), presented only two numerical experiments but due to a very slow computer program performance, the information of the dynamics was limited.

Our plan is to apply a different numerical method, namely the one-dimensional integrated radial basis function network (1D-IRBFN) method. As a result, we will develop numerical code to accurately solve the model. A rich variety of dynamical regimes, primarily in 1D and also in 2D, will be thoroughly explored and analysed. Different settled regimes will be investigated against the size of available space domain under different boundary and initial conditions. In order to validate the method and MATLAB code a comparitive study will be carried out with existing data, which helps us make predictions of the dynamical characteristics of the Eq. (2.1).

3.3.2 Significance

In this PhD project we will develop numerical codes based on the 1D-IRBFN method to solve and analyse the NEP equation. The code on its own will be valueable as a solving tool for high-order nonlinear partial differential equations. The 1D-IRBFN method has been applied to solve many engineering problems such as viscous flows Cong et al. (2012), turbulant dispersion in channel flows Mohammed et al. (2015), Structural analysis (P Le et al., 2008). The advantages of the 1D-IRBFN method over other numerical methods (e.g. FDM) in terms of accuracy, faster approach and efficiancy has been demonstrated in (Mai-Duy, N. Tran-Cong, T., 2001; 2003). Our current 1D code for solving Eq. (2.1) is very efficient when running on a PC with 3.0 GHz CPU and 4 GB RAM. However the code will be further developed for 2D equation with a large elapsed time and large domain, therefore the use of HPC will be helpful to reduce the computational time. This project will substantially advance the numerical modelling of non-stationary reaction front dynamics. It will help us to gain better insight into the dynamics of detonation fronts, which are shock waves in gases accompanied by combustion reaction; solid flames, which are combustion front propagating through solid-phase compounds; super-adiabatic fronts propagating through complex compounds such as solid industrial waste.

Chapter 4

Verification of the 1D-IRBFN method for solving the NEP equation with one spatial dimension

4.1 Introduction

The main purpose of this chapter is to verify the 1D-IRBFN method through several numerical examples to demonstrate the accuracy of the method. Due to the chosen way of testing, this chapter also presents an independent physical interest because it studies a physically interesting case of the forced version of the NEP equation. We select an exact solution of the the forced version of the NEP equation and derive the forced function $f(x,t)$ for this equation. The comparison of the exact and numerical solutions demonstrates satisfactory performance of the numerical code. We solve the forced NEP equation with different sizes of the domain.

4.2 Construction of the forced NEP equation

We consider the equation,

$$\frac{du}{dt} = -A\frac{d^2u}{dx^2}(\frac{du}{dx})^2 + B(\frac{du}{dx})^4 + C\frac{d^6u}{dx^6}\,. \tag{4.1}$$

In order to allow analytical solution we modify the equation by adding a forced term $f(x,t)$ in the above equation, and we arrive at the forced equation

$$\frac{du}{dt} = -A\frac{d^2u}{dx^2}(\frac{du}{dx})^2 + B(\frac{du}{dx})^4 + C\frac{d^6u}{dx^6} + f(x,t)\,. \tag{4.2}$$

The error between the 1D-IRBFN solution $u(x,t)$ and the desired exact solution $u_e(x,t)$ will be determined. Smaller relative error N_e will ensure that the approximation is more accurate.

We desire that the forced Eq.(4.2) have a solution

$$u = \sin(kx + \omega t) \ . \tag{4.3}$$

Assuming $k = 1$, $\omega = -1$ and also $A = 1, B = 1$ and $C = 1$ we get

$$\begin{aligned} &\partial_x u = \cos(x-t)\,, \quad \partial_x^2 u = -\sin(x-t)\,, \quad \partial_x^3 u = -\cos(x-t), \\ &\partial_x^4 u = \sin(x-t)\,, \quad \partial_x^5 u = \cos(x-t)\,, \quad \partial_x^6 u = -\sin(x-t)), \\ &\partial_t u = -\cos(x-t). \end{aligned} \tag{4.4}$$

By sustituting (4.4) into Eq.(4.2) we find,

$$\begin{aligned} -\cos(x-t) = (\sin(x-t))(\cos(x-t))^2 + (\cos(x-t))^4 - \sin(x-t) + \\ f(x,t), \end{aligned} \tag{4.5}$$

$$\begin{aligned} f(x,t) = -\cos(x-t) - (\sin(x-t))(\cos(x-t))^2 - (\cos(x-t))^4 + \\ \sin(x-t). \end{aligned} \tag{4.6}$$

4.3 Exact solutions of the forced equation. Testing the numerical code

We wrote the Matlab numerical code for solving the unforced and the forced NEP equation (4.2) (see Appendix B). The spatial part of the equation is discretized using 1D-IRBFN and the resulting system of differential equations is integrated in time. We carry out the test to ensure a good accuracy as described below. To solve the forced equation we require an initial condition and 6 boundary conditions, so we derive an initial condition and 3 Newmann boundary conditions at $x = 0$ and other 3 at $x = L$, using the exact solution.

For equation (4.2) we would not know apriori whether our chosen solution is stable or not, but if it is stable, our numerical code should be capable of reproducing it. If it proves unstable, we would need to choose a different solution candidate. Of course the solution needs to be nontrivial (non-constant) is space and must satisfy the boundary conditions. For the test we created a nonstationary solution which is represented by the single formula

$$u = \sin(kx + \omega t) \ , \tag{4.7}$$

Write equation (4.2) as

$$\partial_t u = \mathrm{RHS} + f(x,t)\,, \tag{4.8}$$

where RHS stands for the right-hand side of (1.1). Substituting (7.2) into (4.2) we get

$$\partial_t u = \text{RHS} - \cos(x-t) - (\sin(x-t))(\cos(x-t))^2 - (\cos(x-t))^4 + \sin(x-t)\,, \quad (4.9)$$

Table 4.1: Case1: 1D NEP forced equation subject to the Dirichlet boundary conditions. Comparison of the relative error norm (N_e) between the exact solution and the 1D-IRBFN solution with $A = 1$, $B = 1$ and $C = 1$ ($\beta = 1$).

h	1D-IRBFN
0.0510	2.9990E-5
0.0449	2.9548E-5
0.0367	1.8532E-5
0.0347	2.5919E-6
0.0265	1.3105E-6
0.0224	8.3000E-7
0.0184	5.7020E-7
0.0163	3.4163E-7
0.0143	2.3200E-7
0.0122	1.4795E-7

Table 4.2: Case 2: 1D NEP forced equation subject to the Dirichlet boundary conditions. Comparison of relative error norm (N_e) between the exact solution and the 1D-IRBFN solution where $A = 2$, $B = 1$ and $C = 1$ ($\beta = 1$).

h	1D-IRBFN
0.0510	2.1818E-5
0.0449	2.9914E-5
0.0367	1.7421E-5
0.0347	2.6057E-6
0.0265	1.3150E-6
0.0224	8.3763E-7
0.0184	6.4715E-7
0.0163	3.4184E-7
0.0143	2.3243E-7
0.0122	1.4811E-7

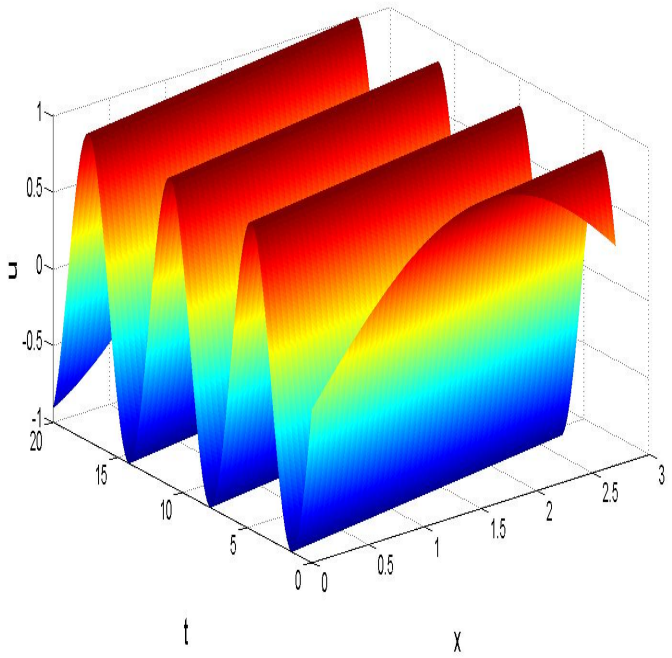

Figure 4.1: Exact solution of Eq. (4.2). $A = 1$, $B = C = 1$, $L = 3$.The axes show grid points.

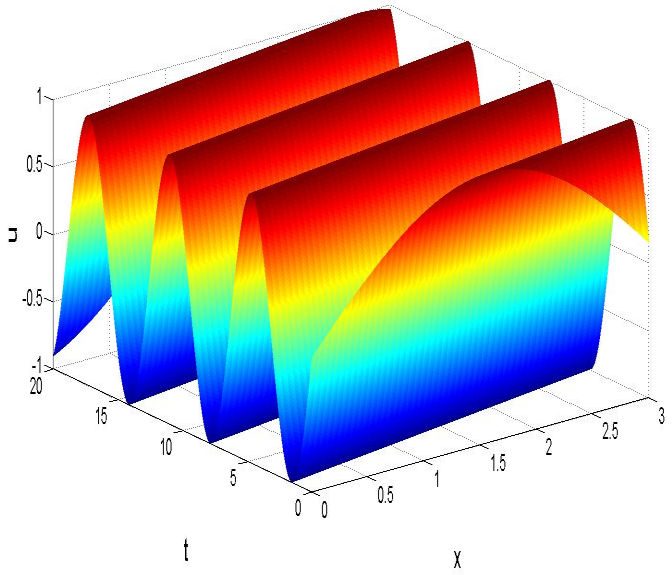

Figure 4.2: The numerical (1D-IRBFN) solution of Eq. (4.2). $A = 1$, $B = C = 1$, $L = 3$. The axes show grid points.

4.3.1 Grid convergence study

Two cases of boundary conditions are considered as follows.

Set 1: Dirichlet and Newmann Bounday conditions are imposed at the both ends of the x-axis.

Set 2: Only Newmann Bounday conditions are imposed at the both ends of the x-axis.

To verify the 1D-IRBFN method, We intend to demonstrate that the numerical solution by the method well agrees with the analytical solution (4.3). The boundary and initial conditions must be consistent with (4.3). The initial time moment is taken at $t_0 = 0$. Table 4.1, 4.2 and Fig. 4.3 present the numerical results, namely, the relative error norms (N_e) of the present numerical method for

Case 1: A=1, B=1, C=1
and
Case 2: A=2, B=1, C=1.

The relative error norm is calculated as

$$N_e = \sqrt{\frac{\sum_{i=1}^{n}[u_e(x_i,t) - u(x_i,t)]^2}{\sum_{i=1}^{n} u_e^2(x_i)}}, \tag{4.10}$$

where $u_e(x,t)$ denotes the analytical solution; and N is the total number of unknown nodal values in the computational domain. Assuming that the solution is convergent with respect to the grid refinement, the behaviour of the error of the solution is assumed to be $N_e \approx \alpha h^{\lambda} = O(h^{\lambda})$, in which h is the grid spacing; and α and λ the parameters of the exponential model ($\lambda > 0$ is the convergence rate). The convergence behaviour for Case 1 and Case 2 is found to be O($h^{2.73}$) and O($h^{2.75}$), respectively. Fig. 4.3 shows that the 1D-IRBFN method can produce accurate numerical results with high convergence rates for both Case1 and Case 2. The convergence study for Set 1 and Set 2 is shown in Fig. 4.4, the numerical results show that 1D-IRBFN method is highly convergent for the both sets but it is a bit more accurate when we apply Dirichlet boundary and Newmann boundary condition (mixed boundary conditions) as compared to only Newmann boundary conditions, where convergence rates are O($h^{2.73}$) and O($h^{2.24}$) for Set 1 and Set 2 respectively.

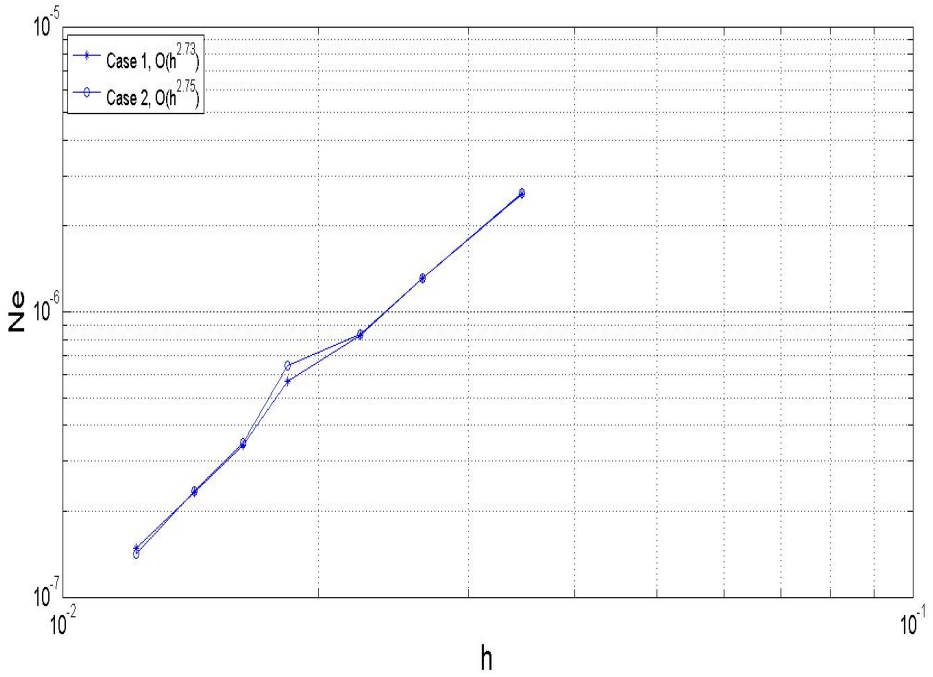

Figure 4.3: The convegence study for Case 1 and Case 2. $L = 1$. The axes show grid points.

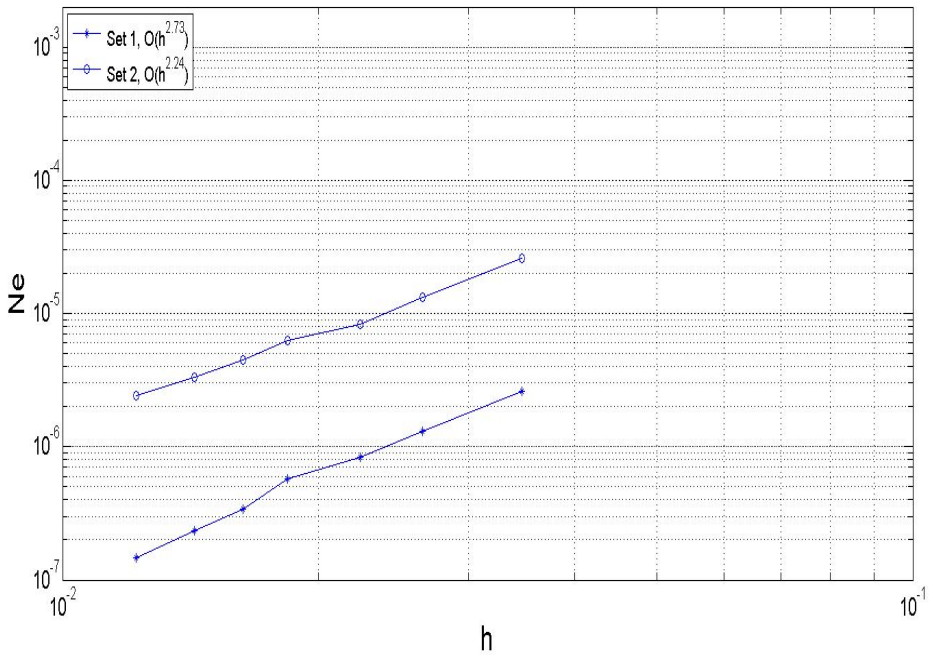

Figure 4.4: The convegence study for set 1 and set 2. $L = 1$. The axes show grid points.

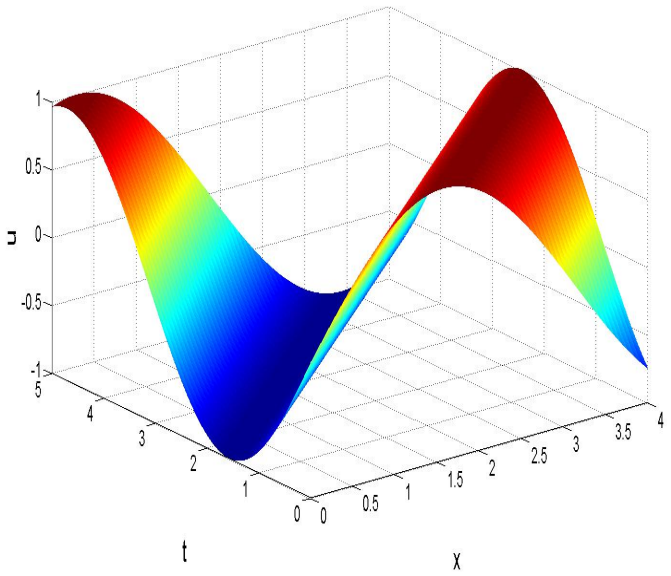

Figure 4.5: Exact solution of equation (4.2). $A = 2$, $B = C = 1$, $L = 4$ $t = 5$. The axes show grid points.

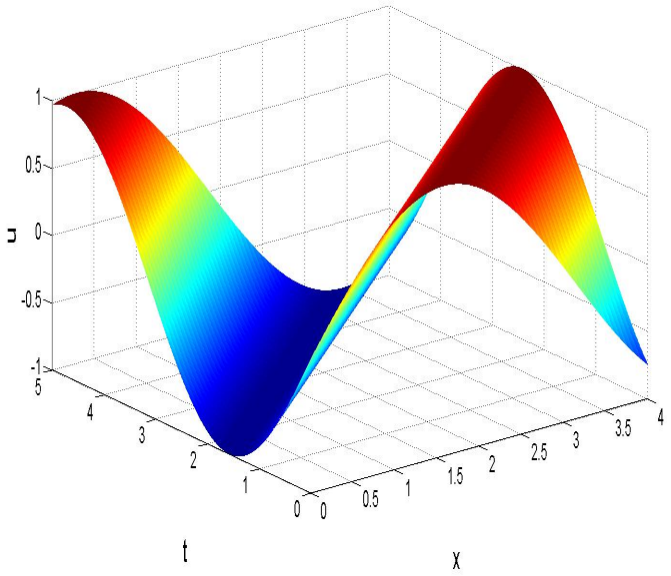

Figure 4.6: The numerical (1D-IRBFN) solution of Eq. (4.2). $L = 4$. The axes show grid points.

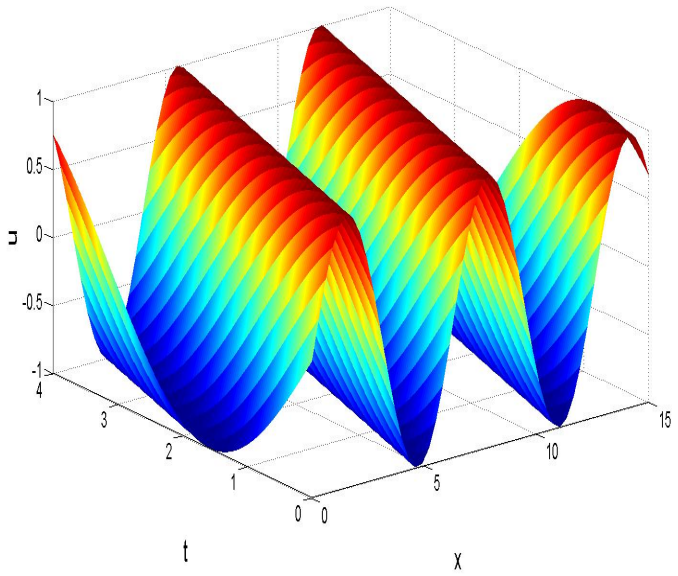

Figure 4.7: Exact solution of equation (4.2). $A = 1$, $B = C = 1$, $L = 15$ $t = 6$. The axes show grid points.

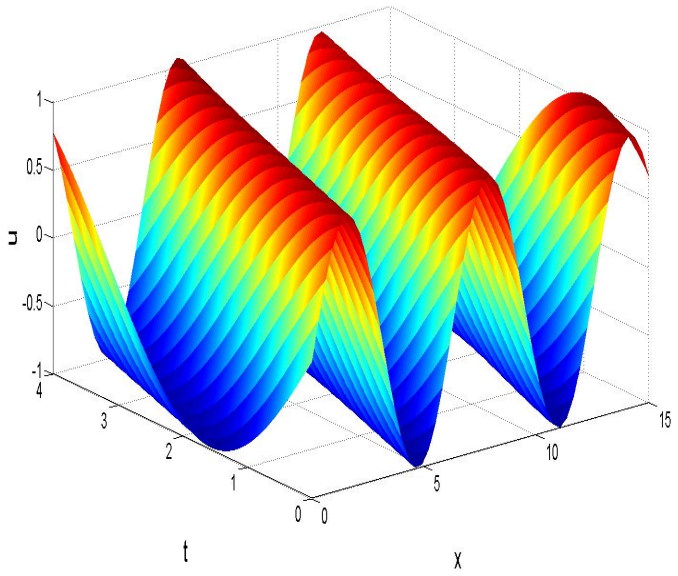

Figure 4.8: The numerical (1D-IRBFN) solution of Eq. (4.2). $L = 15$. The axes show grid points.

4.4 Chapter Summary

In this chapter, we derived the forced version of the NEP equation addressing nonuniformity of the reacting medium in space. Selected exact solutions of this version were constructed. Different non-stationary solutions were obtained for different domain sizes. Stability of the solutions was demonstrated by the numerical experiments. Comparison of the exact and numerical solutions demonstrates satisfactory performance of the numerical code.

Chapter 5

Dynamics of curved reaction fronts

5.1 Introduction

For convenience, we start this section by writing the NEP equation again,

$$\partial_t u = -A(\partial_x u)^2 \partial_x^2 u + B(\partial_x u)^4 + C\partial_x^6 u\,, \tag{5.1}$$

where A, B and C are constants ($A > 0$, $C > 0$). As we mentioned earlier in this thesis, Eq. (5.1) simulates combustion waves (fronts) having the shape of one or more steps and developing instabilities in nonlocal reaction-diffusion systems. In the context of combustion waves, u stands for the distance, measured along, say, axis z, passed by the combustion front through a hollow cylinder, as a function of the coordinate x and time t. The equation generates a rich variety of dynamical regimes, the most spectacular of which is the spinning wave illustrated by Figs. 1.1-1.2. The Fig. 1.1 shows the wave solution of Eq. (5.1) simulating the experiment for Fig.1.2. On the graph the cylinder is rolled out into a plane and two periods are shown. The moving x locations of the steepest sections in Fig 1.1 correspond to luminous spots spinning along the cylinder, due to extremely high temperatures.

Previously Eq. (5.1) has been solved numerically in 1D – with one independent spatial dimension x – using the spectral Galerkin method (Strunin, 1999) and in 2D using a straightforward finite difference scheme. As we mensioned, we aim to apply a different numerical method, which has proved to be fast and accurate in a number of problems, namely the 1D-IRBFN method. First we would like to test the method. Eq. (5.1) is unlikely to allow analytical solutions because of the nonlinearity, so we intend to obtain a single-step travelling wave and compare it with the results shown in Fig. 1.1. Our modelling in this chapter presents a new series of numerical exercises targeting various dynamical regimes generated by Eq. (5.1).

5.2 The numerical method

To solve the main equation (5.1) we developed numerical codes based on the 1D-IRBFN method. This method was tested in many engineering problems incuding viscous flows (Ngo-Cong, Mai-Duy et al., 2012) and structural analysis (Le, Mai-Duy et al., 2008). It was demonstrated that the 1D-IRBFN method has advantage over other numerical methods, for example finite difference and finite element methods, in terms of accuracy, faster approach and efficiancy (Mai-Duy and Tran-Cong 2001; 2003).

In the 1D-IRBFN method highest-order derivative in a differential equation is approximated by radial basis functions (RBFs) and, further, the lower-order derivatives and function itself are then obtained by integration. The purpose of using integration to constuct the approximants is to avoid the reduction in convergence rate caused by differentiation and also to improve the numerical stability of a discrete solution. The integration process naturally gives rise to arbitrary constants that serve as additional expansion coefficients. Therefore they facilitate the employment of some extra equations in the process of converting the RBF weights into the function values, which helps in the implementation of multiple boundary conditions. Results showed that RBFs yield better accuracy, are easy to implement and have the capability to provide a very accurate solution using relatively low numbers of grid points. The so-called multiquadric functions were found to be the most efficient basis function to use in the method we are using in our research. It was found that among RBFNs the multiquartic functions yield more accurate results (Haykin, 1999) then others.The IRBFN ability to capture sharp gradients and the resultant sparse system matrix will enable us to effectively investigate Eq. (5.1). For time integration we used the second order Crank-Nicolson method.

Although RBF methods can be easily implemented in a truly meshless manner based on scattered data points, it proves very efficient and effective to discretise a domain using Cartesian grids. Thus, the purpose of using integration (a smoothing operator) to construct the approximants is to avoid the reduction in convergence rate caused by differentiation, and also to improve the numerical stability of a discrete solution.

This distinguishing feature of the integral formulation provides effective ways to overcome well-known difficulties associated with conventional differential approaches: (i) the implementation of multiple boundary conditions (Mai-Duy and Tanner, 2005); (ii) the description of non-rectangular boundaries on a Cartesian grid (Mai-Duy, See and Tran-Cong, 2008); (iii) the imposition of high-order continuity of the approximate solution across subdomain interfaces (Mai-Duy and Tran-Cong, 2008); and (iv) the incorporation of nodal derivative values into the approximations via compact IRBFN stencils (Mai-Duy and Tran-Cong, 2011).

The ability of the IRBFN methods to capture very sharp gradients, which is highly desirable for Eq. (5.1), has been demonstrated with the effective simulation of shockwave-like behaviours as in the dynamic strain localisation in a quasi-brittle material subjected to a sudden step loading (Le, Mai-Duy, Tran-Cong and Baker, 2008).

5.3 Numerical experiments

5.3.1 Settling of the travelling front under homogeneous boundary conditions

Experiment 1.

Figs 5.1–5.2 show a sequence of snapshots displaying the solution of Eq. (5.1) evolving from the initial condition chosen in the step-like (front-like) form

$$u(x,0) = 8\,\exp[-(x-5)^2] \text{ for } x \geq 5\,,$$

$$u(x,0) \equiv 8 \text{ for } x < 5\,.$$

The idea is to help the solution curve acquire the step-like shape hinted by Fig. 1.1, although we realise that ultimate settled configuration of the solution will not depend of the initial condition.

In our numerical experiments we chose not to transform the equation to the canonical form, in order to be able to adjust the coefficient values as necessary, for example to increase or reduce the energy release in the system in hope to achieve a self-sustained balance between the release and dissipation. The parameter values were: $A = 5$, $B = 1$, $C = 1$, the number of nodes 401, the length of the x-interval 10, time step $2 \cdot 10^{-6}$. The x-interval was constantly shifted to the right to follow the main kink, which, according to the initial shape, was to move to the right. When looking at Fig. 1.1, if one stretches the x-axis enough, the long shoulders would become nearly horizontal.

In fact each shoulder could stretch to infinity on both sides of an isolated single step. Aiming at such a solution, we adopt the boundary conditions

$$\partial_x u = 0\,, \quad \partial_x^2 u = 0\,, \quad \partial_x^3 u = 0$$

on the left and right ends of the (moving) x-interval. The experiment showed that after some period of transitional evolution lasted from $t_0 = 0$ to about $t = 0.03$, the curve practically ceased changing in shape. Continuing the experiments further gave the same frozen shape of the solution moving with constant speed to the right. Looking at the solution displayed in Fig. 1.1 we see the same characteristic tale of ripples in front of the main kink. They were expected to form, caused by the high order of the dissipation acting in the system. Immediately in front of the main kink sits a shorter one, followed, as we look from left to right, by barely distinguishable smaller ripples. The height of the main kink relative to its neighbour is about 4:1 or a bit higher, for the both figures. The fact that the solution settles into a steady moving shape of correct proportions correlates with the earlier result.

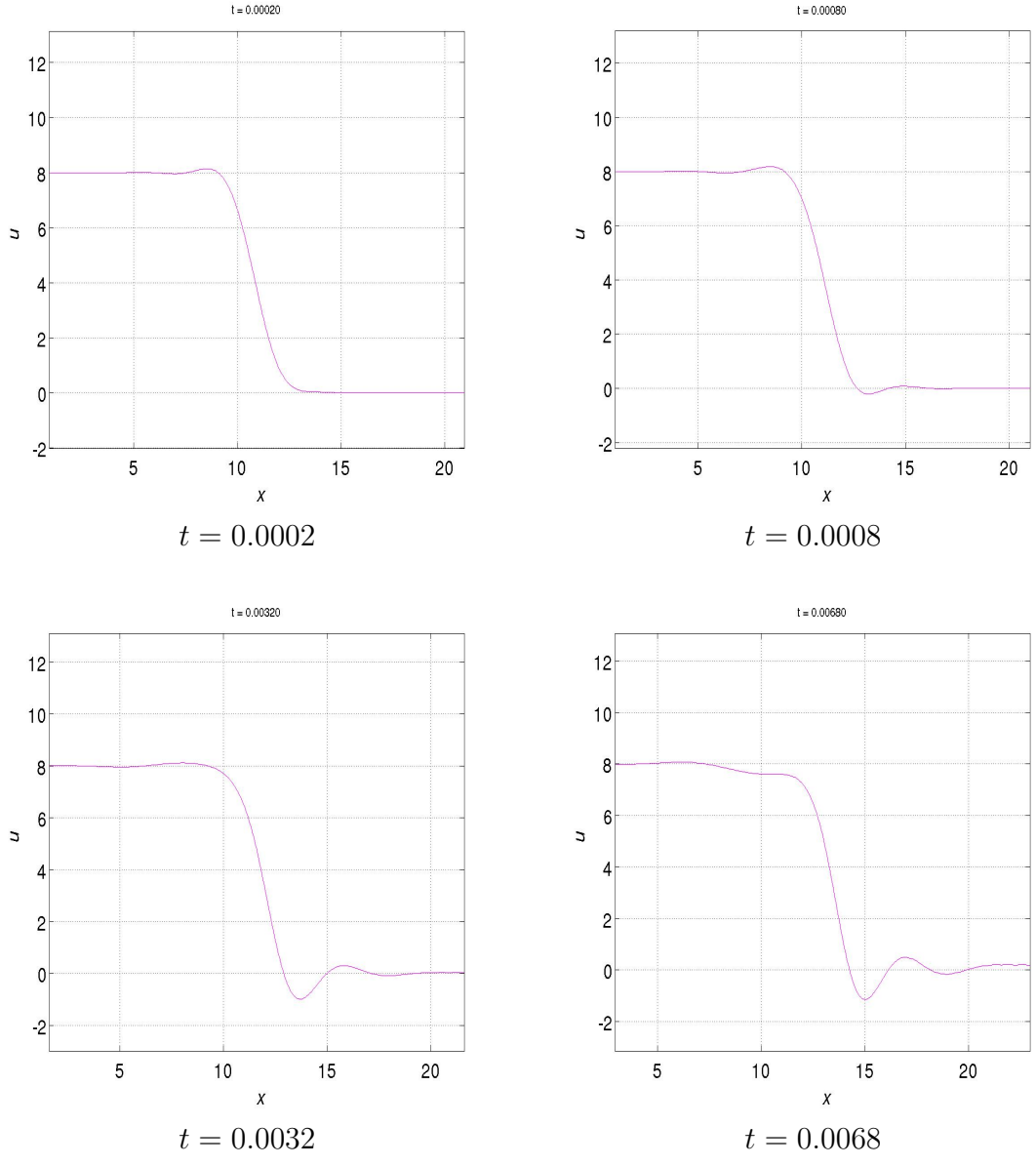

$t = 0.0002$ $t = 0.0008$

$t = 0.0032$ $t = 0.0068$

Figure 5.1: Evolving solution of Eq. (5.1) via the 1D-IRBFN method.

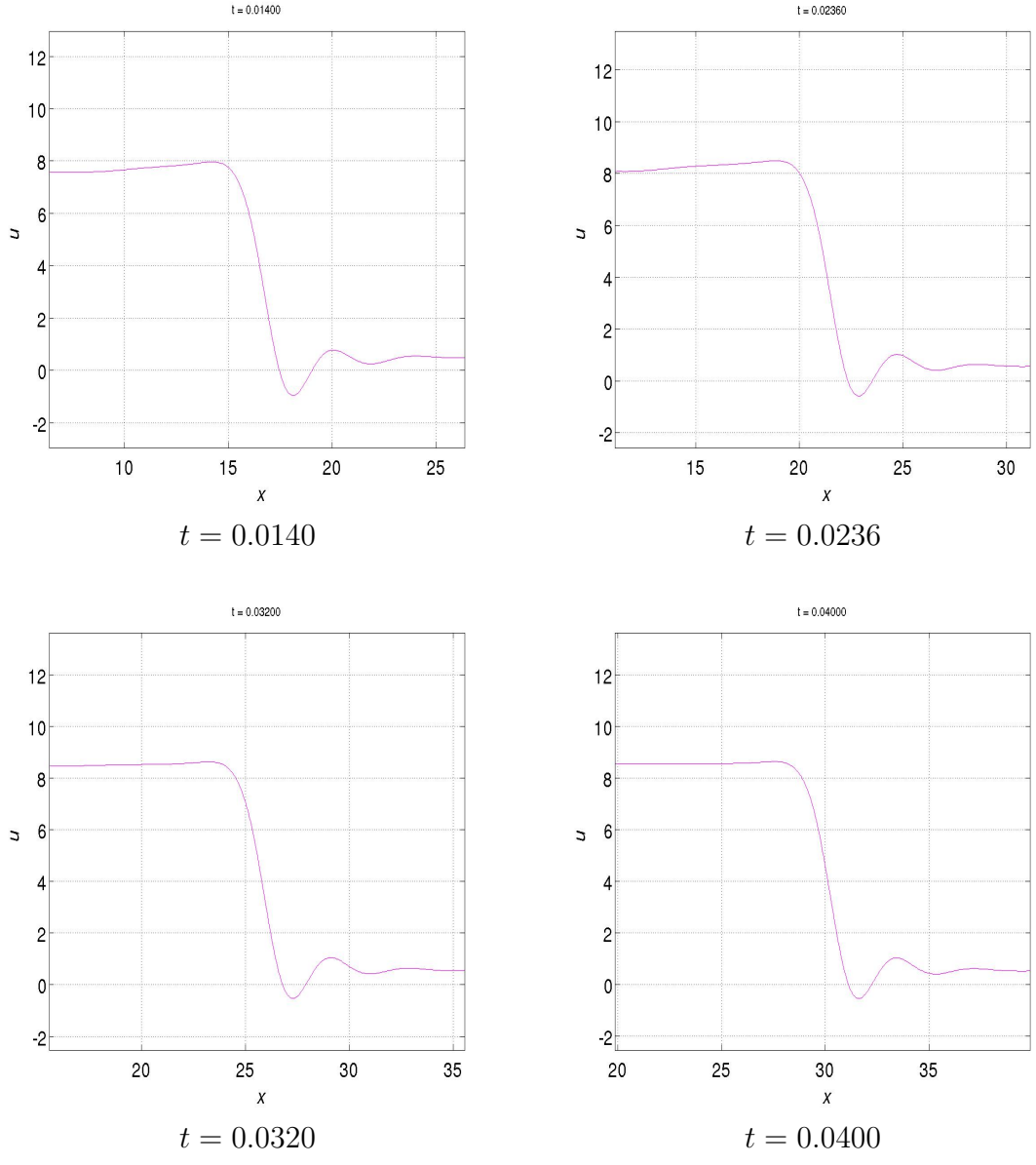

$t = 0.0140$ $t = 0.0236$

$t = 0.0320$ $t = 0.0400$

Figure 5.2: Evolving solution of Eq. (5.1) via the 1D-IRBFN method.

Experiment 2.

In this set of numerical experiments we assume the homogeneous boundary conditions,

$$\partial_x u|_{x=L_1} = \partial_x u|_{x=L_2} = 0\,,$$
$$\partial_x^2 u|_{x=L_1} = \partial_x^2 u|_{x=L_2} = 0\,,$$
$$\partial_x^3 u|_{x=L_1} = \partial_x^3 u|_{x=L_2} = 0\,.$$

The equation coefficients are chosen arbitrarily, $A = 2$, $B = 1$, $C = 1$. We recall that regardless of concrete values of the coefficients, the governing equation can always be transformed to the canonical form with $A = B = C = 1$ by re-scaling x, t and u. The space domain was constantly shifted to the right, following the moving front. The number of nodes was 500, the covered length $L_2 - L_1 = 30$.

The initial condition was

$$u(x,0) = 5\exp\left[-(x-1)^2\right]\,.$$

After some transitional period Fig. 5.3 , the front clearly settles in constant shape (most evident at the later moments), with the nearly horizontal tails Fig. 5.4 . Ahead of the front goes the characteristic chain of small-scale oscillations caused by the high-order dissipation. Effectively this regime represents an isolated step from Fig. 1.1. In the next chapter we present a more direct matching between our results and the periodic solution in Fig. 1.1.

Fig. 5.5 displays the solution dynamics in the form of a surface $u = u(t,x)$. See that the front's motion and shape start to settle around $t = 6$ and then the velocity is practically constant. We obtained similar results when using different initial conditions and values of the parameters. Fig. 5.6 shows the time dependence of the position of the local maximum of u, that is that of the top point of the step. Apparently, after some transitional period characterised by fluctuations of the velocity, the graph becomes a straight line that is the velocity becomes constant.

Experiment 3.

In this numerical experiment we want to achieve periodic solutions and therefore require continuity of u and its five derivatives on the edges,

$$u|_{x=L_1} = u|_{x=L_2}\,, \quad \partial_x u|_{x=L_1} = \partial_x u|_{x=L_2}\,,$$
$$\partial_x^2 u|_{x=L_1} = \partial_x^2 u|_{x=L_2}\,, \quad \partial_x^3 u|_{x=L_1} = \partial_x^3 u|_{x=L_2}\,.$$
$$\partial_x^4 u|_{x=L_1} = \partial_x^4 u|_{x=L_2}\,. \quad \partial_x^5 u|_{x=L_1} = \partial_x^5 u|_{x=L_2}\,.$$

The equation coefficients are chosen to be $A = 1$, $B = 1$ and $C = 1$. We emphasise again that concrete values of the coefficients are not important in terms of the shape of the front and the way it moves, because any of our graphs

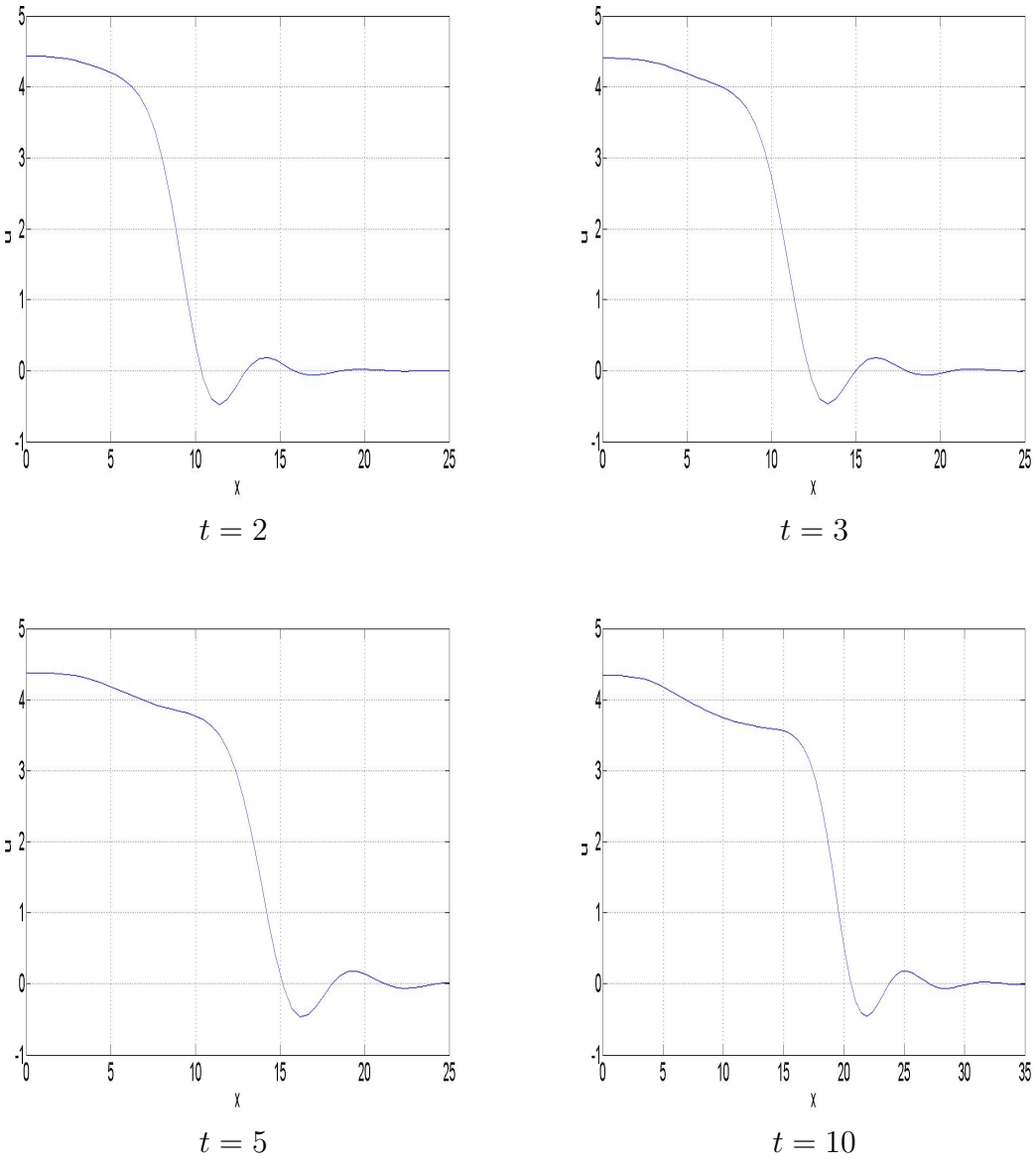

$t = 2$ $t = 3$

$t = 5$ $t = 10$

Figure 5.3: Settling of the fixed-shape front.

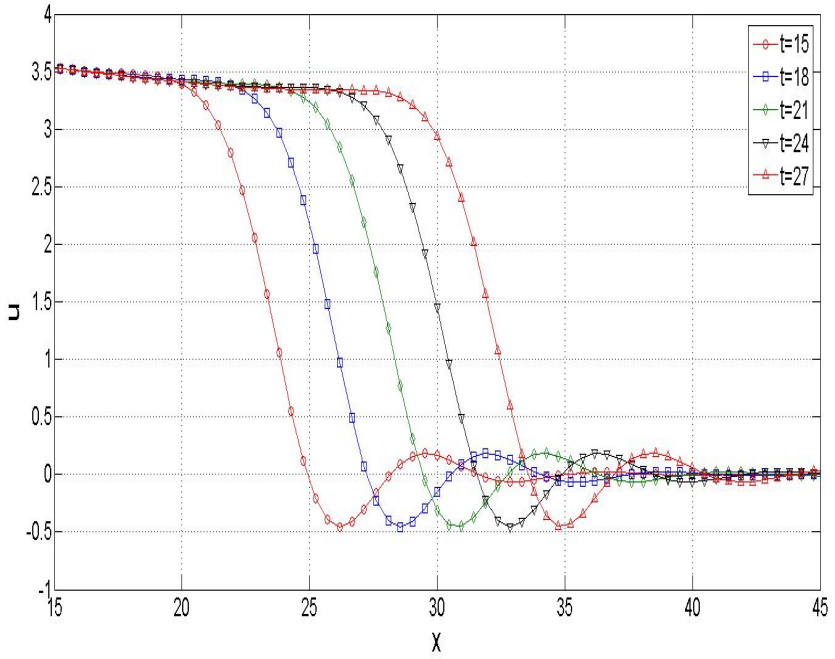

Figure 5.4: A spinning front solution of Eq. (5.1).

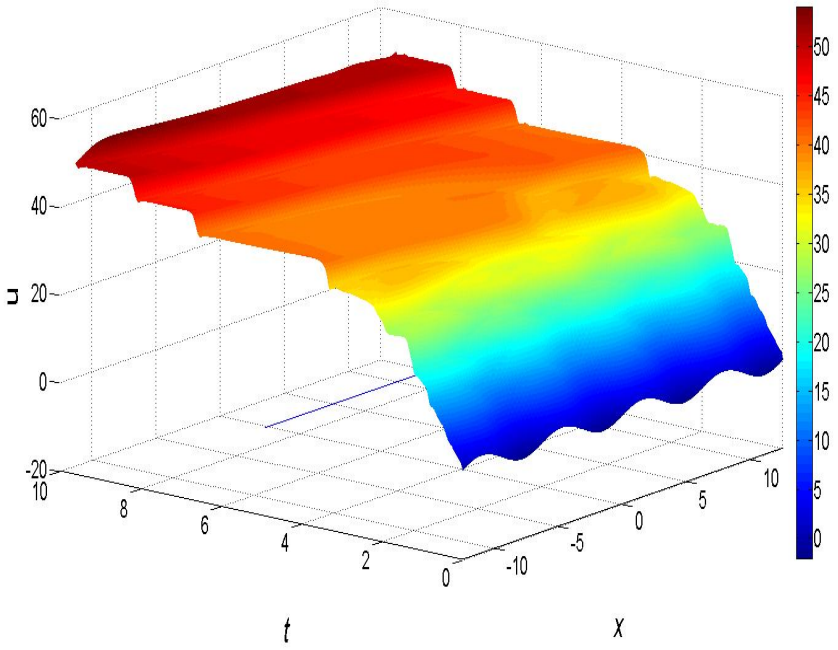

Figure 5.5: The surface diagram for the times between $t = 0$ and $t = 10$.

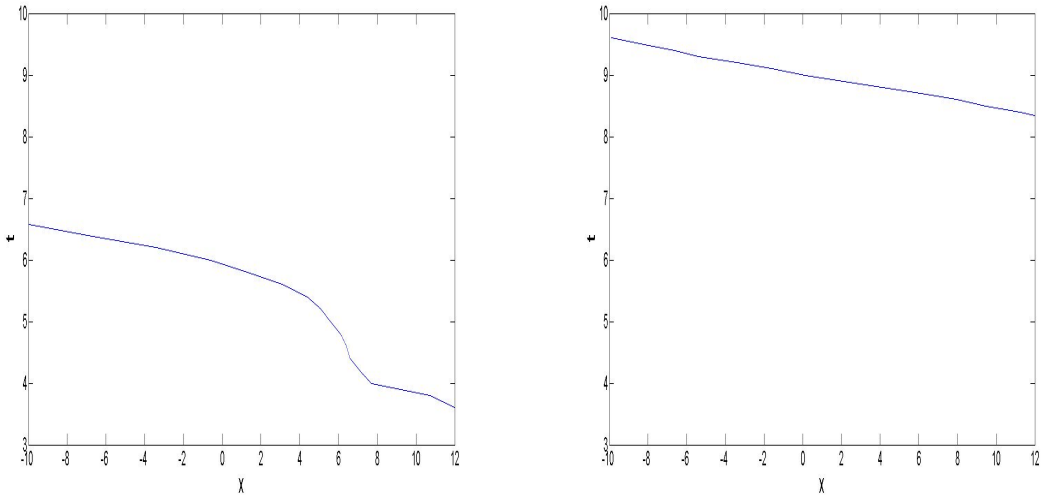

Figure 5.6: The propagation of the local maximum of u for $t = 0$ through $t = 10$.

can be viewed as one corresponding to the canonical form of Eq. (5.1), only in scaled coordinates.

The initial condition is

$$u(x, 0) = \sin x\,, \tag{5.2}$$

see Fig. 5.7. The number of nodes is taken to be 120, the time step 0.001 and $L_2 - L_1 = \pi$. Figs. 5.8-5.9 shows the dynamics at early times. In this particular experiment the initial condition is periodic and hence, is consistent with the boundary conditions. As a result at $t = 0$ the value of the function on the left edge and the right edge is same/equal.

For the NEP equation, by denoting the characteristic scale of the phase variations by $U > 0$ and $L > 0$ and evaluating in absolute value:

$$\nabla^2 u(\nabla u)^2 \sim U^3/L^4, \quad (\nabla u)^4 \sim U^4/L^4, \quad \nabla^6 u \sim U/L^6. \tag{5.3}$$

The balance between the three terms of (1.1),

$$AU^3/L^4 \sim BU^4/L^4 \sim CU/L^6\,, \tag{5.4}$$

governs the scales of the dissipative structures,

$$U \sim A/B, \quad L \sim (B^2C/A^3)^{1/2}. \tag{5.5}$$

In case L is very small the term U/L^6 is largest as compared to the other two terms. As a result dissipation term of the NEP equation prevails and system is heading towards decay. Fig 5.10 demonstrates that under smaller lengths the NEP equation for combustion systems decays forever.

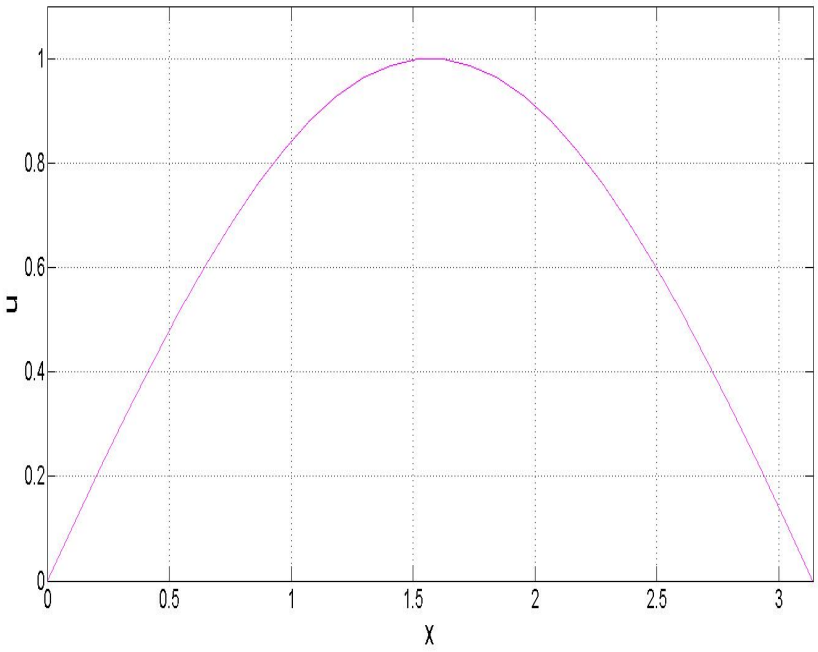

Figure 5.7: The initial condition.

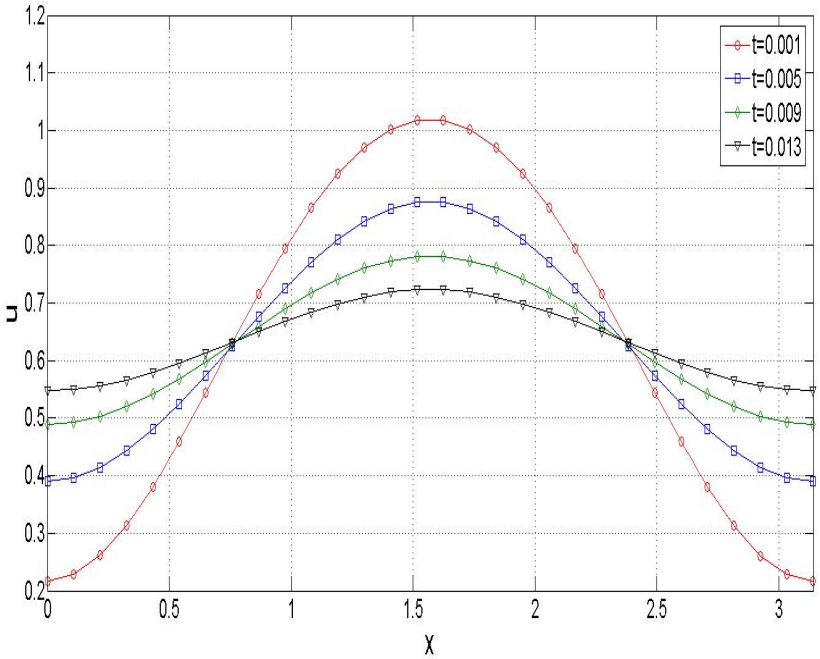

Figure 5.8: The solution at t=0.001 to t= 0.013.

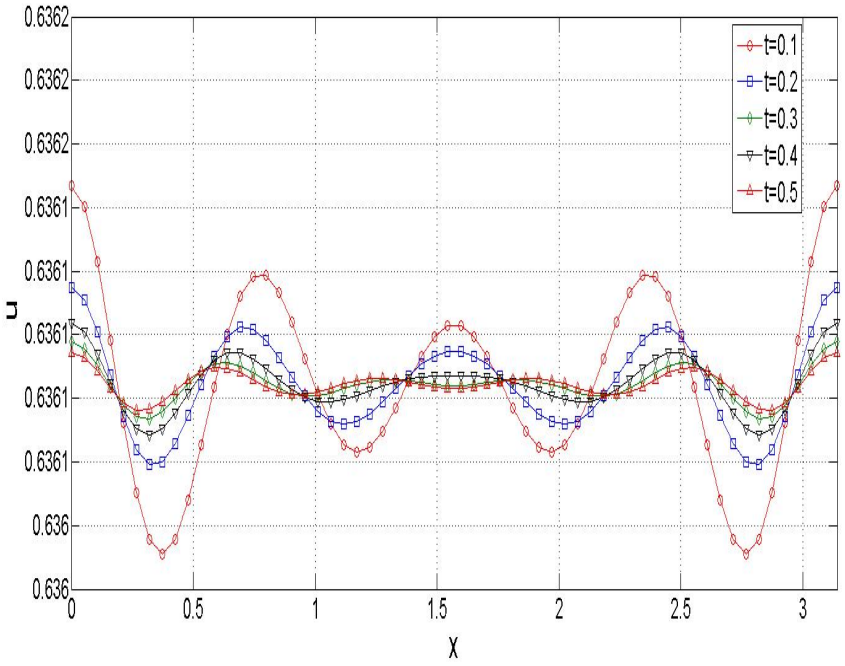

Figure 5.9: The solution at t=0.1 to t= 0.5.

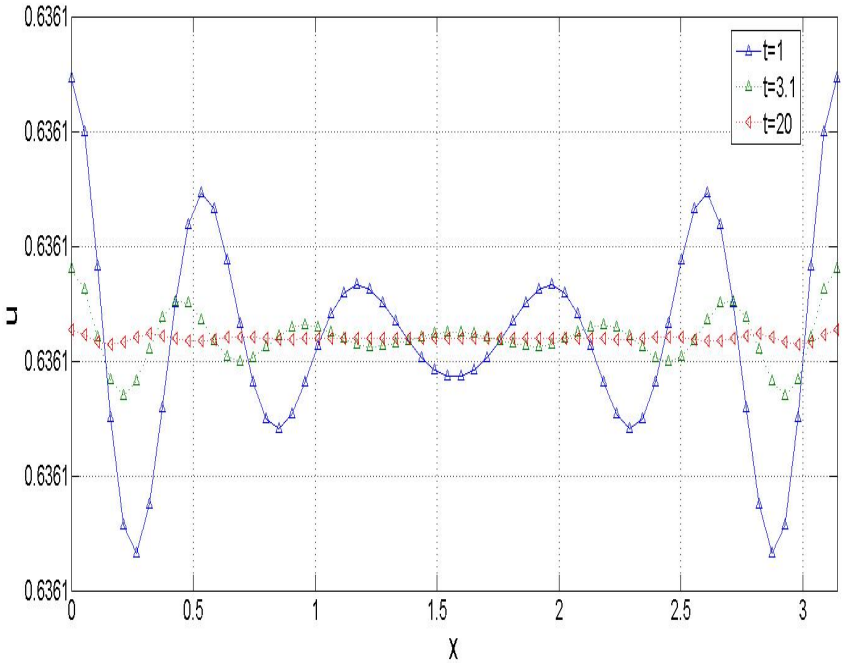

Figure 5.10: The solution at t=1 to t= 20.

Experiment 4.

(a): In this numerical experiment we want to find the bifurcation point in terms of L beyond which a non trivial regime may settle and below which only a trivial (flat) settled state is possible. In such a case there is enough space for dissipative structures to form as discussed in Experiment 3. We set periodic boundary conditions, therefore require continuity of u and its five derivatives on the edges. The equation coefficients are chosen to be $A = 1$, $B = 1$ and $C = 1$.

The initial condition is

$$u(x, 0) = 10 \sin x \,, \tag{5.6}$$

see Fig. 5.11. The number of nodes is taken to be 120, the time step 0.001 and $L_2 - L_1 = \pi$ as in experiment 3. Figs. 5.12–5.13 show the dynamics at early times. In this particular experiment the initial condition is periodic and, hence is consistent with the boundary conditions.

In this experiment, we intentionally take the amplitude bigger than in the Experiment 3, and we get the following numerical results. We see in Figs. 5.12–5.14 that even if the amplitude is ten times the amplitude of the previous experiment the system starts decaying until it becomes flat. This demonstartes that if the length of the domain is smaller than the bifurcation length, the system decays irrespectively of the amplitude of the initial condition. We found that the bifurcation length L_* lies in the interval $15 < L_* < 17$ as supported by Figs.5.15–5.17 and Figs. 5.18-5.20.

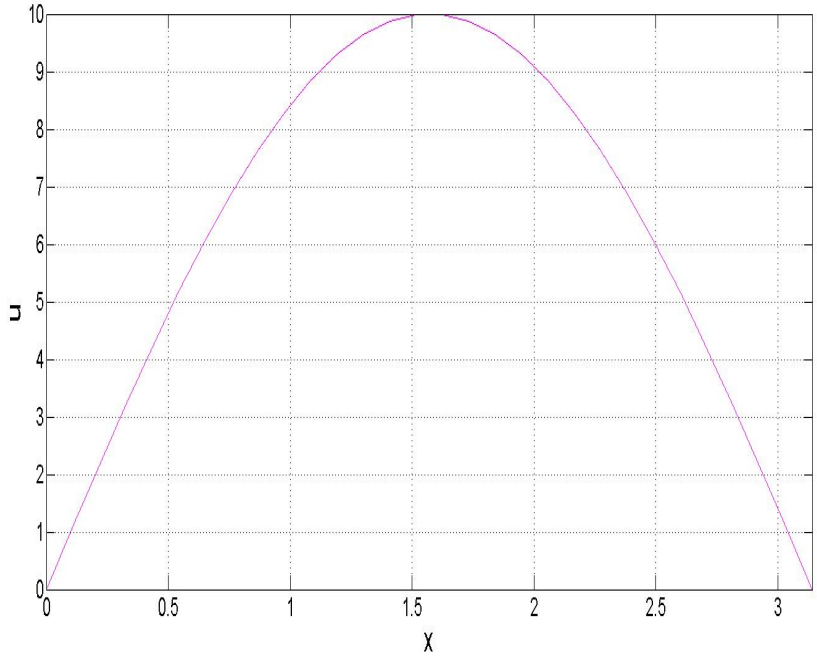

Figure 5.11: The initial condition.

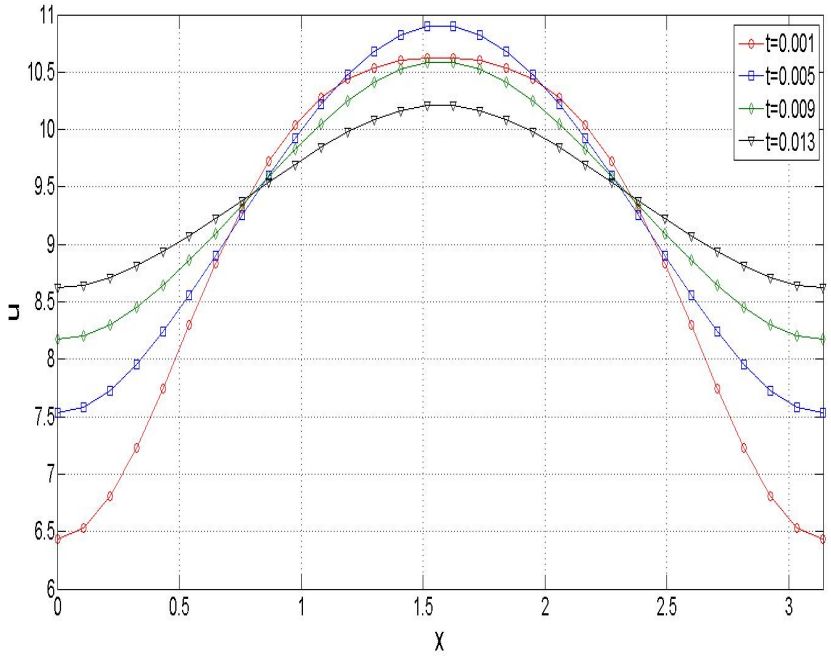

Figure 5.12: The solution at t=0.001 to t= 0.013.

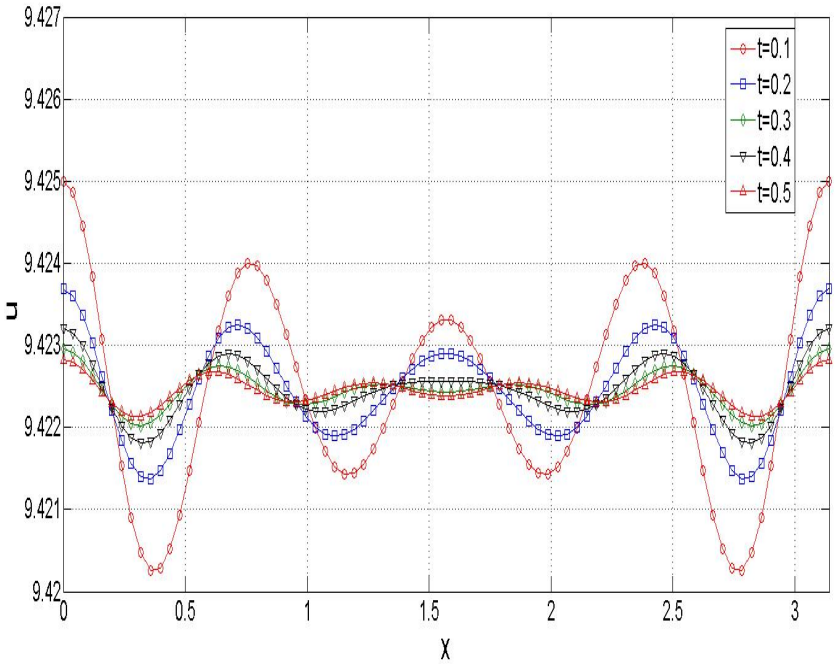

Figure 5.13: The solution at t=0.1 to t= 0.5.

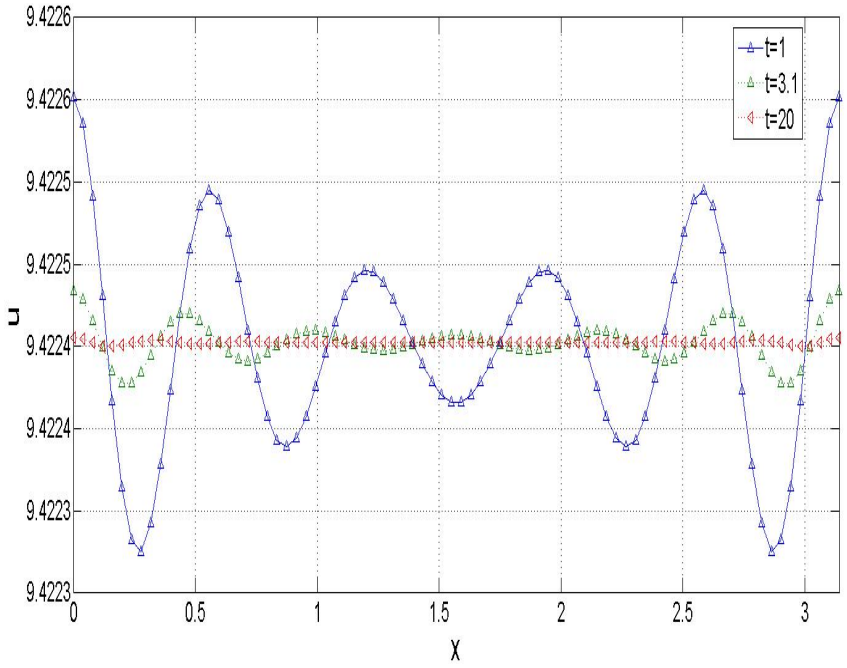

Figure 5.14: The solution at t=1 to t= 20.

(b): For this experiment we set periodic boundary conditions on the edges. The equation coefficients are chosen to be $A = 1$, $B = 1$ and $C = 1$. The initial condition is

$$u(x,0) = u(x,0) = 1.1\left[\sin(3x) + \frac{1}{2}\sin(4x) + \frac{x}{8}\right]. \tag{5.7}$$

The number of nodes is taken to be 180, the time step 0.001 and $L_2 - L_1 = 15$. Figs. 5.15–5.16 show the dynamics at early times. The final solution Fig. 5.17 decays with time, so the dynamics of the solution demonstrates that the length of the domain is smaller than the bifurcation length.

(c): For this experiment we again set periodic boundary conditions on the edges. The equation coefficients are chosen to be $A = 1$, $B = 1$ and $C = 1$. The initial condition is the same as in Experiment 4 (b). The number of nodes is taken to be 180, the time step 0.001 and $L_2 - L_1 = 17$. Figs. 5.18–5.19 show the dynamics at early times. The final solution Fig. 5.20 shows that the length of the domain is larger than the bifurcation length as the fronts survives and finally develops into strong spinning waves.

5.4 Conclusions

We applied the 1D-IRBF numerical method to solve Eq. (5.1) simulating spinning combustion fronts and oscillations in reaction-diffusion systems with non-local effects.

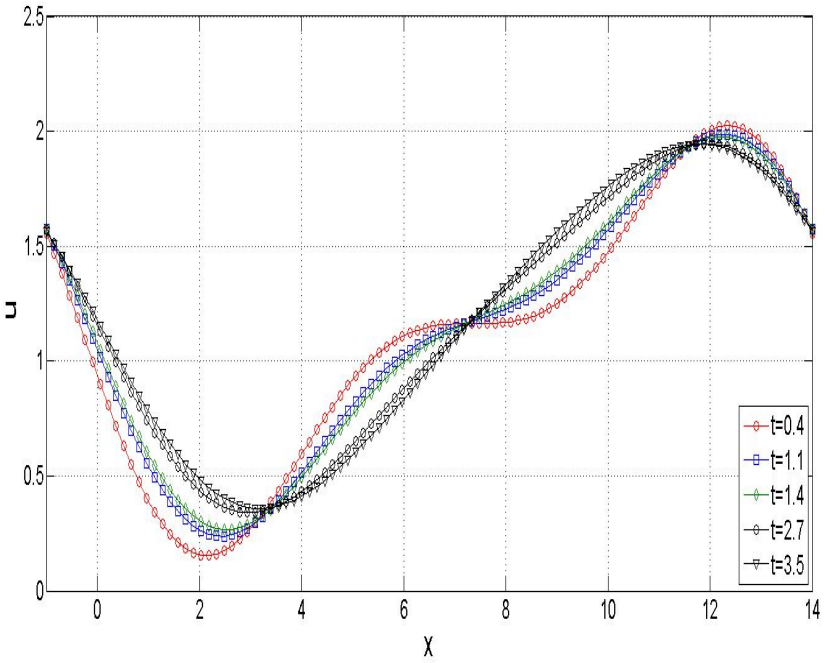

Figure 5.15: The solution at t=0.4 to t= 3.5.

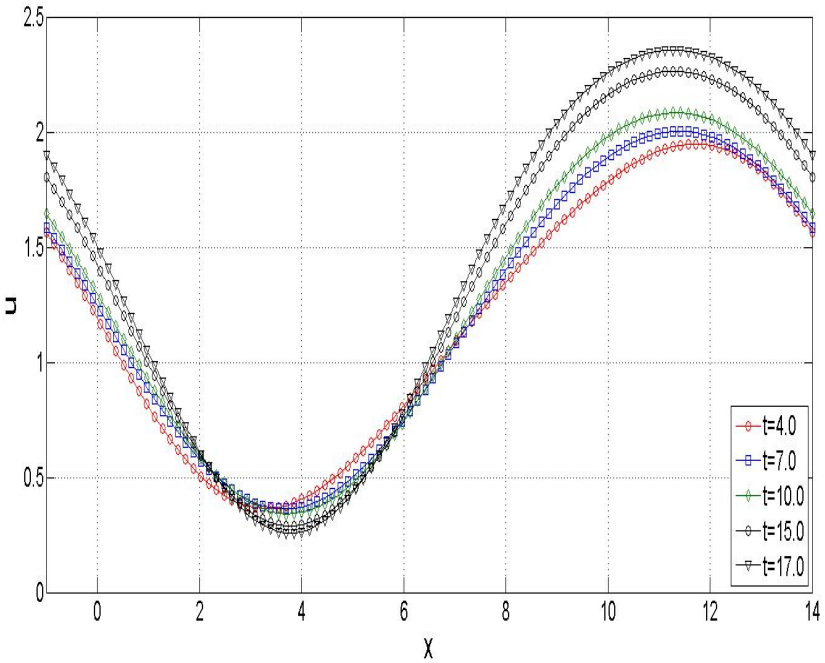

Figure 5.16: The solution at t=4.0 to t= 17.

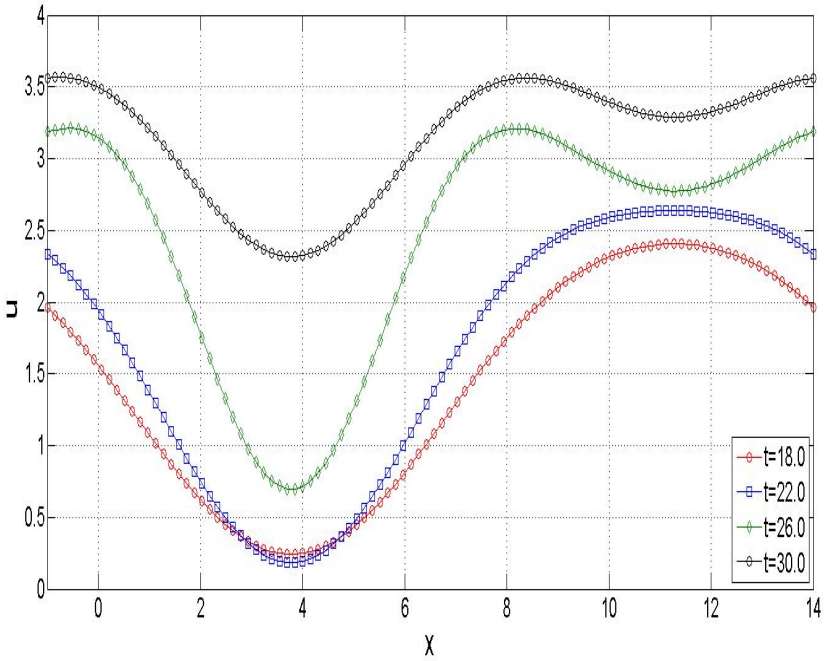

Figure 5.17: The solution at t=18 to t= 30.

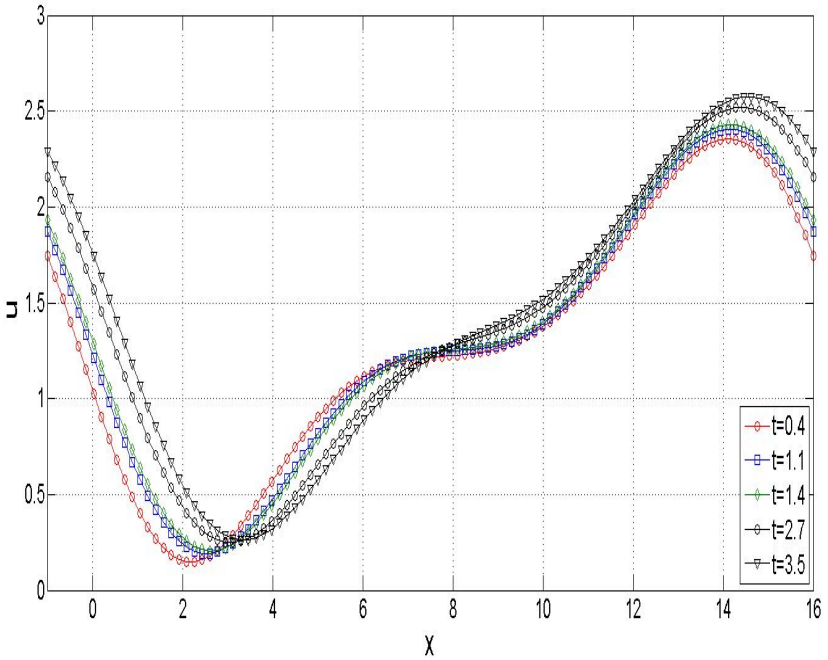

Figure 5.18: The solution at t=0.4 to t= 3.5.

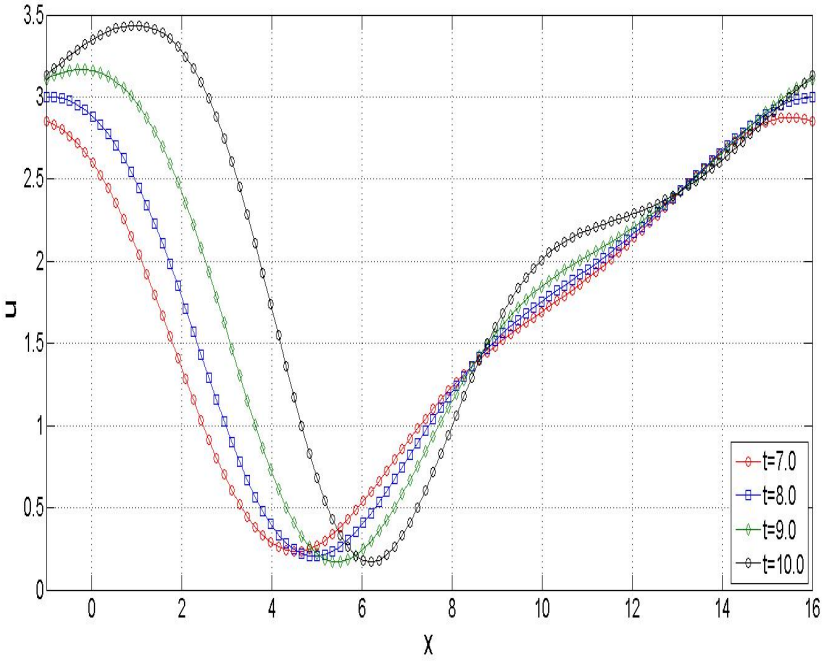

Figure 5.19: The solution at t=7 to t= 10.

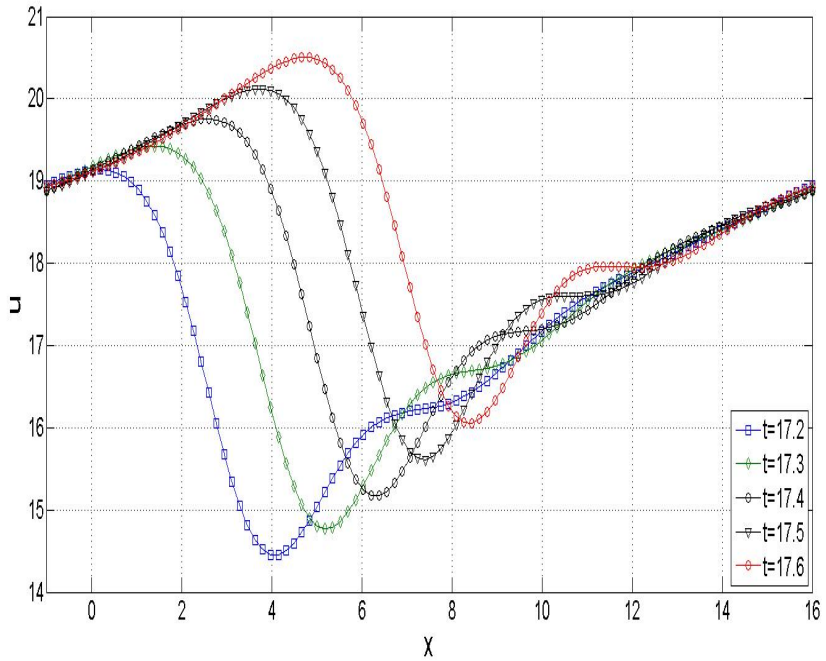

Figure 5.20: The solution at t=17.2 to t= 17.6.

To our satisfaction, the method successfully reproduced a similar shape of the settled spinning regimes as in the earlier study (Strunin, 1999). We also determined the interval within which the bifurcation point lies. In the next chapter we will use the 1D-IRBF approach to study more complicated regimes such as co-directed motion of several fronts, collision of counter-directed fronts etc.

Chapter 6

Numerical simulation of 1D reaction fronts using 1D-IRBFNs

6.1 Introduction

The following equation simulates certain type of active systems with dissipation,

$$\partial_t u = -A(\partial_x u)^2 \partial_x^2 u + B(\partial_x u)^4 + C\partial_x^6 u\,, \tag{6.1}$$

A, B, $C > 0$. In particular, Eq. (6.1) is relevant to fronts of solid-phase combustion waves (Strunin, 1999) and nonlinear instabilities in reaction-diffusion systems with nonlocal effects (Strunin, 2009*b*).The literature on these phenomena is very extensive and we refer to the cited papers for further references. In the context of the combustion fronts, $u(x,t)$ stands for the distance, measured along, say, axis z, passed by the combustion front through a hollow cylinder, as a function of the transversal coordinate x and time t. The equation generates rich variety of dynamics, the most spectacular of which is the spinning front illustrated by Fig. 1.1. It shows spatially periodic solutions of Eq. (6.1) at several consecutive moments of time; two periods are displayed for better visualisation.

If one rolls the plane of the graph into a cylindrical tube by connecting the right and left edges, the solution curves would represent the spinning regime on a hollow cylinder, in agreement with experimental observations. Previously Eq. (6.1) was solved in 1D – with one independent spatial coordinate x – using the spectral Galerkin method (Strunin, 1999) and in 2D using finite difference scheme (Strunin and Mohammed, 2015). In the present research we apply a different numerical method formulated relatively recently, which has proved efficient in a number of modelling problems – the 1D Integrated Radial Basis Function Networks, 1D-IRBFN. As part of our numerical exercises we will reproduce the solution in Fig. 1.1.

Although the method has been tested successfully before in a number of papers, getting the spinning regime with this method would provide yet another test. In Fig. 1.1 see a train of step-like fronts, each featuring a steep section (step itself) followed by a long nearly flat plateau. The latter appears inclined on the

graph, however the slope is small relative to the step. The velocity of the steps, its height and width are controlled by the equation and not initial conditions. This is a consequence of the fact that the step-like structure is a result of the balance between the energy release, represented by the term $-A(\partial_x u)^2\partial_x^2 u$, and the dissipation, represented by the term $C\partial_x^6 u$. The term $B(\partial_x u)^4$ plays the role of the bridge between the two; it is responsible for the energy flow from the energy source towards dissipation.

Note that by re-scaling t, x and u, Eq. (6.1) can always be transformed into canonical form where all the coefficients, A, B, and C, become units.

6.2 The numerical method

The 1D-IRBFN method has been successfully verified through several engineering problems such as turbulent flows (Mohammed, Ngo-Cong, Strunin, Mai-Duy and Tran-Cong, 2014), laminar viscous flows (Tran-Cong and Mai-Duy, 2001; Mai-Duy and Tanner, 2007; Ngo-Cong, Mai-Duy, Karunasena and Tran-Cong, 2012), structural analysis (Ngo-Cong, Mai-Duy, Karunasena and Tran-Cong, 2011), and fluid-structure interaction (Mai-Duy, Ngo-Cong, Karunasena and Tran-Cong, 2012). Radial basis function networks are used to accurately approximate scattered data (Haykin, 1999). A function $f(\mathbf{x})$, to be approximated, can be represented by a RBFN as

$$f(\mathbf{x}) \approx u(\mathbf{x}) = \sum_{i=1}^{N} w_i G_i(\mathbf{x}) \,, \tag{6.2}$$

where $\mathbf{x}$ is the input vector, N the number of RBFs, $\{w_i\}_{i=1}^N$ the set of network weights to be found, and $\{G_i(\mathbf{x})\}_{i=1}^N$ the set of RBFs. According to Micchelli's theorem (Franke, 1982), there is a large class of RBFs, e.g. the multiquadric, inverse multiquadric and Gaussian functions, whose design/interpolation matrices obtained from Eq.(6.2) are always invertible. It is proved that RBFNs are capable of representing any continuous function to a prescribed degree of accuracy.

Furthermore, according to the Cover theorem, the higher the number of RBFs used, the more accurate the approximation will be, indicating the property of "mesh convergence" of RBFNs. Among RBFs, the multiquadric functions ($G_i(\mathbf{x}) = \sqrt{(\mathbf{x}-\mathbf{c}_i)^T(\mathbf{x}-\mathbf{c}_i)+a_i^2}$, $\mathbf{c}_i$ is called the centre and a_i the width) are ranked as the most accurate and possess an exponential convergence with the spatial discretisation refinement (Franke, 1982). A review of the application of RBFNs for solving partial differential equations can be found, e.g., in (Fasshauer, 2007). The usual approach (Kansa, 1990) is to differentiate Eq. (6.2) as often as required to obtain approximate derivatives of $f(\mathbf{x})$. If the error in $f(\mathbf{x})$ is $O(h^s)$, where h is the mesh size and $s > 0$, the error in the n-th derivative of $f(\mathbf{x})$ is $O(h^{s-n})$. Therefore, there is a reduction in convergence rate for derivatives and this reduction is an increasing function of derivative order.

Thus, differentiation will magnify any error that might exist in the approximation of $f(\mathbf{x})$. To avoid this problem, recognising that integration is a smoothing

process, the integral formulation was proposed (Mai-Duy and Tran-Cong, 2001; Mai-Duy and Tran-Cong, 2003), where spectral approximants, e.g. RBFNs, are utilised to represent highest-order derivatives under consideration and then integrated analytically to yield approximate expressions for lower-order derivatives and the function itself, to construct the approximations for the field variables in a problem. Although RBF methods can be easily implemented in a truly meshless manner based on scattered data points, it proves very efficient and effective to discretise a domain using Cartesian grids. Thus, the purpose of using integration (a smoothing operator) to construct the approximants is to avoid the reduction in convergence rate caused by differentiation, and also to improve the numerical stability of a discrete solution.

The integration process naturally gives rise to arbitrary constants that serve as additional expansion coefficients, and therefore facilitate the employment of some extra equations in the process of converting the RBF weights into the function values. This distinguishing feature of the integral formulation provides effective ways to overcome well-known difficulties associated with conventional differential approaches: (i) the implementation of multiple boundary conditions (Mai-Duy and Tanner, 2005); (ii) the description of non-rectangular boundaries on a Cartesian grid (Mai-Duy et al., 2008); (iii) the imposition of high-order continuity of the approximate solution across subdomain interfaces (Mai-Duy and Tran-Cong, 2008); and (iv) the incorporation of nodal derivative values into the approximations via compact IRBFN stencils (Mai-Duy and Tran-Cong, 2011).

The ability of the IRBFN methods to capture very sharp gradients such as the steps in Fig. (3.3), is particularly valuable for the purposes of our research.

Generally the RBFN schemes based on the multiquadric (MQ) functions result in highly accurate results as compared to other RBFNs. In the present study we use the MQ functions $G_i(x) = \sqrt{(x - x_i)^2 + a_i^2}$, where the width a_i is assumed equal to the distance between the i-th centre and its nearest neighbour.

As we already discussed in Chapter 3, we descretise an interval $L_1 < x < L_2$ using a uniform cartesian grid having n number of nodes. Following the basic idea of the integral RBF method (Tran-Cong and Mai-Duy, 2001) we decompose the highest p-th-order derivative ($p = 6$ in our case) of the function u into RBFs,

$$\frac{\partial^p u}{\partial x^p} = \sum_{i=1}^{n} w_i G_i(x) = \sum_{i=1}^{n} w_i I_i^{(p)}(x)\,, \tag{6.3}$$

where $[w_i]_{i=1}^n$ is the set of network weights, and $[G_i(x)]_{i=1}^n = [I_i^{(p)}(x)]_{i=1}^n$ is the set of known RBFs. Lower-order derivatives and the function itself are then obtained through further integration,

$$\frac{\partial^{p-1} u}{\partial x^{p-1}} = \sum_{i=1}^{n} w_i I_i^{(p-1)}(x) + c_1\,, \tag{6.4}$$

$$\frac{\partial^{p-2} u}{\partial x^{p-2}} = \sum_{i=1}^{n} w_i I_i^{(p-2)}(x) + c_1 x + c_2\,, \tag{6.5}$$

$$\cdots\cdots\cdots$$

$$\frac{\partial^3 u}{\partial x^3} = \sum_{i=1}^{n} w_i I_i^{(3)}(x) + c_1 \frac{x^{p-4}}{(p-4)!} + c_2 \frac{x^{p-5}}{(p-5)!} + \cdots + c_{p-4}x + c_{p-3}\,, \tag{6.6}$$

$$\frac{\partial^2 u}{\partial x^2} = \sum_{i=1}^{n} w_i I_i^{(2)}(x) + c_1 \frac{x^{p-3}}{(p-3)!} + c_2 \frac{x^{p-4}}{(p-4)!} + \cdots + c_{p-3}x + c_{p-2}\,, \tag{6.7}$$

$$\frac{\partial u}{\partial x} = \sum_{i=1}^{n} w_i I_i^{(1)}(x) + c_1 \frac{x^{p-2}}{(p-2)!} + c_2 \frac{x^{p-3}}{(p-3)!} + \cdots + c_{p-2}x + c_{p-1}\,, \tag{6.8}$$

$$u = \sum_{i=1}^{n} w_i I_i^{(0)}(x) + c_1 \frac{x^{p-1}}{(p-1)!} + c_2 \frac{x^{p-2}}{(p-2)!} + \cdots + c_{p-1}x + c_p\,, \tag{6.9}$$

where $I_i^{(p-1)}(x) = \int I_i^{(p)}(x)dx$, $I_i^{(p-2)}(x) = \int I_i^{(p-1)}(x)dx$, $I_i^{(0)}(x) = \int I_i^{(1)}(x)dx$ and c_1, c_2, ..., c_p are the constants of integration. The number of constants generated by continuous integration is always equal to highest order present in the differential equation. Further in this research we use the following notations: n is number of collocation points, u approximant of the exact solution, $\widehat{[\,]}$ for a vector/matrix $[\,]$ that is associated with a grid line, $[\,]_{(n,m)}$ to denote selected n rows and m columns of the matrix , $[\,]_{(n)}$ to pick out selected components n of the vector, $[\,]_{(:,m)}$ to denote all m rows of the matrix, and $[\,]_{(n,:)}$to denote all n columns of the matrix.

The evaluation of (6.3)–(6.9) at a set of collocation points $[x_j]_{j=1}^{n}$ leads to

$$\widehat{\frac{\partial^p u}{\partial x^p}} = \widehat{\mathbf{I}_{[p]}^{(p)}}\,\widehat{w}\,, \tag{6.10}$$

$$\widehat{\frac{\partial^{p-1} u}{\partial x^{p-1}}} = \widehat{\mathbf{I}_{[p]}^{(p-1)}}\,\widehat{w}\,, \tag{6.11}$$

$$\cdots\cdots\cdots$$

$$\widehat{\frac{\partial^2 u}{\partial x^2}} = \widehat{\mathbf{I}_{[p]}^{(2)}}\,\widehat{w}\,, \tag{6.12}$$

$$\widehat{\frac{\partial u}{\partial x}} = \widehat{\mathbf{I}_{[p]}^{(1)}}\,\widehat{w}\,, \tag{6.13}$$

$$\widehat{u} = \widehat{\mathbf{I}_{[p]}^{(0)}}\,\widehat{w}\,, \tag{6.14}$$

Here $\widehat{w} = (w_1, w_2, \ldots, w_n, c_1, c_2, \ldots, c_p)^T$. The $\widehat{\mathbf{I}_{[p]}^{(0)}}$ is an n by $(n+6)$ matrix, the subscript [.] and superscript (.) are used to denote the order of the IRBFN scheme and the order of a derivative function, respectively. We find $\widehat{\mathbf{I}_{[p]}^{(p)}}$ where p is $0, 1, 2, ...p$ and can be used to estimate Eq. (6.10)-(6.14).

$$\widehat{\mathbf{I}_{[p]}^{(p)}} = \begin{bmatrix} I_1^{(p)}(x_1) & I_2^{(p)}(x_1) & \dots & I_n^{(p)}(x_1) & 0 & 0 & \dots & 0 & 0 \\ I_1^{(p)}(x_2) & I_2^{(p)}(x_2) & \dots & I_n^{(p)}(x_2) & 0 & 0 & \dots & 0 & 0 \\ \dots & & & & & & & & \\ I_1^{(p)}(x_n) & I_2^{(p)}(x_n) & \dots & I_n^{(p)}(x_n) & 0 & 0 & \dots & 0 & 0 \end{bmatrix},$$

$$\widehat{\mathbf{I}_{[p]}^{(p-1)}} = \begin{bmatrix} I_1^{(p-1)}(x_1) & I_2^{(p-1)}(x_1) & \dots & I_n^{(p-1)}(x_1) & 1 & 0 & \dots & 0 & 0 \\ I_1^{(p-1)}(x_2) & I_2^{(p-1)}(x_2) & \dots & I_n^{(p-1)}(x_2) & 1 & 0 & \dots & 0 & 0 \\ \dots & & & & & & & & \\ I_1^{(p-1)}(x_n) & I_2^{(p-1)}(x_n) & \dots & I_n^{(p-1)}(x_n) & 1 & 0 & \dots & 0 & 0 \end{bmatrix},$$

$$\dots\dots\dots$$

$$\widehat{\mathbf{I}_{[p]}^{(1)}} = \begin{bmatrix} I_1^{(1)}(x_1) & I_2^{(1)}(x_1) & \dots & I_n^{(1)}(x_1) & \frac{x_1^{p-2}}{(p-2)!} & \frac{x_1^{p-3}}{(p-3)!} & \dots & 1 & 0 \\ I_1^{(1)}(x_2) & I_2^{(1)}(x_2) & \dots & I_n^{(1)}(x_2) & \frac{x_2^{p-2}}{(p-2)!} & \frac{x_2^{p-3}}{(p-3)!} & \dots & 1 & 0 \\ \dots & & & & & & & & \\ I_1^{(1)}(x_n) & I_2^{(1)}(x_n) & \dots & I_n^{(1)}(x_n) & \frac{x_n^{p-2}}{(p-2)!} & \frac{x_n^{p-3}}{(p-3)!} & \dots & 1 & 0 \end{bmatrix}.$$

$$\widehat{\mathbf{I}_{[p]}^{(0)}} = \begin{bmatrix} I_1^{(0)}(x_1) & I_2^{(0)}(x_1) & \dots & I_n^{(0)}(x_1) & \frac{x_1^{p-1}}{(p-1)!} & \frac{x_1^{p-2}}{(p-2)!} & \dots & x_1 & 1 \\ I_1^{(0)}(x_2) & I_2^{(0)}(x_2) & \dots & I_n^{(0)}(x_2) & \frac{x_2^{p-1}}{(p-1)!} & \frac{x_2^{p-2}}{(p-2)!} & \dots & x_2 & 1 \\ \dots & & & & & & & & \\ I_1^{(0)}(x_n) & I_2^{(0)}(x_n) & \dots & I_n^{(0)}(x_n) & \frac{x_n^{p-1}}{(p-1)!} & \frac{x_n^{p-2}}{(p-2)!} & \dots & x_n & 1 \end{bmatrix}.$$

6.3 Implementation of 1D-RBFNs for solving PDEs on a single domain

6.3.1 Space and time discretisation

Consider the following time dependent differential equation,

$$\frac{\partial u}{\partial t} = F\left(u, \frac{\partial u}{dx}, \frac{\partial^2 u}{\partial x^2}, \dots ..., \frac{\partial^p u}{\partial x^p}\right), \tag{6.15}$$

in fully discrete schemes, Eq. (6.15) is discretized with respect to both time and space variables. Firstly, the time interval $[0, T]$ is partitioned into N_T subintervals $[t^{(n)}, t^{(n+1)}]$ of length $\Delta t = \frac{T}{N_T}$ with $t^{(0)} = 0$ $t^{(N_{T+1})} = T$. The temporal discretization is then accomplished by a time-stepping scheme, followed by the spatial discretization based on the IRBFN method. Among many possible time-stepping schemes, the standard θ-scheme , $(0 \leq \theta \leq 1$) is used in this work.

It should be noted that the extreme cases $\theta = 0$ and $\theta = 1$ correspond to the well-known forward (fully explicit) and backward (fully implicit) Euler schemes, respectively. Applying the θ-scheme to Eq. (6.15) gives

$$\frac{u^{(n+1)} - u^{(n)}}{\Delta t} = \theta F^{(n+1)} + (1 - \theta) F^{(n)}, \tag{6.16}$$

the scheme with $\theta = 1/2$ is known as the (semi-implicit) Crank-Nicolson method which is second-order accurate,

$$\frac{u^{(n+1)} - u^{(n)}}{\Delta t} = \frac{1}{2}F^{(n+1)} + \frac{1}{2}F^{(n)}\,. \tag{6.17}$$

Making use (6.17), Eq. (6.1) becomes

$$\frac{u^{(n+1)} - u^{(n)}}{\Delta t} = \frac{1}{2}\Big[- A(\partial_x u)^2\partial_x^2 u + B(\partial_x u)^4 + C\partial_x^6 u\Big]^{(n+1)}$$

$$+ \frac{1}{2}\Big[- A(\partial_x u)^2\partial_x^2 u + B(\partial_x u)^4 + C\partial_x^6 u\Big]^{(n)} \tag{6.18}$$

To linearize the nonlinear terms, we use the linearization form given by (Rubin and Graves, 1975).

$$\frac{u^{(n+1)} - u^{(n)}}{\Delta t} = \frac{1}{2}\Big\{-A[(\partial_x u)^2]^{(n)}(\partial_x^2 u)^{(n+1)}+B[(\partial_x u)^3]^{(n)}(\partial_x u)^{(n+1)}+C(\partial_x^6 u)^{(n+1)}\Big\}$$

$$+ \frac{1}{2}\Big\{ - A[(\partial_x u)^2]^{(n)}(\partial_x^2 u)^{(n)} + B[(\partial_x u)^4]^{(n)} + C(\partial_x^6 u)^{(n)}\Big\} \tag{6.19}$$

where $\Delta t = t^{(n+1)} - t^{(n)}$ is the time step; the superscript (n) and $(n+1)$ denotes the time levels, $u^{(n+1)} = u(x, t^{(n+1)})$, $u^{(0)} = u(x, 0)$ initial condition and $u^{(n)}$ represents the approximate value of u at time level n. We consider $\mathbf{H}_0 = \widehat{\mathbf{I}^{(0)}_{[6]}}, \mathbf{H}_1 = \widehat{\mathbf{I}^{(1)}_{[6]}}, \mathbf{H}_2 = \widehat{\mathbf{I}^{(2)}_{[6]}}$ and $\mathbf{H}_6 = \widehat{\mathbf{I}^{(6)}_{[6]}}$. Eq. (6.19) is then discretised in space based on the 1D-IRBFN method as follows,

$$\left[\frac{\mathbf{H}_0}{\Delta t} - \frac{1}{2}\big[- A\mathbf{H}_2(\mathbf{H}_1\widehat{w}^{(n)})^2 + B(\mathbf{H}_1\widehat{w}^{(n)})^3(\mathbf{H}_1) + C(\mathbf{H}_6)\big]\right]\widehat{w}^{(n+1)} =$$

$$\left[\frac{\mathbf{H}_0}{\Delta t} + \frac{1}{2}\big[- A\mathbf{H}_2(\mathbf{H}_1\widehat{w}^{(n)})^2 + B(\mathbf{H}_1\widehat{w}^{(n)})^3(\mathbf{H}_1) + C(\mathbf{H}_6)\big]\right]\widehat{w}^{(n)} \tag{6.20}$$

For simplicity above equation. can be written as,

$$\mathbf{E}_1\widehat{w}^{(n+1)} = RHS_1, \tag{6.21}$$

and boundary conditions are

$$u = \mathbf{H}_0\widehat{w}^{(n+1)} = j_1$$

$$\partial_x u = \mathbf{H}_1\widehat{w}^{(n+1)} = j_2,$$
$$\partial_x^2 u = \mathbf{H}_2\widehat{w}^{(n+1)} = j_3,$$

$$\partial_x^3 u = \mathbf{H}_3 \widehat{w}^{(n+1)} = j_4,$$
$$\partial_x^4 u = \mathbf{H}_4 \widehat{w}^{(n+1)} = j_5,$$

and so on where j_1,j_2,j_3 ,j_4 and j_5 are known values.

All boundary conditions are changed into single matrix $\mathbf{E}_2$ as

$$\mathbf{E}_2 \widehat{w}^{(n+1)} = RHS_2, \tag{6.22}$$

The system of equations Eq. (6.21) and Eq. (6.22) is solved simultaneously at each time step for $\widehat{w}^{(n+1)}$ until the prescribed time T is reached using the corresponding nodal values at the previous time $t = t^{(n)}$, $\widehat{w}^{(n)}$. We can obtain the all values of u by putting back the values of $\widehat{w}$ in Eq. (6.14).

6.4 Results of the numerical experiments

In this section we present numerical solutions of Eq. (6.1) which we repeat here for convenience,

$$\partial_t u = -A(\partial_x u)^2 \partial_x^2 u + B(\partial_x u)^4 + C\partial_x^6 u\,.$$

Various initial conditions will be used, and for the boundary conditions we will either set zero value for first three derivatives of u on each edge of the domain, or stipulate spacial periodicity of u implying equal values of u and its first five derivatives on the edges, respectively.

6.4.1 Single-step regimes under periodic boundary conditions

In these numerical experiments we want to achieve periodic solutions and therefore require continuity of u and its five derivatives on the edges,

$$u|_{x=L_1} = u|_{x=L_2}\,, \quad \partial_x u|_{x=L_1} = \partial_x u|_{x=L_2}\,,$$
$$\partial_x^2 u|_{x=L_1} = \partial_x^2 u|_{x=L_2}\,, \quad \partial_x^3 u|_{x=L_1} = \partial_x^3 u|_{x=L_2}\,.$$
$$\partial_x^4 u|_{x=L_1} = \partial_x^4 u|_{x=L_2}\,. \quad \partial_x^5 u|_{x=L_1} = \partial_x^5 u|_{x=L_2}\,.$$

The solutions obtained here can be associated with the reaction front moving on a cylinder in the same manner as shown in Fig. 3.3. In this context the covered x-length corresponds to the perimeter of the cylinder.

The equation coefficients are chosen to be $A = 4$, $B = 1$ and $C = 2$. We emphasise again that concrete values of the coefficients are not important in terms of the shape of the front and the way it moves, because any of our graphs can be viewed as one corresponding to the canonical form of Eq. (6.1), only in scaled coordinates.

The initial condition is

$$u(x,0) = 6.1\frac{\exp[-0.25(x+1.1)] - \exp[-0.25(x+1.1)]}{\exp[-0.25(x+1.1)]] + \exp[-0.25(x+1.1)]}\,, \tag{6.23}$$

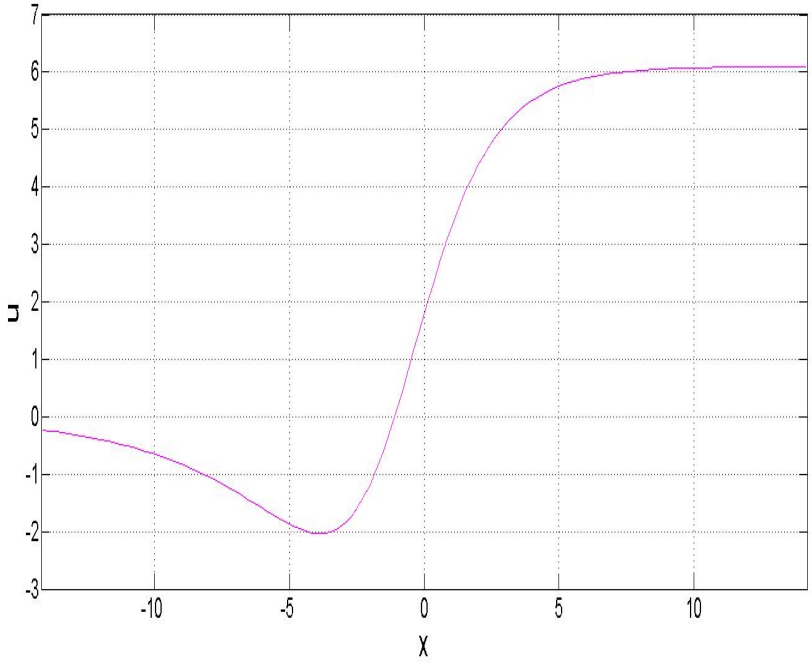

Figure 6.1: The initial condition.

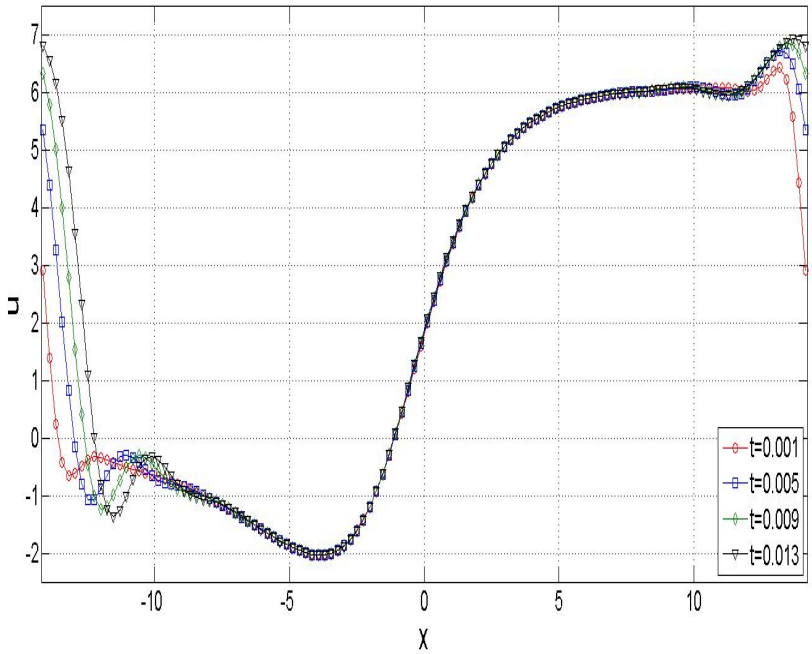

Figure 6.2: The solutions at $t = 0.001$ to $t = 0.013$.

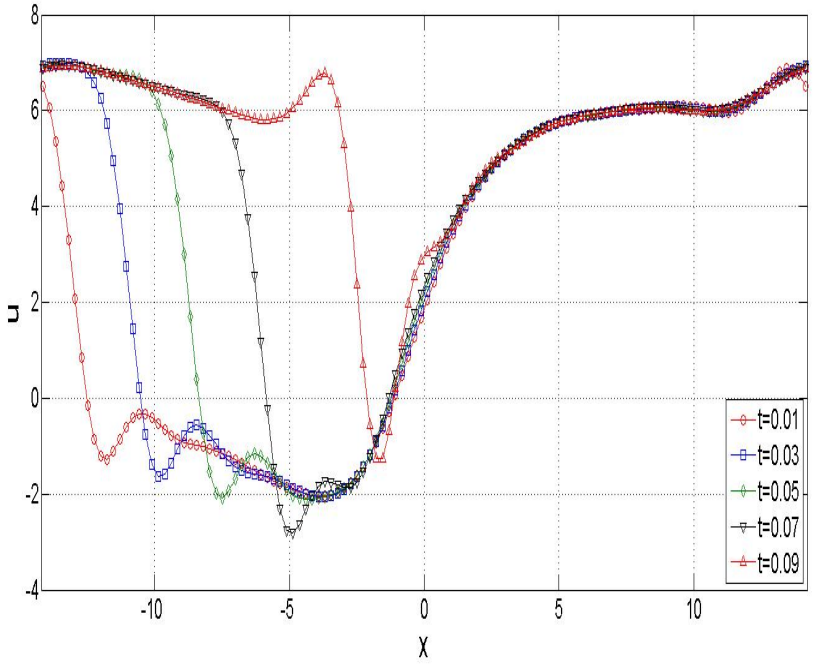

Figure 6.3: The solutions at $t = 0.01$ to $t = 0.09$.

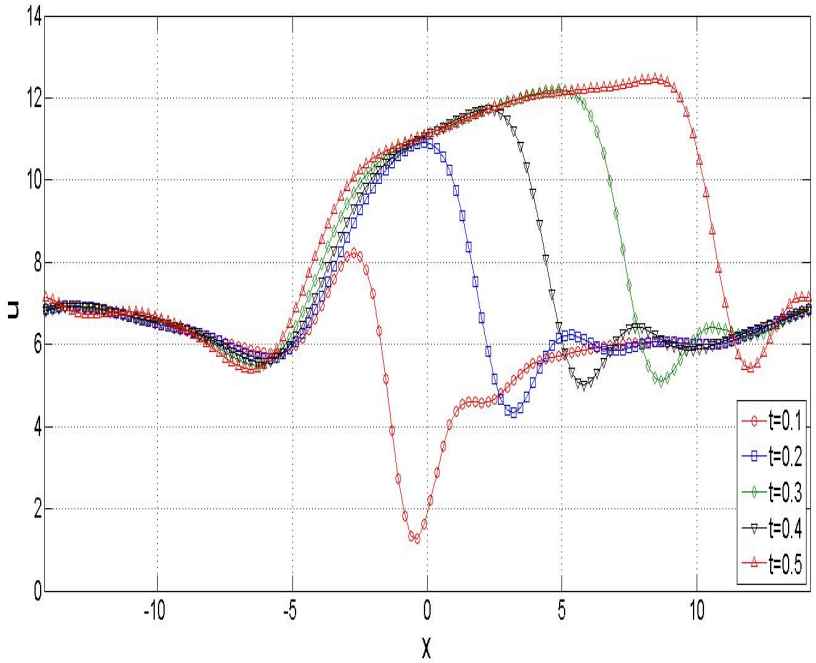

Figure 6.4: The solutions at $t = 0.1$ to $t = 0.5$.

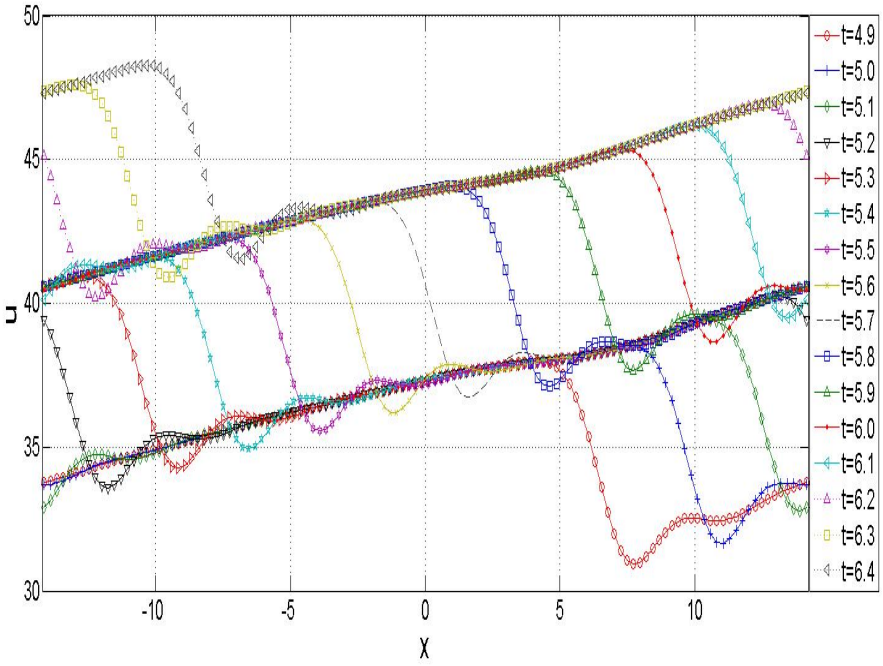

Figure 6.5: The solutions at $t = 4.9$ to $t = 6.4$.

see Fig. 3.3. The number of nodes is taken to be 340, the time step 0.001 and $L_2 - L_1 = 9\pi$. Fig. 6.2 shows the dynamics at early times. Remarkably, in this particular experiment the initial condition does not match the boundary conditions, because at $t = 0$ the value of the function on the left edge and the right edge is not the same.

However, the code quickly makes the ends of the curve meet; this creates the large step which is opposite in orientation to the smooth step represented by the formula (6.23). As a result, an intensive energy release starts within the large step, pushing it to the right. This motion happens to be so powerful that the new step climbs over the "original" step and continues to move on top of it. Eventually the right-moving regime settles, representing the spinning reaction front (Fig. 6.3-6.5).

For the next experiments we used $A = 6$, $B = 2$ and $C = 2$, and the initial condition

$$u(x, 0) = 1.1 \left[\sin(3x) + \frac{1}{2} \sin(4x) + \frac{x}{8} \right]$$

displayed in Fig. 6.6. The number of nodes is 400, the time step 0.001, the period $L_2 - L_1 = 12\pi$.

As is seen, the initial shape looks like a saw. However, the dissipation quickly smoothens out the sharp angles. After a while the settled spinning regime establishes with the direction of motion to the right (Fig.6.7-6.9).

As in the previous example, this direction is dictated by the orientation of the large step which is created from the initial jump between the values of the function on the left and on the right.

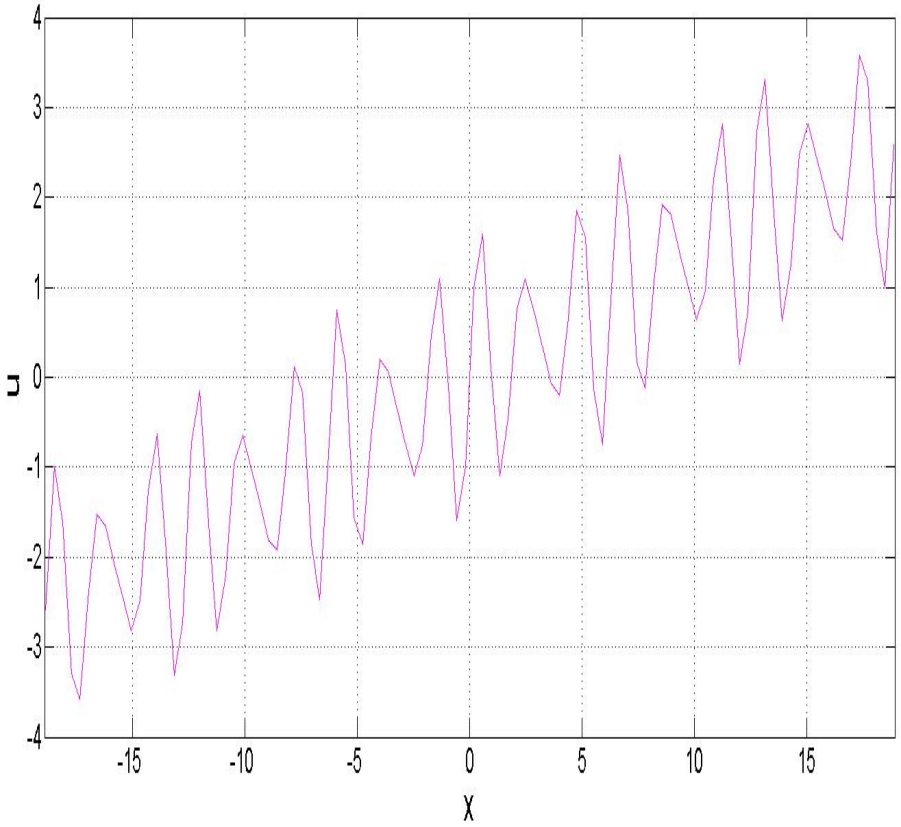

Figure 6.6: The initial condition

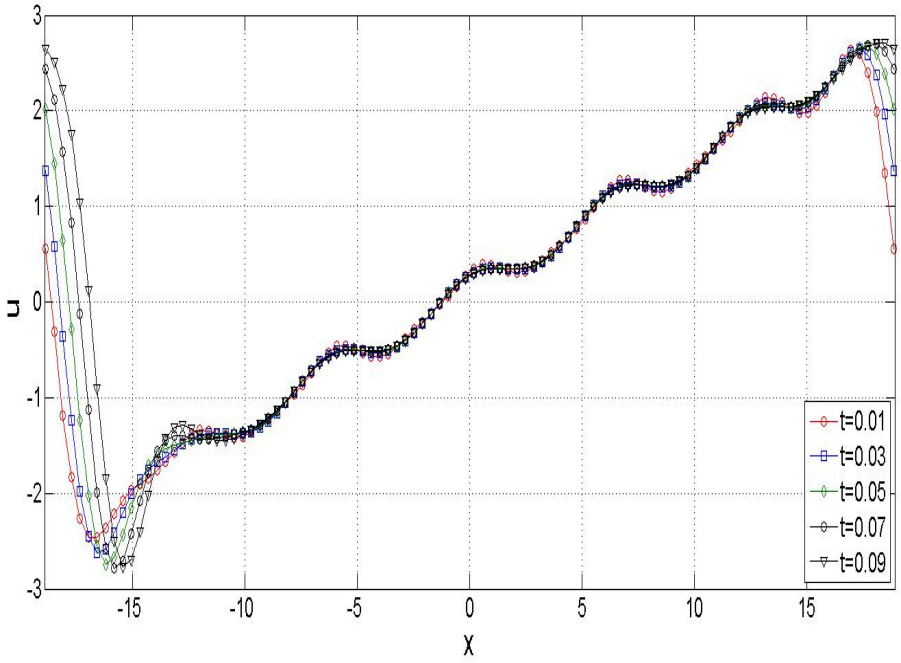

Figure 6.7: Early stage of the evolution (a) $t = 0$ (b) $t = 0.01$ to $t = 0.09$.

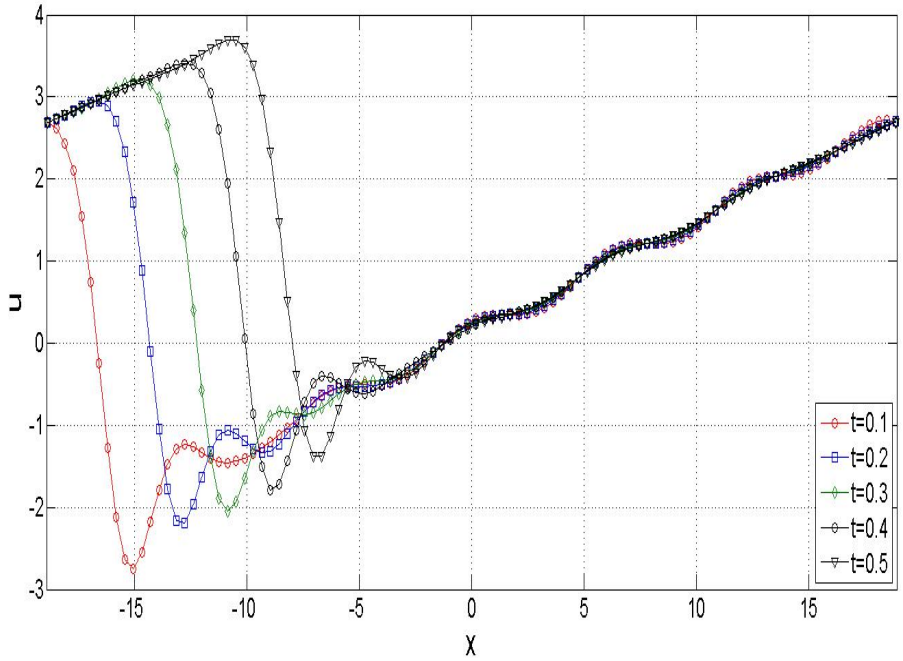

Figure 6.8: Late stage of the evolution $t = 0.1$ to $t = 0.5$.

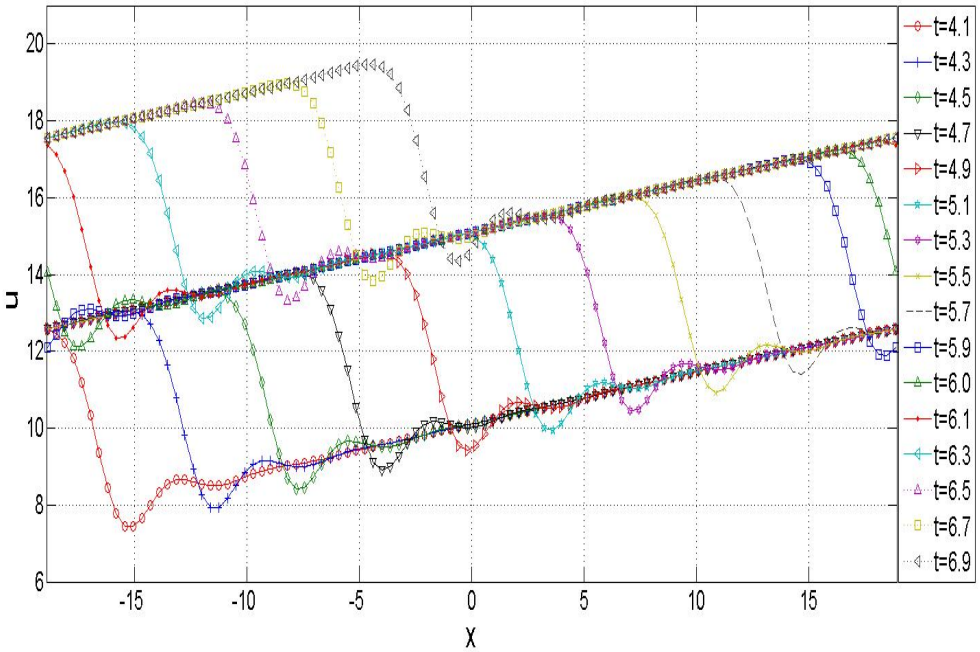

Figure 6.9: Late stage of the evolution $t = 4.1$ to $t = 6.9$.

In the next numerical experiment we used $A = 8$, $B = 3$ and $C = 2$ and the lumpy initial condition (Fig. 6.10)

$$u(x, 0) = 2 \sin x \, .$$

The initial condition is periodic and, hence, is consistent with the boundary conditions. The number of nodes was 340, the time step is 0.001, the period $L_2 - L_1 = 25$. Figs. 6.11-6.14 show the early evolution of the front. See that the initially symmetric shape gradually becomes asymmetic. We explain this effect by the small initial asymmetry introduced by spatial discretisation. With time the asymmetry amplifies, with the four initial crests gradually merging into one. Fig. 6.15 presents the later stages of the evolution during which a single-step regime forms. Thus, the small initial asymmetry eventually progressed into a fully developed step travelling to the left. This case again demonstrates independence of the final regime (do be precise, the hight and width of individual steps, but not their number) of the details of the initial condition.

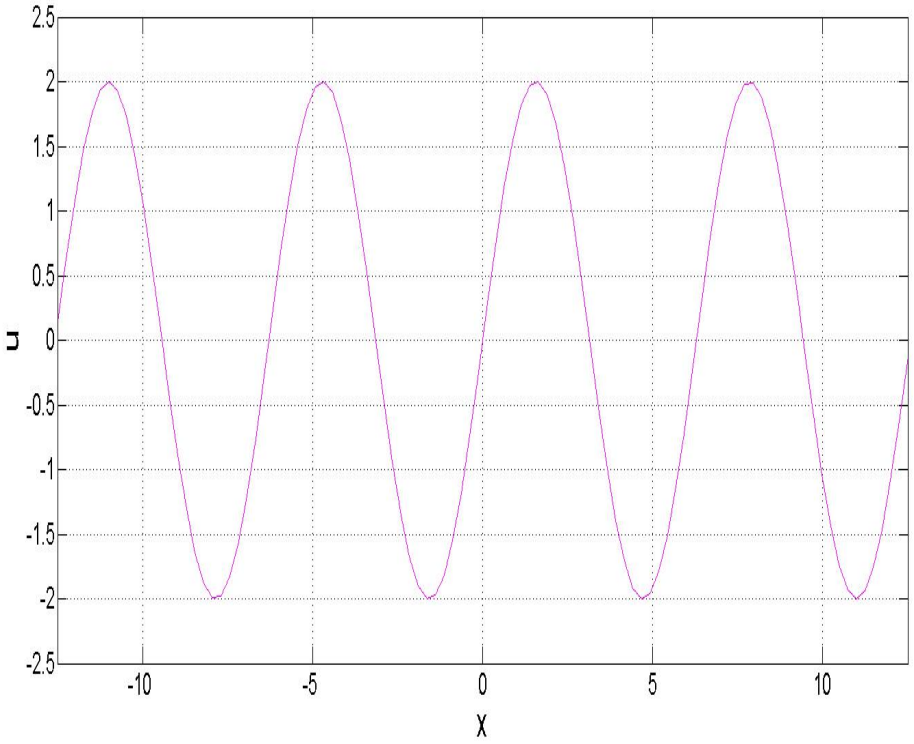

Figure 6.10: The initial condition $u(x, 0) = 2 \sin x$.

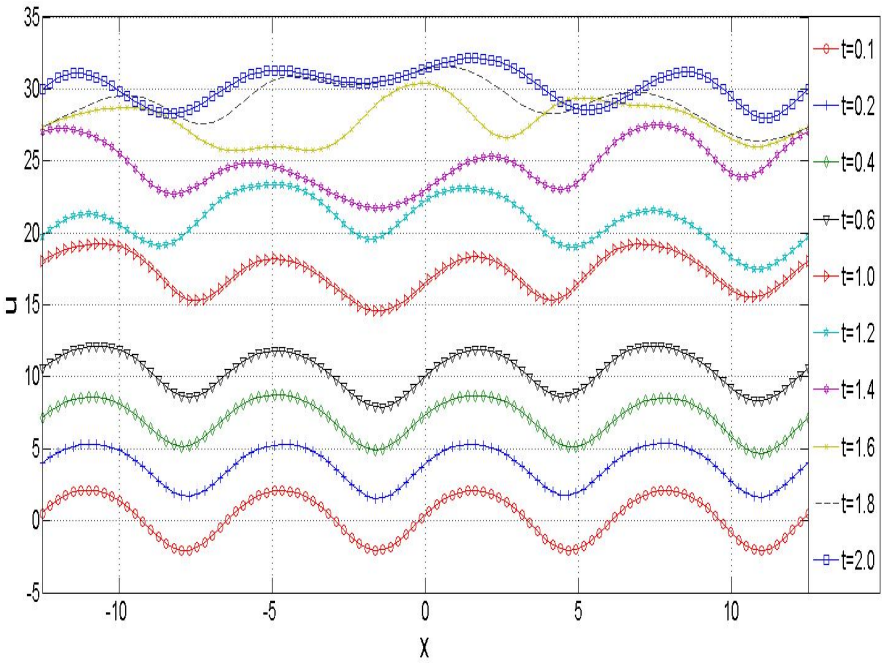

Figure 6.11: The solution evolved from $u(x,0) = 2\sin x$ between $t = 0$ and $t = 2$.

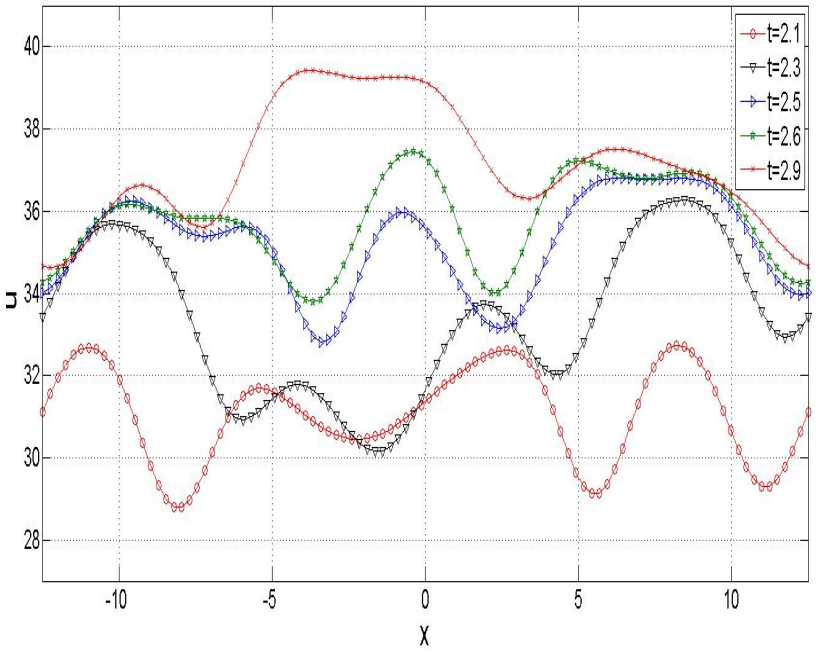

Figure 6.12: The solution evolved from $u(x,0) = 2\sin x$ between $t = 2.1$ and $t = 2.9$.

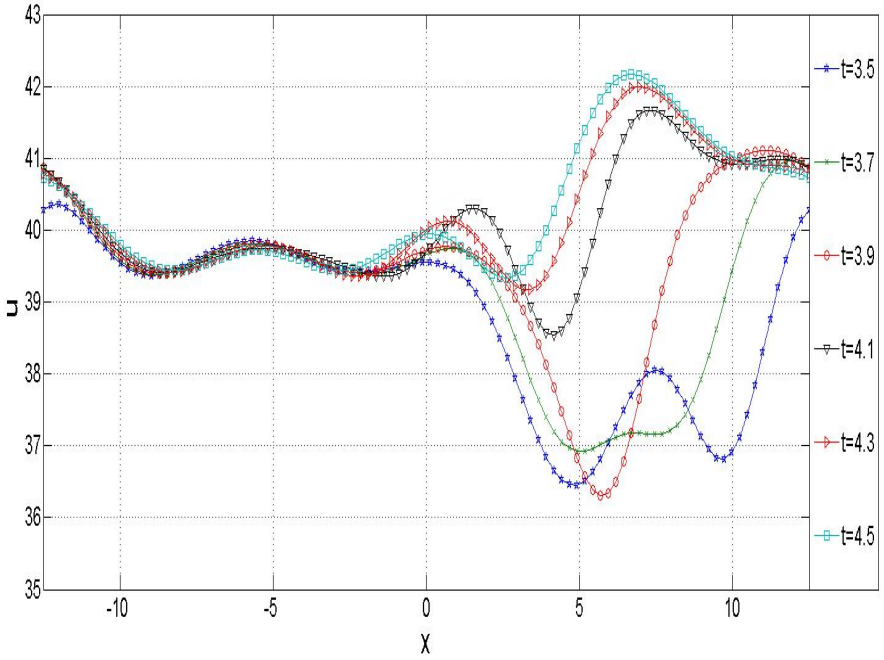

Figure 6.13: The solution evolved from $u(x,0) = 2\sin x$ between $t = 3.5$ and $t = 4.5$.

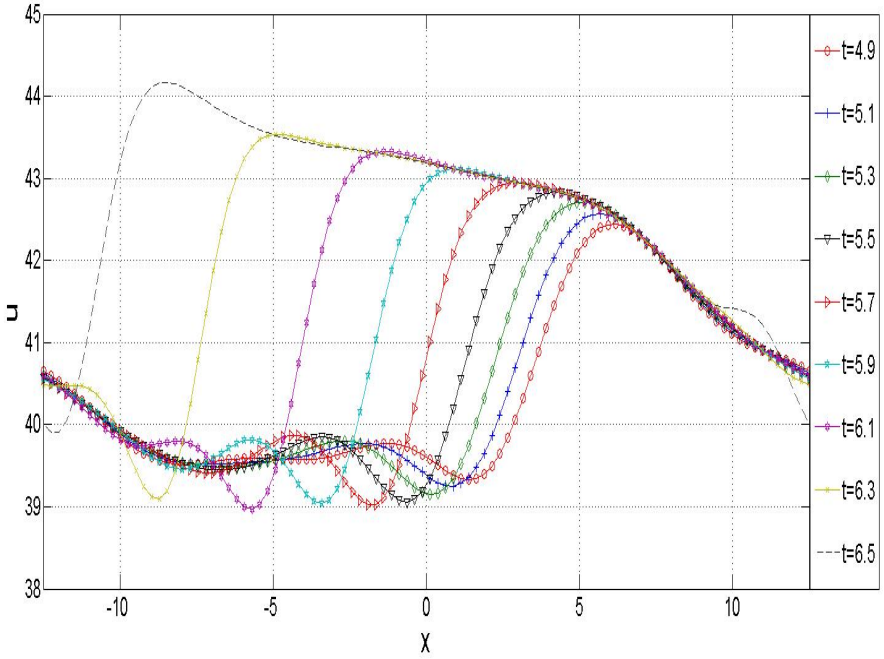

Figure 6.14: The solution between $t = 4.9$ and $t = 6.5$.

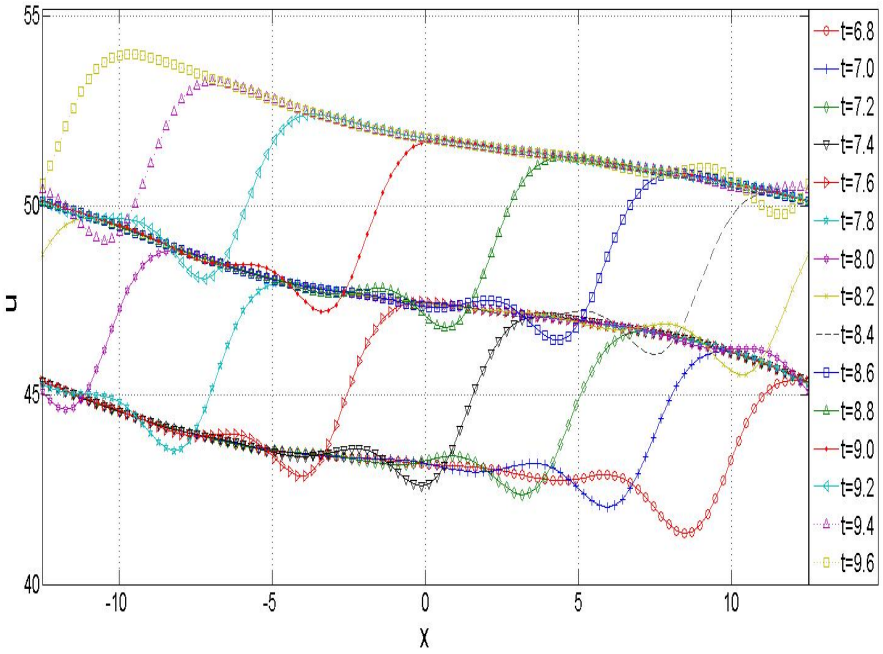

Figure 6.15: The solution between $t = 6.8$ and $t = 9.6$.

6.4.2 Two-step regimes under homogeneous boundary conditions

Here we use homogeneous boundary conditions and the initial condition

$$u(x, 0) = 7.8 \exp[-(x - 5)^2] .$$

The coefficients are $A = 2$, $B = 1$, $C = 1$; the period $L_2 - L_1 = 70$, the number of nodes 1000, the time step is 0.001. The initial peak turns out to be large enough to create two-step formation, see Figs 6.18-6.19.

Notice the close proximity of the steps.

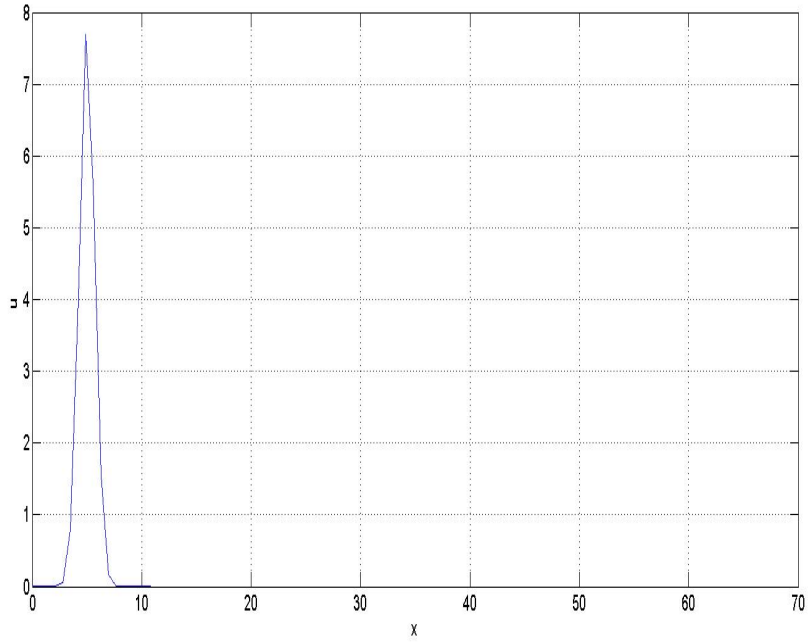

Figure 6.16: The initial condition.

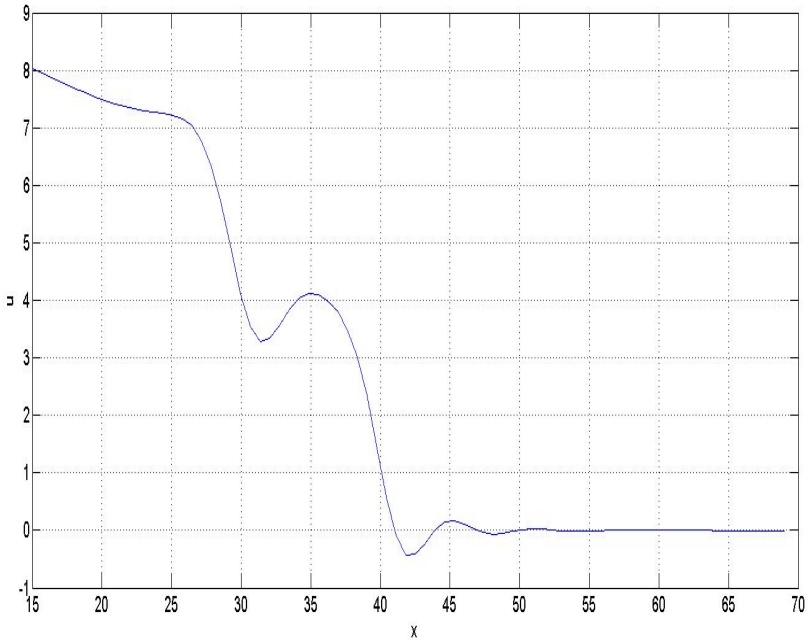

Figure 6.17: The solution evolved at $t = 3.5$.

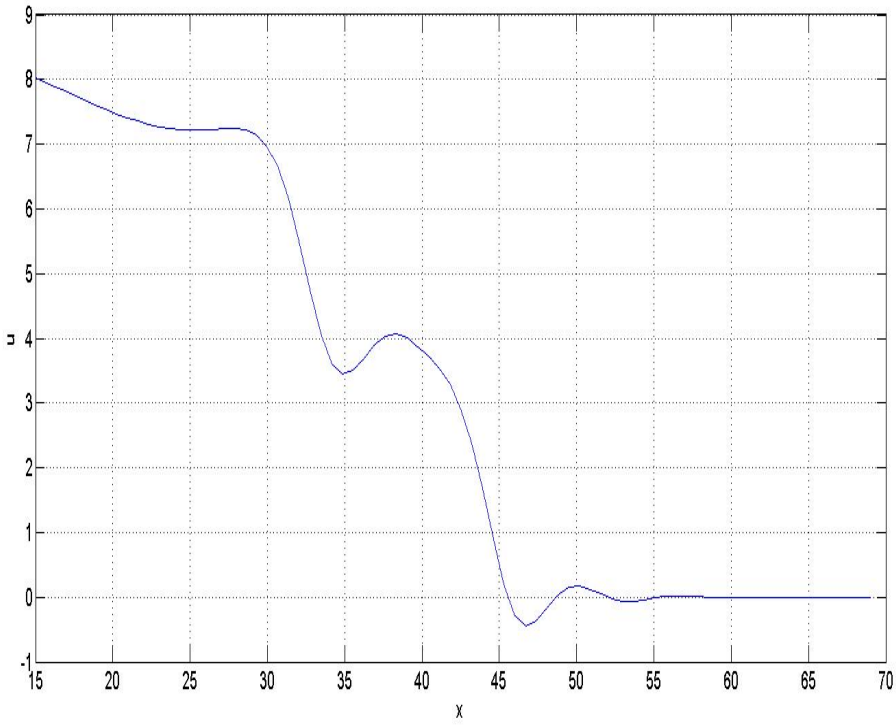

Figure 6.18: The solution at $t = 4.9$.

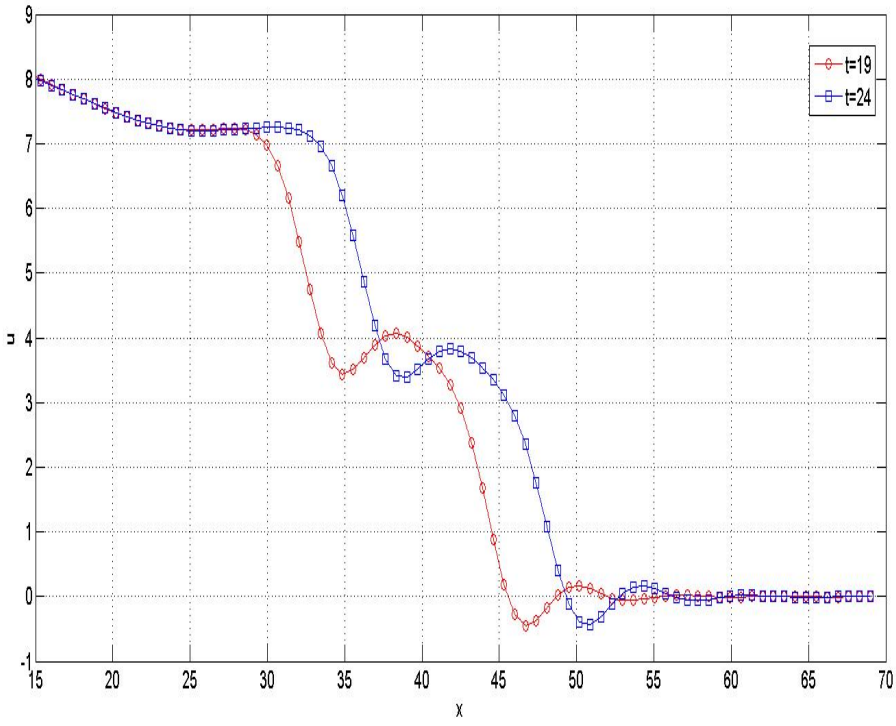

Figure 6.19: The solution between $t = 19$ and $t = 24$.

6.4.3 Two-step regimes under periodic boundary conditions

Here we use periodic boundary conditions and the initial condition

$$u(x,0) = 1.5\sin(x)\,.$$

Our selection of the coefficients was $A = 3$, $B = 1$, $C = 1$; the period $L_2 - L_1 = 70$, the number of nodes 1000, the time step is 0.001.

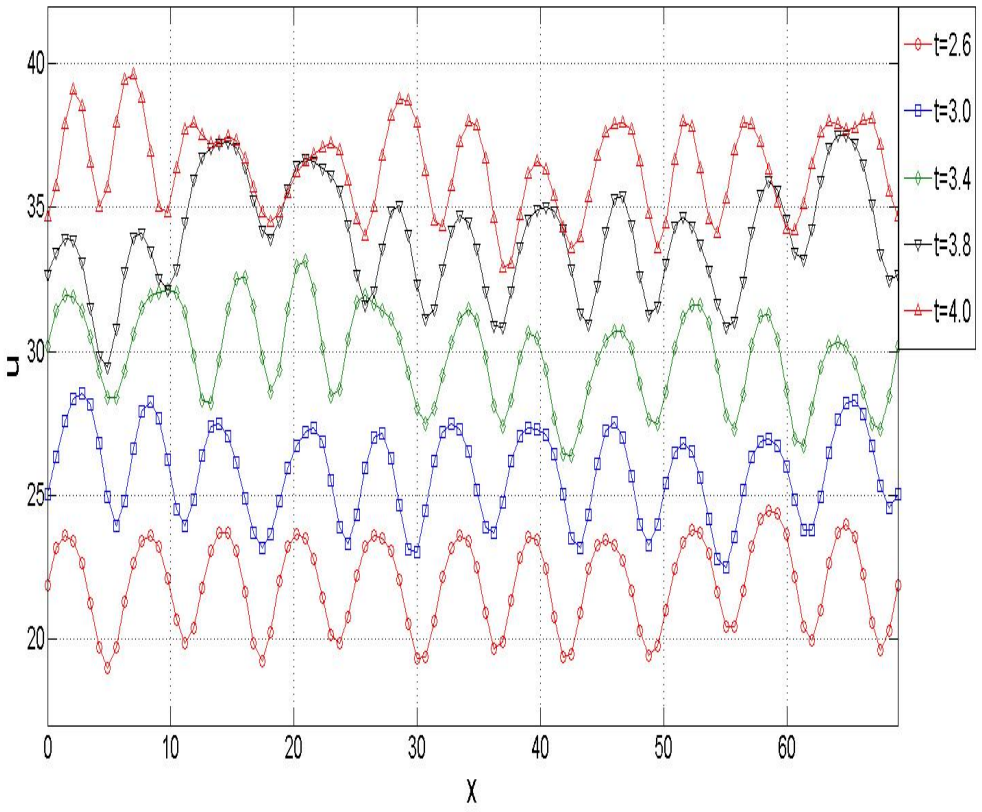

Figure 6.20: The solution from $t = 2.6$ to $t = 4$.

As in the previous section, the initial condition was symmetric which gradually transformed into an asymmetric shape. The final settled shape had two steps shown in Fig. 6.25.

We were particularly interested in the question whether or not the two steps (defined as the local maxima of the profile f) eventually locate equidistantly from each other over the length of the spacial period, or, in terms of the motion on the cylinder diametrally opposite to each other. The answer turned out to be that in the settled regime, the answer is no. The distance between the steps measured in the direction from the left to right is not equal to the distance measured from the opposite direction.

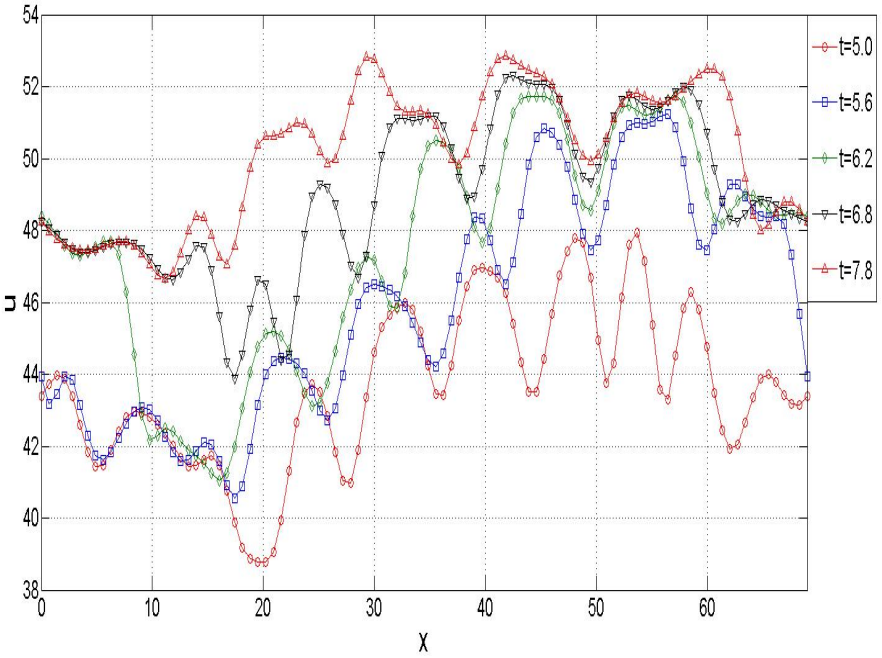

Figure 6.21: The solution from $t = 5$ to $t = 7.8$.

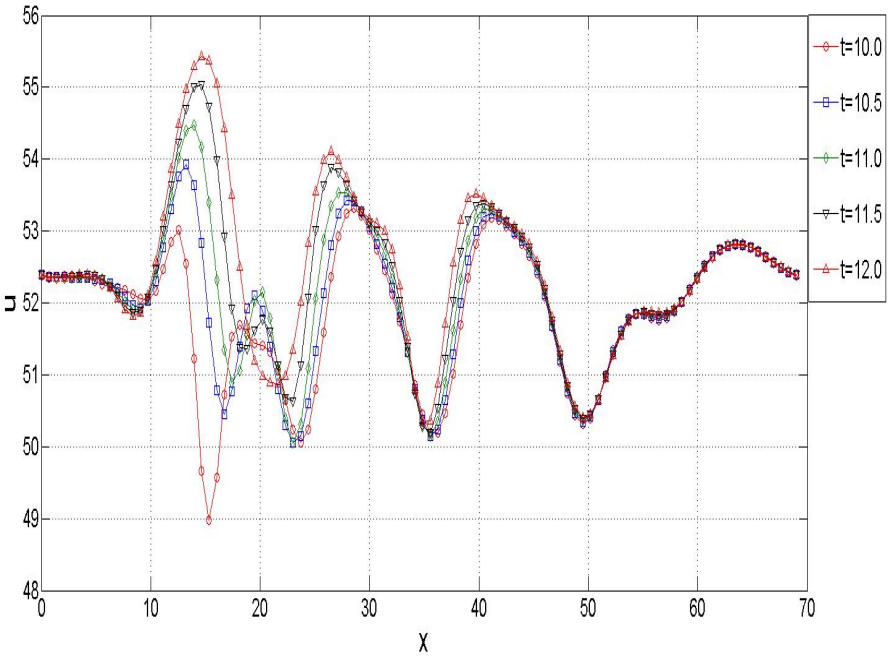

Figure 6.22: The solution from $t = 10$ to $t = 12$.

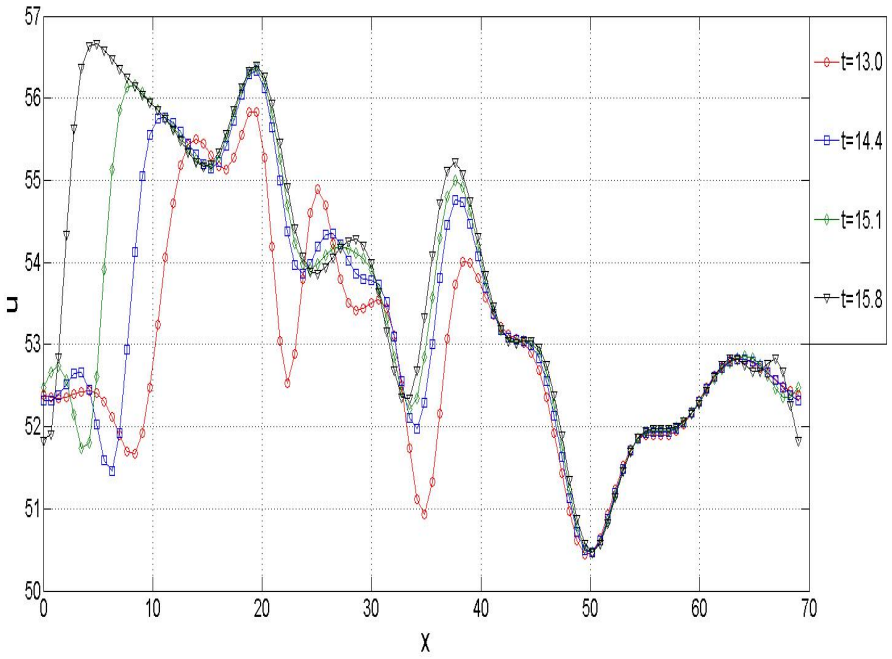

Figure 6.23: The solution from $t = 13$ to $t = 15.8$.

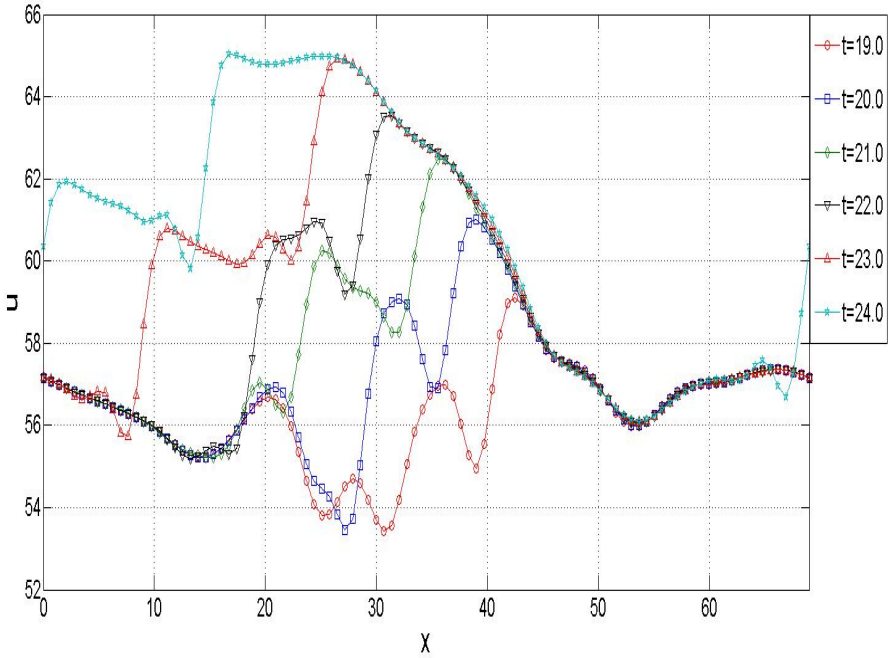

Figure 6.24: The solution from $t = 19$ to $t = 24$ (above) and the settled regime between $t = 410$ and $t = 415$ (below).

One can view this regime as two steps moving as a joint formation. To describe the motion quantitatively, we measured the distance between the steps against time. Fig. 6.26-6.28 show how the distance is measured. At $t = 16$ the distance D reaches its largest value, which is allmost half the period, or perimeter if translated into a cylindrical geometry. The distance decreases sharply between $t = 16$ to $t = 19.5$. At about $t = 20$ the two steps couple with each other (Fig. 6.28) and, from the moment on, move together in close proximity. Fig. 6.29 shows that after $t = 100$, the distance D becomes practically constant.

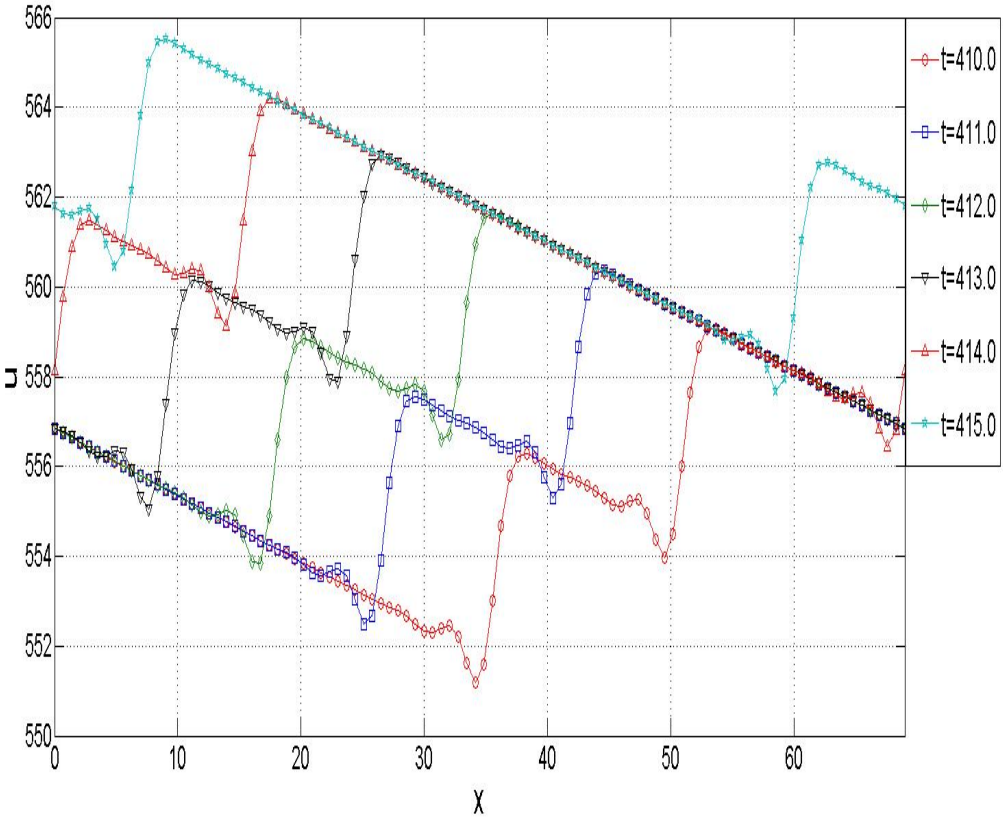

Figure 6.25: The settled regime between $t = 410$ and $t = 415$.

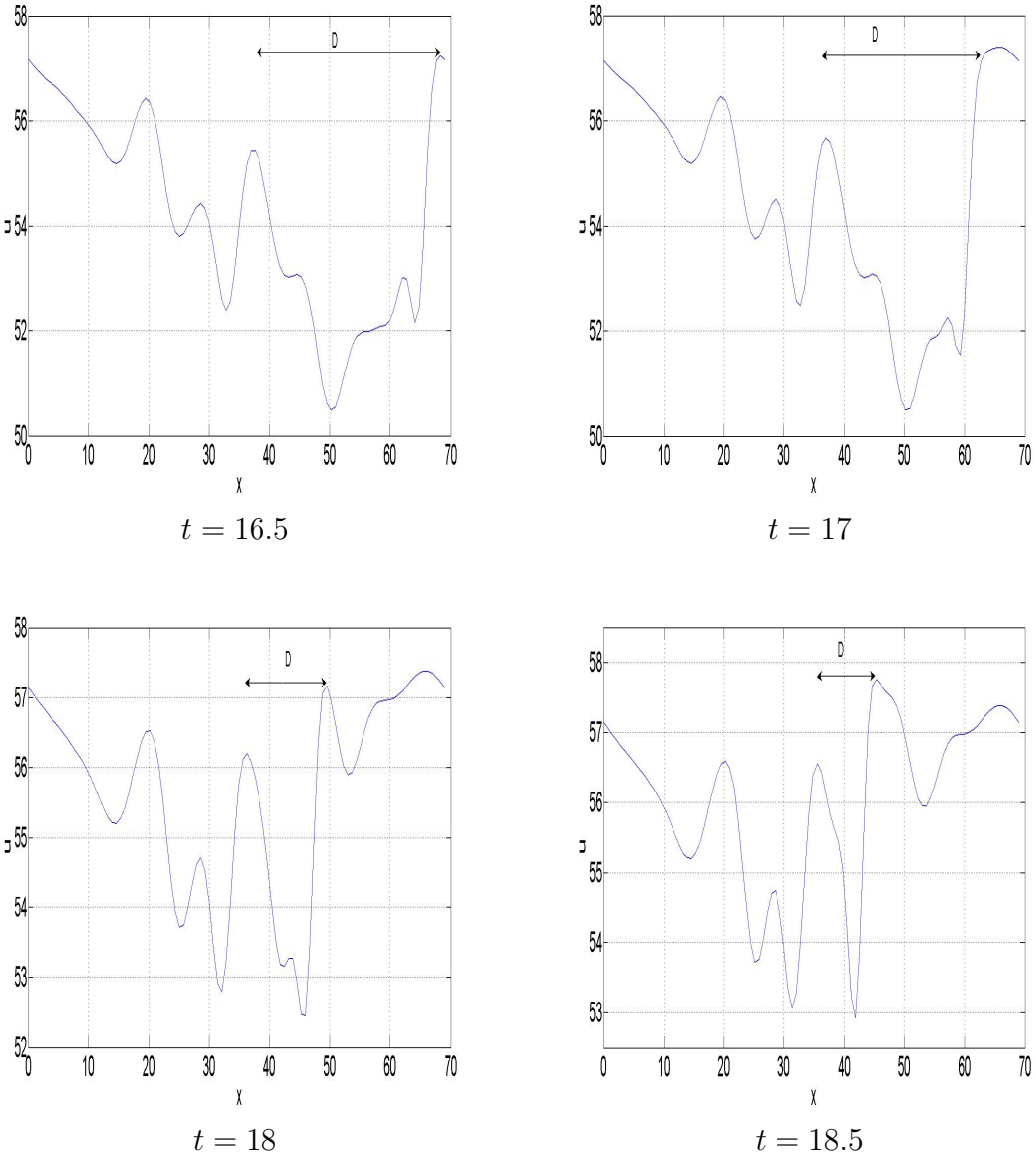

$t = 16.5$ $t = 17$

$t = 18$ $t = 18.5$

Figure 6.26: Measuring the distance between the steps.

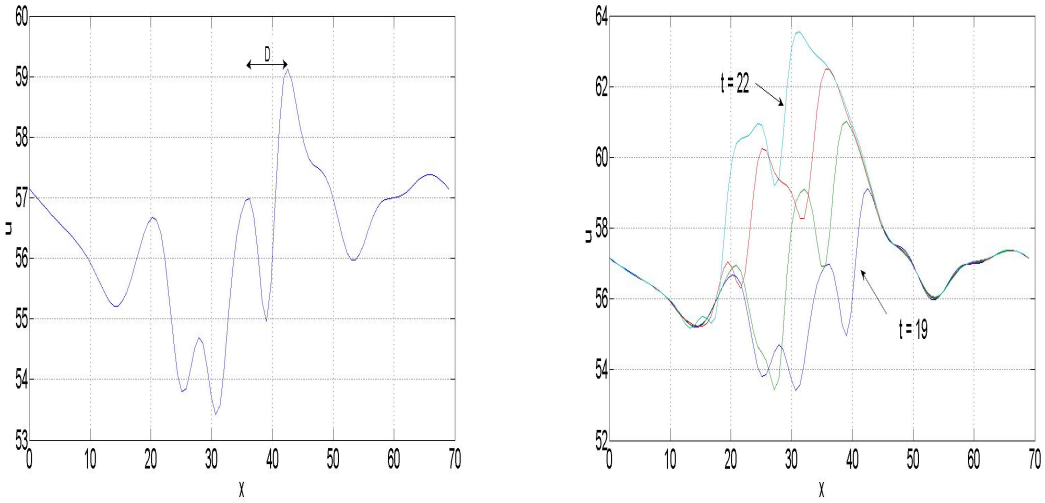

t= 19 t=19–22

Figure 6.27: Measuring the distance between the steps.

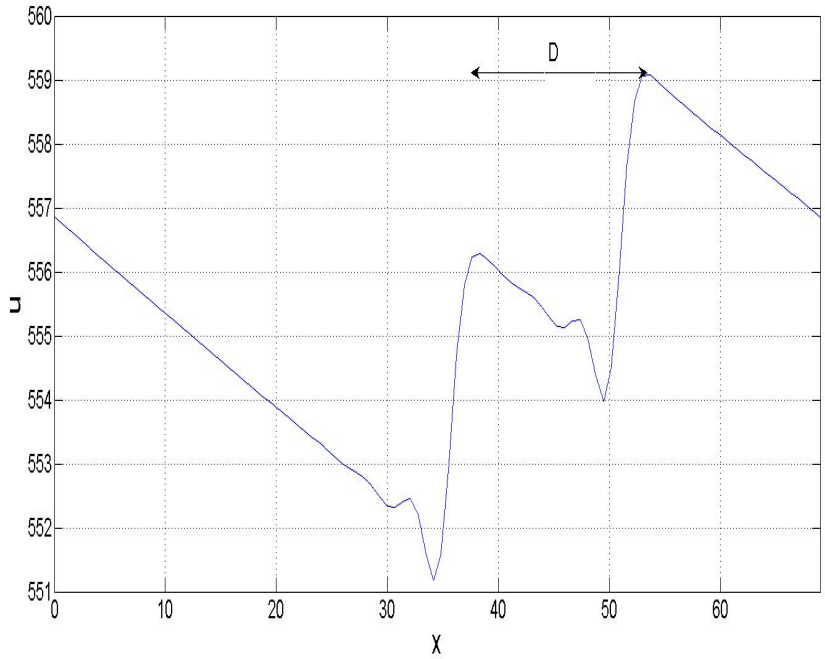

Figure 6.28: A snapshot of the fully settled regime, $t = 410$.

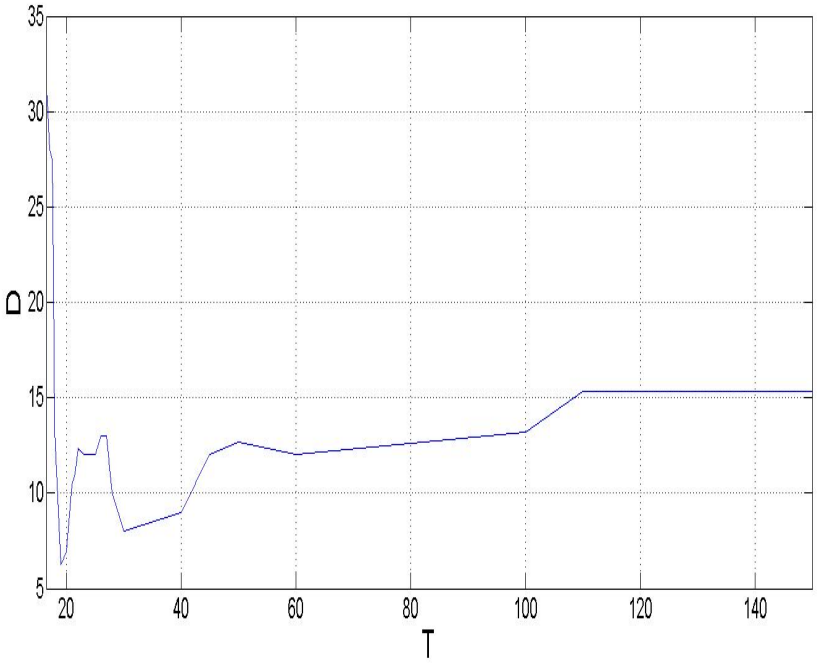

Figure 6.29: Evolution of the distance between the steps.

6.4.4 Three-step regimes under homogeneous boundary conditions

In our last experiment we again used the homogeneous boundary conditions and the initial condition in the form of a peak,

$$u(x,0) = 8.5 \exp\left[-(x-5)^2\right] .$$

The parameters were $A = 2, B = 1, C = 1$, the number of nodes 700, the time step 0.001, L = 120.It is interesting to compare the results with Section 3.3 where the similar initial condition was used, but the peak was a bit shorter, Fig. 18. However, the increase in height from 7.8 to 8.5 (by 9 %) was sufficient to create the third step, see Figs. 6.30-6.32. As is seen, the two leading steps are settled, and the distinct horizontal plateaus are formed stretching to the right of the leading (1st) step and to the left from the following (2nd) step. The 3rd step is not quite settled yet as it still remembers the initial condition via the non-horizontal plateau to the left. A remarkable feature of this dynamic is close proximity of the two leading steps. The highest point of the 1st step sits right on the crest of the small sub-peak in front of the 2nd step. It would be interesting to investigate whether such a tight formation is the closest possible; we leave this question for further study.

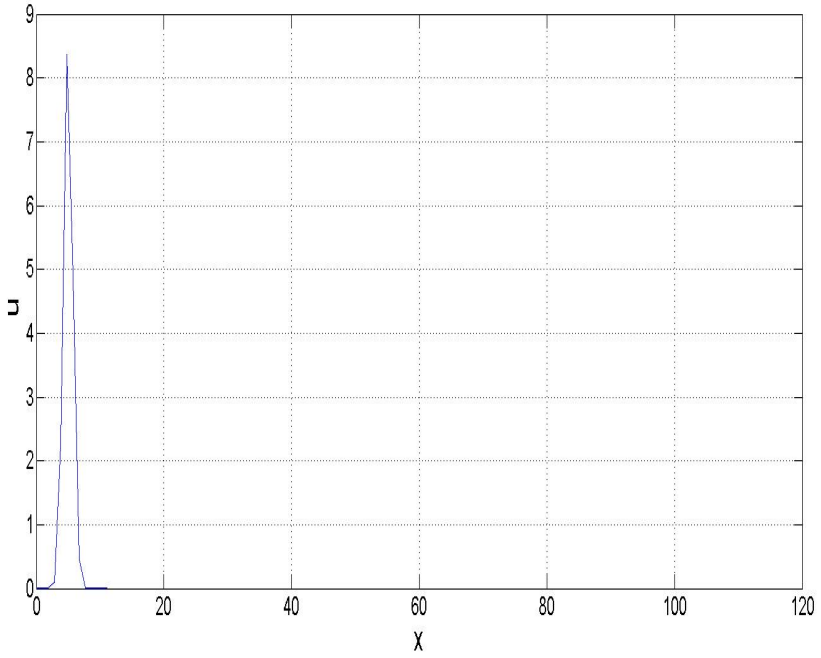

Figure 6.30: The initial condition.

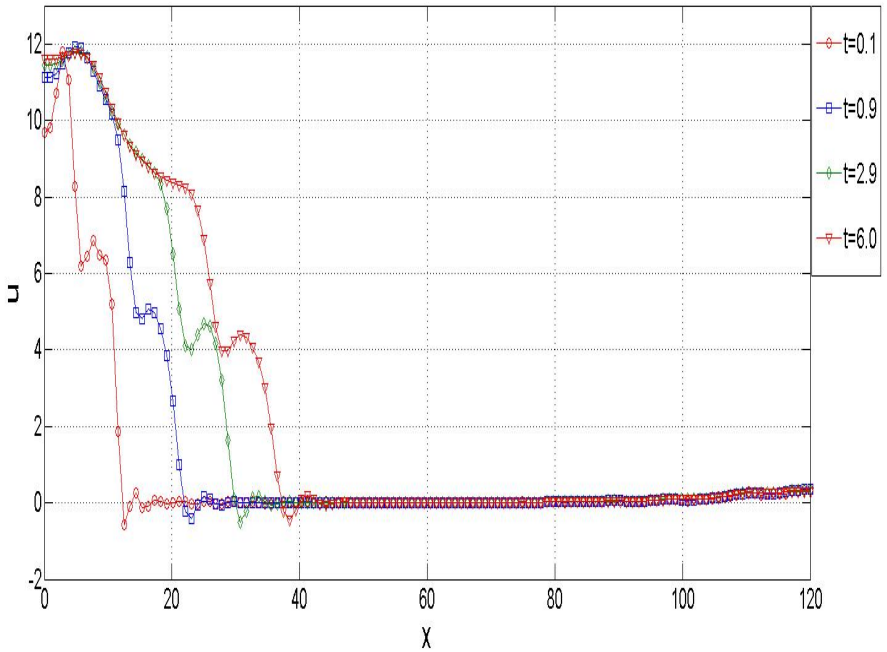

Figure 6.31: Early stage of the evolution.

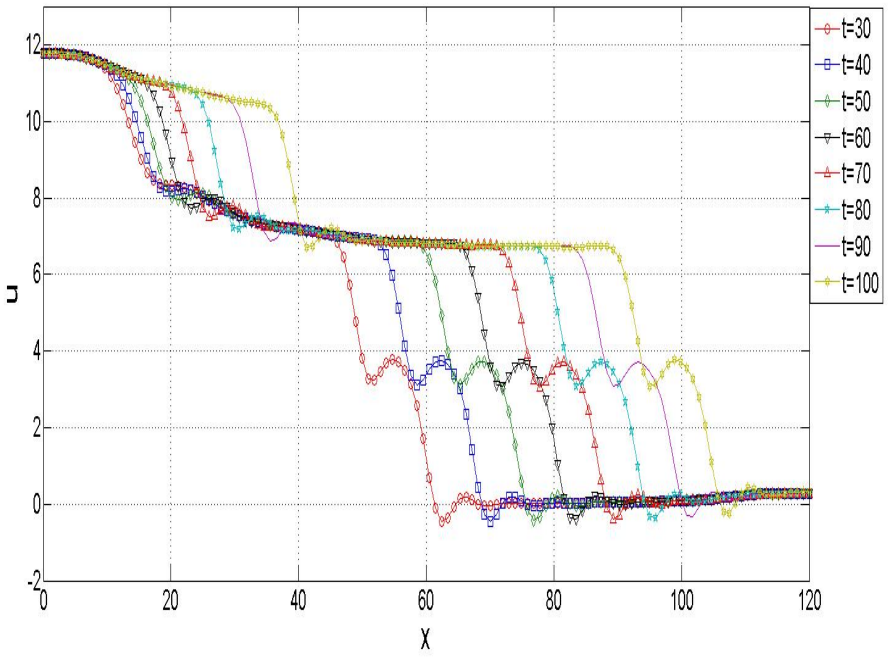

Figure 6.32: The three-step regime.

6.5 Conclusions

We applied the 1D-IRBF numerical method to solve Eq. (6.1) governing the behaviour of the spinning combustion fronts and oscillations in certain class of reaction-diffusion systems with nonlocal interactions. The method successfully reproduced the settled spinning regimes of the earlier modelling (Strunin, 1999). We presented and analysed the complex process of formation of the spinning fronts, in which the energy pumping within the most sharp segments of the front control the dynamics : it determines the direction of motion and, jointly with the dissipation, erases memory about the details of the initial conditions. Single-step, two-step and three-step regimes are investigated under homogeneous and/or periodic boundary conditions.

Chapter 7

2D numerical solutions for the NEP equation

7.1 Introduction

The spinning waves occur in solid flames and detonation fronts when the plane uniformly propagating reaction front loses stability. As a result, the front breaks down into localized zones of intensive reaction. In this chapter we study a 2D time dependent phenomenological model aimed at modeling such phenomena.This work contains results demonstrating the capacity of the model to reproduce basic experimental features of the front inside a solid cylinder in case of solid flame and a gas tube in case of detonation wave: metastability of the uniform state and formation of self-sustained regime with predominantly lateral propagation of the front curvature.

As we discussed in the previous chapters, spinning combustion is an interesting nonlinear phenomenon initially discovered in detonation (Zel'dovich and Kompaneets, 1960) and later on in solid-phase combustion (Merzhanov et al., 1973) and others. By comparison, small amplitude waves in fluids are linear and the nonlinear effects become significant when the amplitude is relatively large. Any combustion wave is already nonlinear by its nature. However, small perturbations to the traveling wave solution of the original reaction-diffusion equations satisfy linearized equations. If instability develops, the nonlinear effects come into play. The spinning waves in solid-phase combustion were extensively studied since the early 1970s experimentally (Dvoryankin et al., 1982) and theoretically (Ivleva et al., 1980; Aldushin et al., 1981) and still attract considerable attention.

In deriving a 1D model (6.1) the goal was to reproduce three main qualitative features of the actual process, which are : (1), The decay of a front with relatively smooth curvatures; this would correspond to the decay of a front with insufficient initial concentration of energy. (2), The self-sustained non- trivial dynamics of a front with relatively sharp curvatures so that a typical amplitude of the settled curvatures is governed by the equation, not the initial condition. (3), the self-propagating front moving predominantly in lateral direction at any particular

moment. These properties are ensured by the dynamical structure of (6.1): the purely dissipative linear part, nonlinear nature of the source and overall dynamical balance involving all three terms in the right-hand side. Equ. (6.1) was shown to give spinning wave solutions corresponding to the front moving around a hollow cylinder with thin walls.

Here we solve the NEP equation in 2D using the 1D-IRBFN method. Previously, a two-dimensional version of the equation was formulated and solved under zero boundary conditions (Strunin and Mohammed, 2015; Strunin and Suslov, 2005) using a less accurate finite difference method.

7.2 Two-dimensional model

Here we generalize equation (6.1) to incorporate the second transversal dimension, y, in order to model the front propagation through a 3D continuum. With the distance u measured along the third axis, z, we aim to obtain a three-dimensional pattern. In 2D equation (6.1) has the form

$$\begin{aligned}\partial_t u = &-A(\partial_x^2 u + \partial_y^2 u)\Big[(\partial_x u)^2 + (\partial_y u)^2\Big] \\ &+B\Big[(\partial_x u)^4 + 2(\partial_x u)^2(\partial_y u)^2 + (\partial_y u)^4\Big] \\ &+C\Big[\partial_x^6 u + 3\partial_x^4\partial_y^2 u + 3\partial_x^2\partial_y^4 u + \partial_y^6 u\Big]. \end{aligned} \tag{7.1}$$

In this set of numerical experiments we use circular domain and the homogeneous boundary conditions on the circular boundary expressed by,

$$\partial_x u = 0\,, \quad \partial_x^2 u = 0\,, \quad \partial_x^3 u = 0\,,$$

$$\partial_y u = 0\,, \quad \partial_y^2 u = 0\,, \quad \partial_y^3 u = 0,$$

at each point on the boundary.

The simulated system is assumed adiabatic so that energy is nither coming into the system nor going out of the system. The zero first derivatives/zero slope of the front towards the boundary represents the adiabatic condition.

7.3 Results of the numerical experiments

As stated above, we assume the homogeneous boundary conditions on the circumference of the circular domain. The equation coefficients are chosen arbitrarily, $A = 80$, $B = 4$, $C = 1$. We recall that, regardless of concrete values of the coefficients, the governing equation can always be transformed to the canonical form with $A = B = C = 1$ by re-scaling x, t and u. The number of grid nodes are 60×60.

The initial condition is

$$u = \cos(x/2 \times y/5) \ , \tag{7.2}$$

To solve the equation, as discussed in the previous chapter the temporal discretization is accomplished by a time-stepping scheme, followed by the spatial discretization based on the IRBFN method. Among many possible time-stepping schemes, the standard θ-scheme , ($0 \leq \theta \leq 1$) is used in this work. We used all the derivatives in x and y from Eq. (3.20)-(3.29).

Note that the extreme cases $\theta = 0$ and $\theta = 1$ correspond to the well-known forward (fully explicit) and backward (fully implicit) Euler schemes, respectively. The scheme with $\theta = 1/2$ is known as the (semi-implicit) Crank-Nicolson method which is second-order accurate.

Equation (7.1) and boundary conditions are discretised in space on a uniform equilateral grid using the1D-IRBFN method, within a circle of radius L. Since Equation (7.1) is nonlinear, to avoid expensive iterative solution of a system of nonlinear difference equations at each time step, Crank-Nicolson method was chosen for time discretization. To avoid numerical instability in time integration a sufficiently small time step was used. It was found that for the spatial discretization steps of $x = y = 0.03$ (for which the numerical solution was obtained) the time step $t = 0.001$ was sufficiently small to ensure numerical stability for all regimes.The computations were performed up to time $t = 50$. The average position of a front always increases with time as shown in Figs. 7.2–7.12 which confirms the relevance of the proposed model to realistic situation of a propagating combustion front. The dynamics of u (represented by z-axis) shows that the front propagates with a non-constant speed.

We started with the initial condition displayed in Fig. 7.1 . The initial amplitude, that is the vertical distance between the highest and lowest points of the u surface, was 1.2×10^{-3} and there were four humps. Early stages of the evolution were quite violent and obviously unsettled so we do not show those stages. Around t=36 the dynamics calmed down as shown by Fig. 7.2. The amplitude was of the order 1. Some of our graphs are presented using small vertical scale, in order to demonstrate that the front never decayed completely. Apparently this would not be clear had we used the same scale.

At t=37 (Fig 7.3) after some interaction between the remnants of the initial humps they merge into a single centrally located hump. It shifts towards the boundary (Fig 7.4) with the amplitude about 3 and moves anticlockwise is a spinning fashion. However, this motion did not continue and the hump moved towards the centre (Figs. 7.5-7.6). Remarkably, by t=41 its amplitude decreased to roughly one tength of the initial amplitude. Keep decreasing in amplitude the hump passed through the center to the other side of the domain (Fig. 7.7) but later by t=46 it grew back (Figs. 7.8-7.11)and reached the amplitude 4 (Fig. 7.12) from what we observe, the dynamics did not reach a settled stage yet, but we obtained a spinning motion of the front at certain interval of time and amplitude a fully settled spinning regime to eventually occur at this on slightly different diameter.

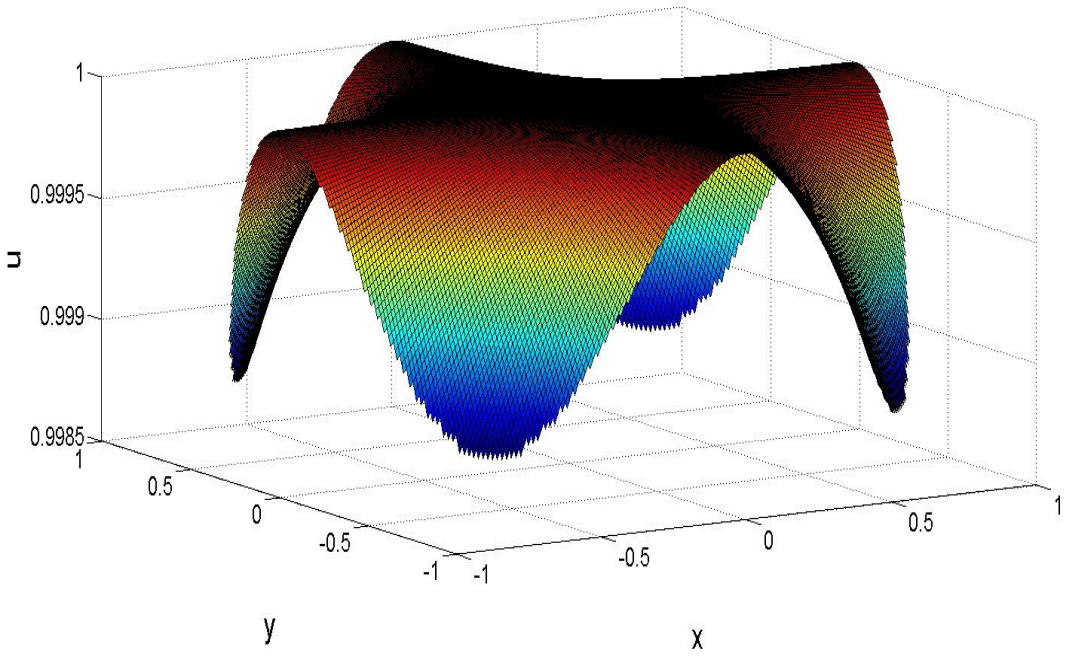

Figure 7.1: The initial condition.

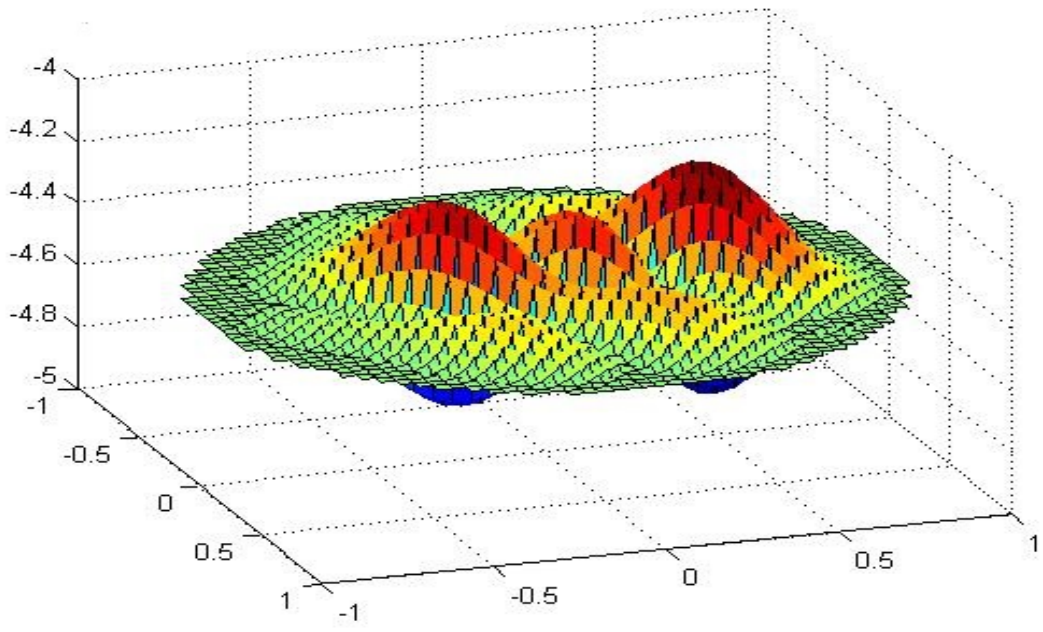

Figure 7.2: The front at $t = 36.28$.

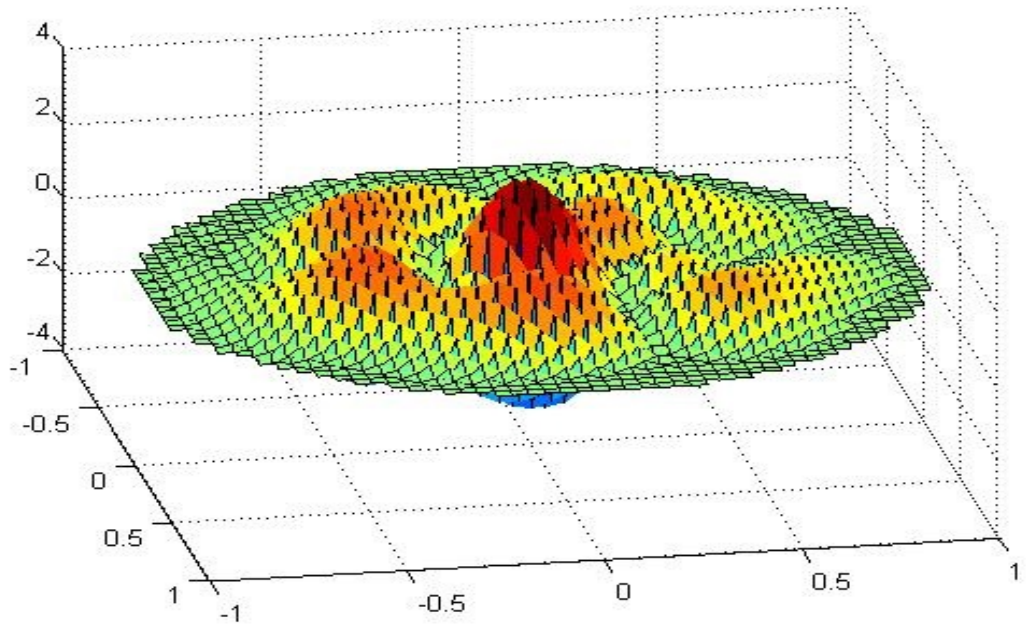

Figure 7.3: The front at $t = 37$.

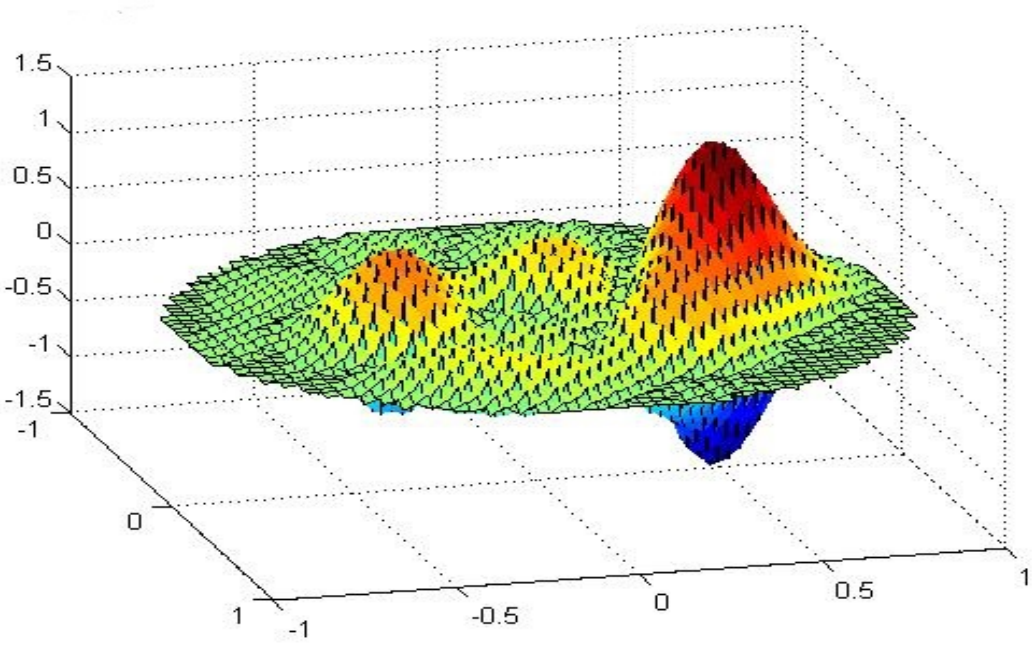

Figure 7.4: The front at $t = 37.9$.

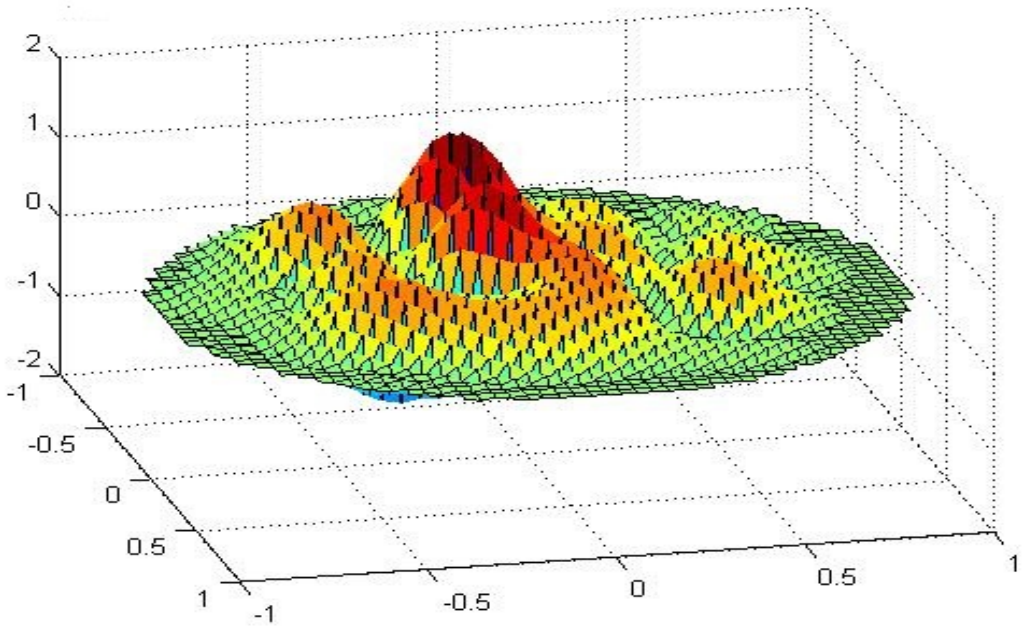

Figure 7.5: The front at $t = 38.1$.

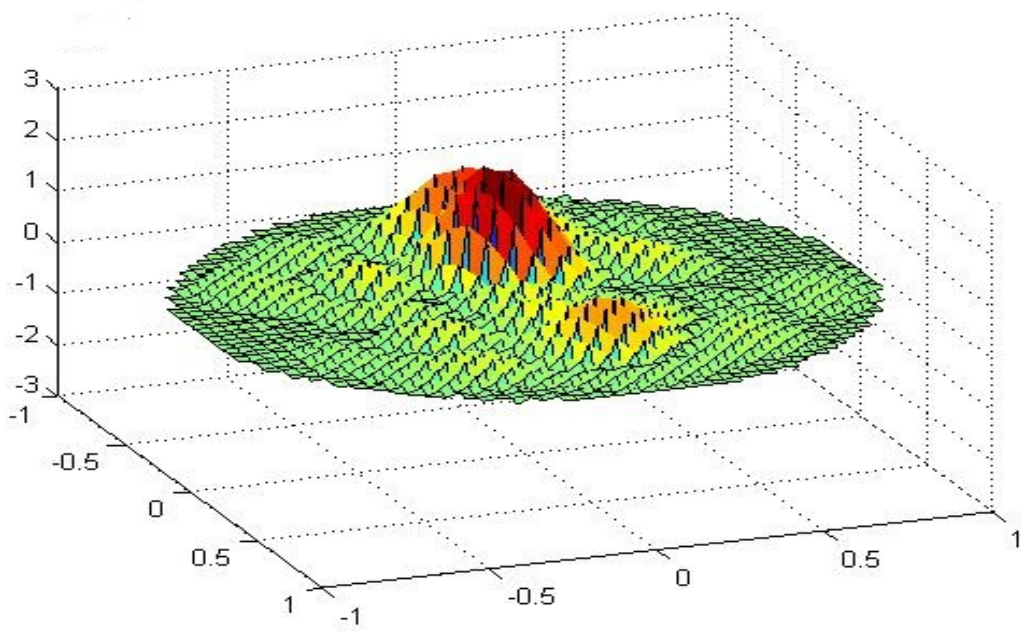

Figure 7.6: The front at $t = 38.8$.

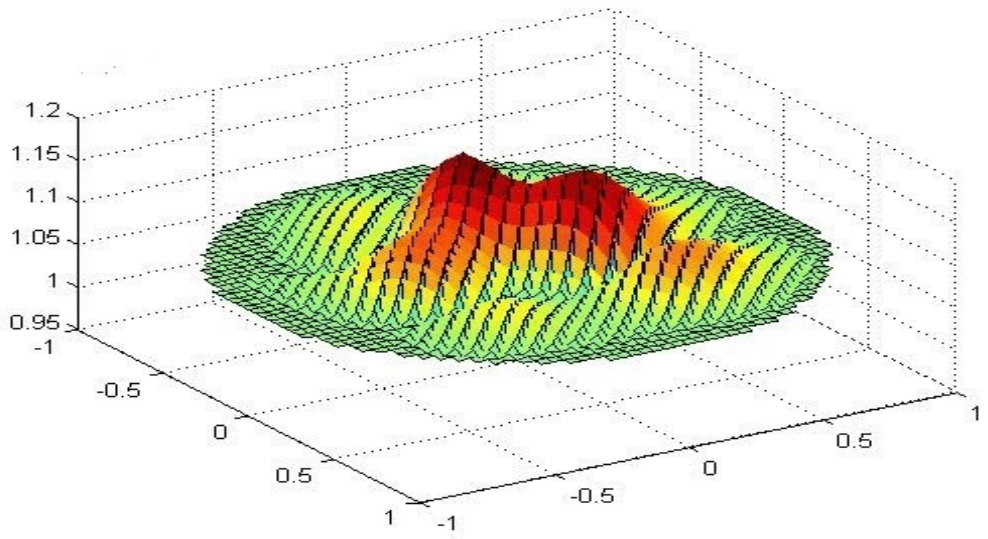

Figure 7.7: The front at $t = 41$.

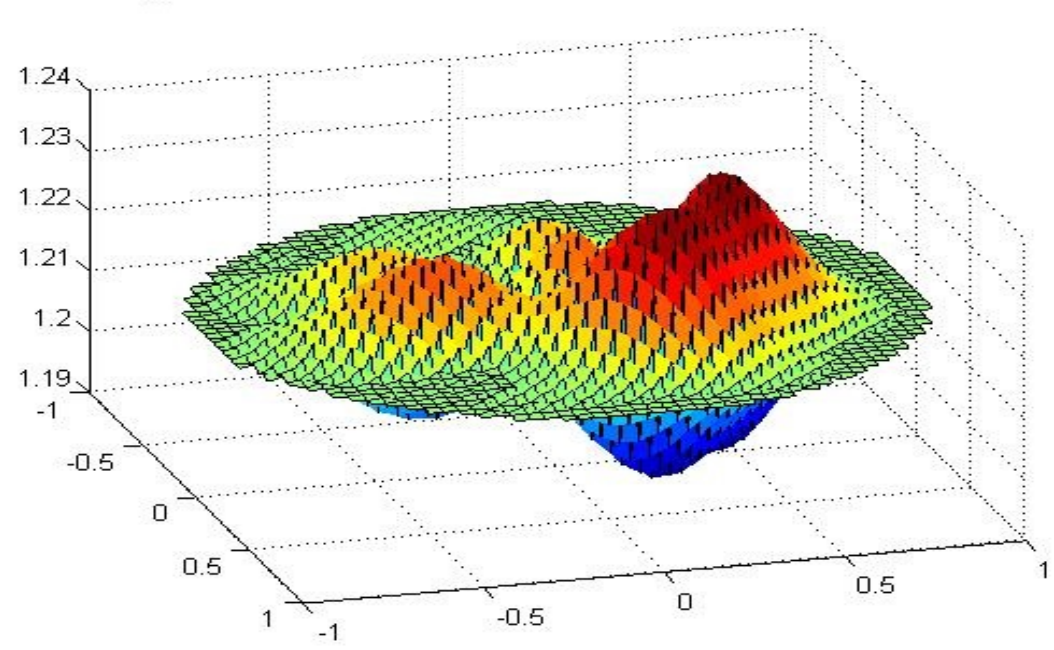

Figure 7.8: The front at $t = 42$.

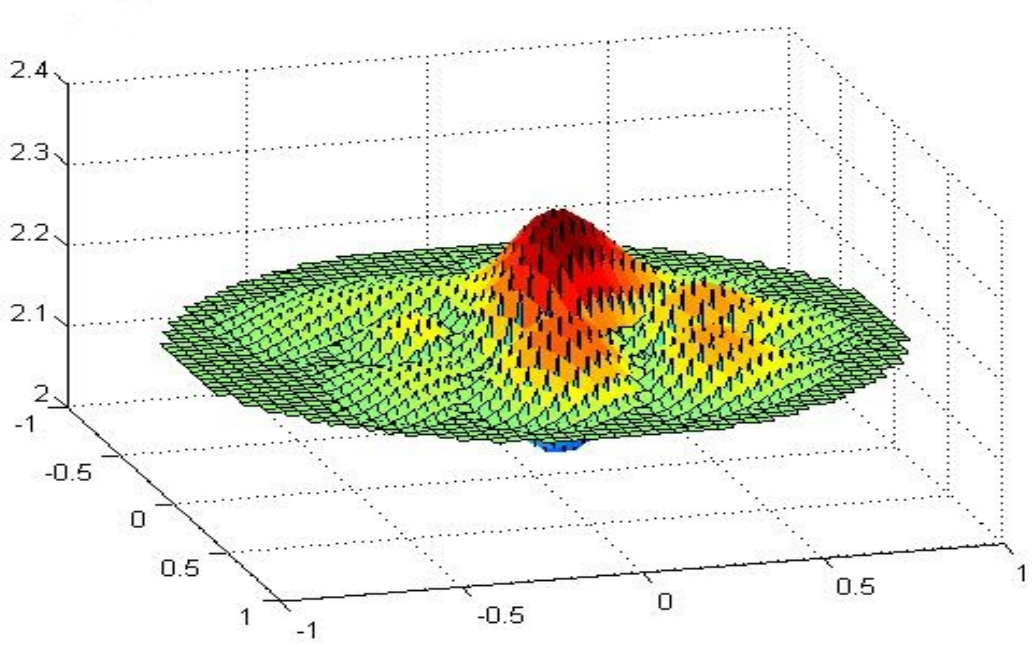

Figure 7.9: The front at $t = 43$.

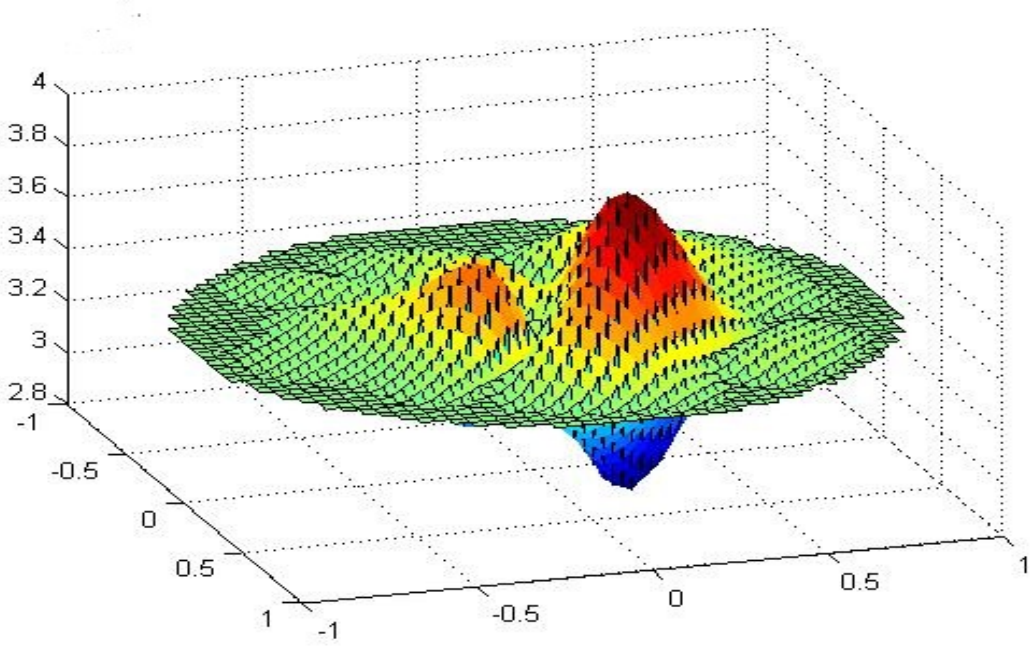

Figure 7.10: The front at $t = 45$.

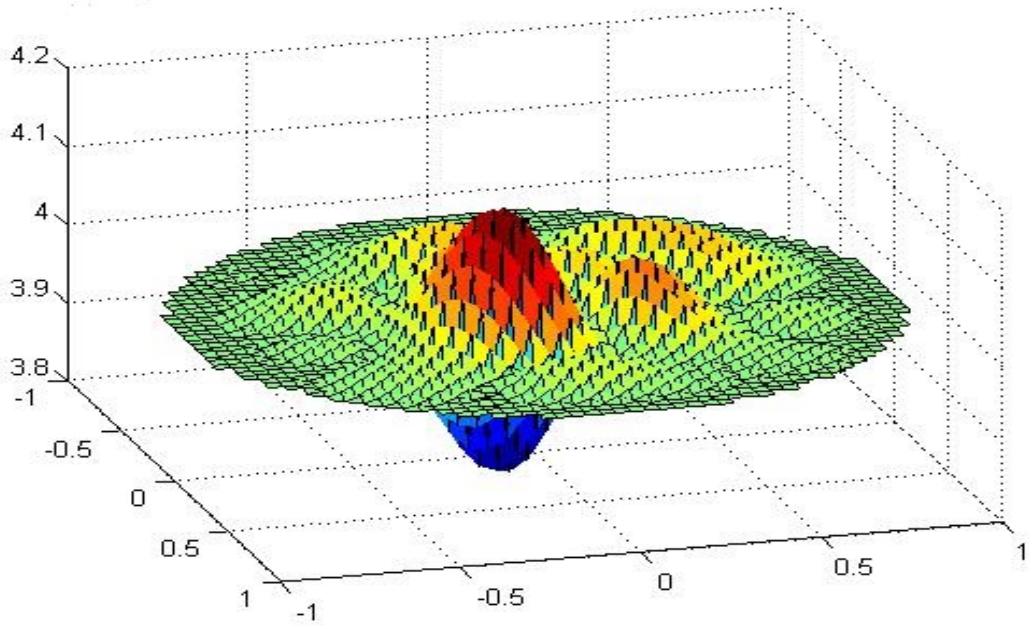

Figure 7.11: The front at $t = 46$.

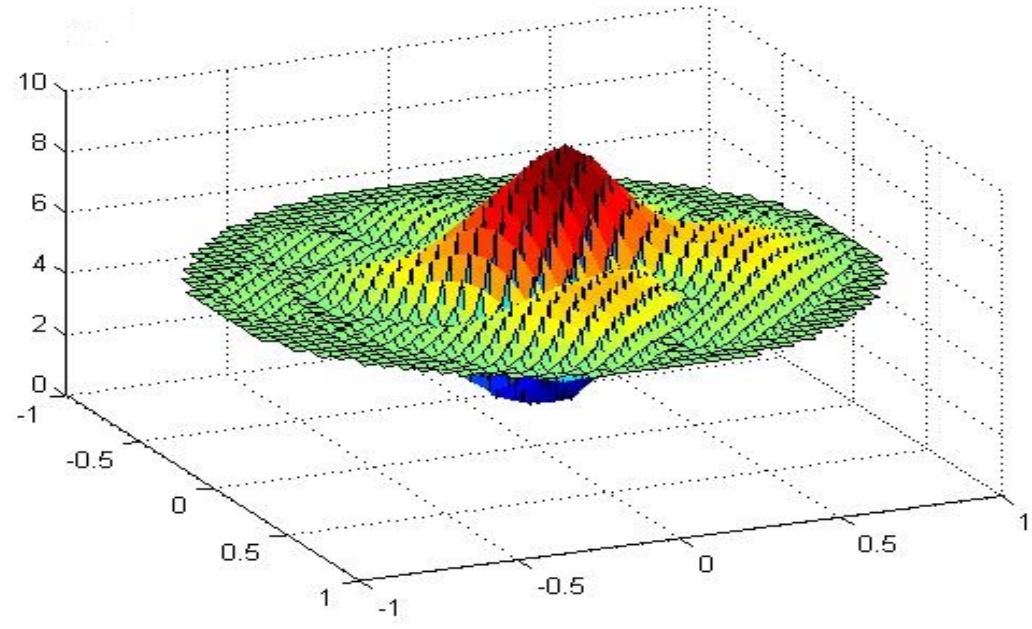

Figure 7.12: The front at $t = 49.7$.

7.4 Conclusions

In this chapter we have successfully applied the 1D-IRBF numerical method to solve Eq. (7.1) governing the behaviour of the spinning combustion front in 3D space. The method successfully produced the spinning motion of the front during limited time.

Chapter 8

Conclusions

8.1 Research outcomes

This research is focused on the active-dissipative partial differential equation

$$\partial_t u = -(\nabla u)^2 \nabla^2 u + (\nabla u)^4 + \nabla^6 u.$$

simulating the dynamics of the reaction fronts (combustion) in different physical systems such as solid flames, detonation and super-adiabatic waves. This equation is referred to as the nonlinearly excited phase (NEP) equation .This equations is based on nonlinear excitation in its most simple form, and hence, the equation is interesting as a basic model of pattern formation as well as regular and irregular dynamics in such systems.

Our approach is also applicable to other equations which have similar structure to the NEP equation (Strunin, 2009). The following results have been obtained in this research:

A forced version of the NEP **equation is derived and used to test the numerical code** We derived a forced version of the NEP equation addressing combustion fronts. Selected exact solutions are constructed. Stability of the solutions is demonstrated in the course of the numerical experiments. The numerical code uses 1D-IRBFN in space; the resulting system of partial differential equations is integrated in time. The comparison of the exact and numerical solutions demonstrated satisfactory performance of the code.

The unforced NEP **equation is solved and analysed numerically in 1D** We used the code to solve the unforced NEP equation in one spatial dimension. Onset of non-trivial regimes from the trivial state is analysed as the domain size is increased. We presented new results in the form of one, two and three step regimes.

The unforced NEP **equation is solved and analysed numerically in 2D** We used the code to solve the unforced NEP equation in two spatial dimension. We presented new results in the form of solid spining waves revolving in a circular boundary.

8.2 Future Directions

As we have already mentioned, Eq. (1.1) describes a generic scenario of pattern formation in a fairly wide group of active systems of different physical or biological nature. Another application of this model concerns superadiabatic combustion waves used for waste treatment. Processing of waste by superadiabatic combustion is an effective clean technology (Institute of Problems of Chemical Physics, Russian Academy of Sciences, www.icp.ac.ru/eng/developments/; yet practically overlooked in Australia. Model (1.1) presents a single-equation simulation tool for the superadiabatic waves.

However, we have already explained that the numerical scheme which is used to solve Eq. (1.1) was 1D-IRBFN for the spatial terms and a Matlab code for the time stepping of the system of differential equations.

So, further research in the direction of this thesis can be done by considering the following points:

1. Explore to a greater precision the onset of spatio-temporal chaos from the regular dynamics with the expansion of space domain.

2. Evaluate the Lyapunov exponents and fractal dimensions characterising the chaotic regimes.

3. Focus on circular 2D geometry in order to achieve regular and chaotic spinning regimes.

8.3 Significance

The further work will help us to understand fundamentals of environmentally friendly technologies of waste treatment and material synthesis. Yet, the project's significance goes beyond this field since Eq. (1.1) describes a generic scenario of pattern formation in a fairly wide group of active systems of different physical, chemical or biological nature.

References

Aldhushin, A. and Braverman, B. S. (2010), 'Saffman-taylor problem in filtration combustion', *Russ. Phys. Chem.* **4**, 788–792.

Aldhushin, A. and Ivleva, T. (2013), 'Hydrodynamic instability of the coflow filtration combustion: numerical simulation', *Dokl. Phys. Chem.* **451**, 157–160.

Aldushin, A. P., Malomed, B. A. and Zel'dovich (1981), 'Phenomenological theory of spin combustion', *Combust.Flame* **42**, 1–6.

Aranson, I. S. and Kramer, L. (2002), 'The world of the Complex Ginzburg-Landau equation', *Reviews of Modern Physics* **74**(1), 99.

Aranson, I. and Tsimring, L. (2006), 'Pattern and collective behavior in granular media: Theoretical concepts', *Reviews of Modern Physics* **78**, 641.

Ayers, R., Burkes, D., Gottoli, G., Yi, H., Guigné, J. and Moore, J. (2005), The application of energetic shs reactions in the synthesis of multi-functional bone tissue engineering and drug delivery systems, *in* 'MRS Proceedings', Vol. 896, Cambridge Univ Press.

Cross, M. C. and Hohenberg, P. C. (1993), 'Pattern formation outside of equilibrium', *Rev.Mod.Phys* **65**, 851–1111.

Dangelmayr, G. and Kramer, L. (1998), Mathematical tools for pattern formation, *in* 'Evolution of Spontaneous Structures in Dissipative Continuous Systems', Springer, pp. 1–85.

Das, S. and Puri, S. (2003), 'Pattern formation in the inhomogeneous cooling state of granular fluids', *Europhysics Letters* **61**, 749.

Dvoryankin, A. V., Strunina, A. G. and Merzhanov, A. G. (1982), 'Trends in the spin combustion of thermites.', *Combust. Explos. Shock Waves* **18**, 134–139.

Fasshauer, G. F. (2007), 'Meshfree approximation methods with matlab'.

Franke, R. (1982), 'Scattered data interpolation: Test of some methods', **38**, 181–200.

García-Morales, V. and Krischer, K. (2012), 'The Complex Ginzburg–Landau equation: an introduction', *Contemporary Physics* **53**(2), 79–95.

Haykin, S. (1999), 'Neural networks- a comprehensive foundation', **6**.

Hyman, J. M. and Nicolaenko, B. (1986), 'The Kuramoto-Sivashinsky equation: a bridge between pde's and dynamical systems', *Physica D: Nonlinear Phenomena* **18**(1), 113–126.

Ivleva, T. P., Merzhanov, A. G. and Shkadinsky, K. G. (1980), 'Principles of the spin mode of combustion front propagation', *Combust. Explos. Shock Waves* **16**, 133–139.

Kansa, E. (1990), 'Multiquadrics-a scattered data approximation scheme with applications to computational fluid dynamics -i. surface approximations partial derivative estimates', **19**, 127–145.

Kerner, B. and Osipov, V. (1989), 'Autosolitons', *Physics-Uspekhi* **32**(2), 101–138.

Kostin, S. V., Krishenik, P. M., Ozerkovskaya, N., Firsov, A. and Shkadinskii, K. G. (2012), 'Cellular filtration combustion of porous layers', *Combustion, Explosion and Shock Waves* **48**, 1–9.

Kostin, S. V., Krishenik, P. M. and Shkadinskii, K. G. (2014), 'Experimental study of the hetrogeneous filtration combustion mode', *Combustion, Explosion and Shock Waves* **50**, 42–50.

Kostin, S. V., Krishenik, P. M. and Shkadinskii, K. G. (2015), 'Pulsating cellular regimes of infiltration combustion of porous media', *Russian Journal of Physical Chemistry B* **9**, 385–391.

Kudryashov, N. (1990), 'Exact solutions of the generalized Kuramoto-Sivashinsky equation', *Physics Letters A* **147**(5), 287–291.

Kuramoto, Y. (1984*a*), *Chemical Oscillations, Waves, and Turbulence*, Berlin: Springer-Verlag.

Kuramoto, Y. (1984*b*), 'Phase dynamics of weakly unstable periodic structures', *Progress of theoretical physics* **71**(6), 1182–1196.

Kuramoto, Y. (1995), 'Scaling behavior of turbulent oscillators with non-local interaction', *Progress of Theoretical Physics* **94**(3), 321–330.

Kuramoto, Y. and Tsuzuki, T. (1976), 'Persistent propagation of concentration waves in dissipative media far from thermal equilibrium', *Prog. Theor. Phys* **55**(2), 356–369.

Landau, L. D. and Lifshits, E. M. (1987), 'Fluid mechanics', *Oxford: Pergamon* .

Le, P., Mai-Duy, N., Tran-Cong, T. and Baker, G. (2008), 'A meshless modeling of dynamic strain localization in quasi-brittle materials using radial basis function networks', **25**, 43–66.

Mai-Duy, N., Ngo-Cong, D., Karunasena, W. and Tran-Cong, T. (2012), 'Free vibration analysis of laminted composite plates based on fsdt using one dimensional irbfn method', **83**, 459–498.

Mai-Duy, N., See, H. and Tran-Cong, T. (2008), 'An integral collocation based fictitious domain technique for solving elliptic problems', **24**, 1291–1314.

Mai-Duy, N. and Tanner, R. (2005), 'Solving high order partial differential equations with radial basis function networks', **63**, 1636–1654.

Mai-Duy, N. and Tanner, R. (2007), 'A multidomain integrated radial basis function collocation method for elliptic problems', **17**, 165–186.

Mai-Duy, N. and Tran-Cong, T. (2001), 'Numerical solution of differential equations using multiquadric radial basis functions networks', **14**, 185–199.

Mai-Duy, N. and Tran-Cong, T. (2003), 'Approximation of function and its derivative using radial basis function networks', **17**, 197–220.

Mai-Duy, N. and Tran-Cong, T. (2008), 'A multidomain integrated radial basis function collocation method for elliptic problems', **24**, 1301–1320.

Mai-Duy, N. and Tran-Cong, T. (2011), 'Compact local integrated-rbf approximations for second order elliptic differential problems', **230**, 4772–4794.

Manneville, P. (1990), *Dissipative structures and weak turbulence*, Academic Press. INC.

Manneville, P. (2010), *Instabilities, chaos and turbulence, An Introduction to Nonlinear Dynamics and Complex Systems*, Vol. 1, World Scientific.

Merzhanov, A. (1996), 'Combustion processes that synthesize materials', *Journal of materials processing technology* **56**(1), 222–241.

Merzhanov, A. (1997), 'Fundamentals, achievements, and perspectives for development of solid-flame combustion', *Russian Chemical Bulletin* **46**(1), 1–27.

Merzhanov, A. G. (2004), 'The chemistry of self-propagating high-temperature synthesis', *Journal of Materials Chemistry* **14**(12), 1779–1786.

Merzhanov, A. G., Filonenko, A. K. and Borovinskaya, I. P. (1973), 'New phenomena in combustion of condensed systems.', *Doklady Phys. Chem.* **208**, 122–125.

Merzhanov, A. G., Rogachev, A. S. et al. (1992), 'Structural macrokinetics of shs processes', *Pure Appl. Chem* **64**(7), 941–953.

Merzhanov, A. and Rumanov, E. (1999), 'Physics of reaction waves', *Reviews of Modern Physics* **71**(4), 1173.

Mohammed, F., Ngo-Cong, D., Strunin, D., Mai-Duy, N. and Tran-Cong, T. (2014), 'Modelling dispersion in laminar and turbulent flows in an open channel based on centre manifolds using 1d-irbfn method', **38**, 3672–3691.

Mohammed, M. (2015), 'Dynamics of active systems with nonlinear excitation of the phase', *USQ PhD thesis* .

Newell, A. C., Passot, T. and Lega, J. (1993), 'Order parameter equations for patterns', *Annual review of fluid mechanics* **25**(1), 399–453.

Newell, A. C. and Whitehead, J. (1969), 'Finite bandwidth, finite amplitude convection', *Journal of Fluid Mechanics* **38**(02), 279–303.

Ngo-Cong, D., Mai-Duy, N., Karunasena, W. and Tran-Cong, T. (2011), 'Free vibration analysis of laminted composite plates based on fsdt using one dimensional irbfn method', **89**, 1–13.

Ngo-Cong, D., Mai-Duy, N., Karunasena, W. and Tran-Cong, T. (2012), 'Local moving least square one dimensional irbfn technique for incompressible viscous flows', *Int.J.Numer.Meth.Fluids* **70**, 1443–1474.

Nikolaevskii, V. N. . (1989), 'Dynamics of viscoelastic media with internal oscillator', *Recent Advances in Engineering Science in Lecture Notes in Engineering* **39**, 210.

Park, J. and Sandberg, I. (1991), 'Universal approximation using radial basis function networks', *Neural Computation* **3**, 246–257.

Pismen, L. M. (1999), *Vortices in nonlinear fields: From liquid crystals to superfluids, from non-equilibrium patterns to cosmic strings*, Vol. 100, Oxford University Press.

Rabinovich, M. I., Ezersky, A. B. and Weidman, P. D. (2000), *The dynamics of patterns*, World Scientific.

Rozenberg, A., Lempert, D., Grigoryan, L., Medvedev, A. and Manelis, G. (2005), 'Mass transfer of metal containing products in filtaration combustion under superadiabatic heating conditions', *Doklady Physical Chemistry* **405**, 249–252.

Rubin, S. G. and Graves, R. A. (1975), 'Cubic spline approximation for problems in fluid mechanics', *NASA TR R-436, Washington D.C,* .

Sivashinsky, G. (1977), 'Nonlinear analysis of hydrodynamic instability in laminar flamesi. derivation of basic equations', *Acta Astronautica* **4**(11), 1177–1206.

Slimane, R., Lau, F., Dihu, R., Khinkis, M., Bingue, J., Saveliev, A., Fridman, A. and Kennedy, L. (2002), 'Production of hydrogen by superadiabatic decomposition of hydrogen sulphide', *Gas Technology Institute Final Report for contract no. DE-FC36-99GO10450, submitted to US Department of Energy* .

Stewartson, K. and Stuart, J. (1971), 'A non-linear instability theory for a wave system in plane poiseuille flow', *Journal of Fluid Mechanics* **48**(03), 529–545.

Strunin, D. (2009*a*), 'Fluid flow between active elastic plates', *ANZIAM Journal* **50**, C871–C883.

Strunin, D. and Suslov, S. (2005), 'Phenomenological approach to 3d spinning combustion waves: numerical experiments with a rectangular rod', *International Journal of Self Propagating High Temperature Synthesis* **14**(1), 33–39.

Strunin, D. V. (1999), 'Autosoliton model of the spinning fronts of reaction', *IMA journal of applied mathematics* **63**(2), 163–177.

Strunin, D. V. (2009*b*), 'Phase equation with nonlinear excitation for nonlocally coupled oscillators', *Physica D: Nonlinear Phenomena* **238**(18), 1909–1916.

Strunin, D. V. and Mohammed, M. G. (2015), 'Range of validity and intermittent dynamics of the phase of oscillators with nonlinear self excitation', *ANZIAM Journal* **53**, C236–C248.

Tanaka, D. (2004), 'Chemical turbulence equivalent to Nikolaevskii turbulence', *Physical Review E* **70**(1), 015202.

Tanaka, D. (2005), 'Critical exponents of Nikolaevskii turbulence', *Physical Review E* **71**(2), 025203.

Tanaka, D. (2006), 'Turing instability leads oscillatory systems to spatiotemporal chaos', *Progress of theoretical physics. Supplement* (161), 119–126.

Tanaka, D. and Kuramoto, Y. (2003), 'Complex Ginzburg-Landau equation with nonlocal coupling', *Physical Review E* **68**(2), 026219.

Tran-Cong, T. and Mai-Duy, N. (2001), 'Numerical solution of navier-stokes equations using multi quadric radial basis function', **37**, 65–86.

Tribelsky, M. and Velarde, M. (1996), 'Short-wavelength instability in systems with slow long-wavelength dynamics', *Physical Review E* **54**(5), 4973.

Zel'dovich, Y. B. and Kompaneets, A. S. (1960), 'Theory of detonation', *New York: Academic Press* .

Appendix A

Matlab program to solve the NEP equation with one spatial dimension

We developed the Matlab code to solve the Strunin equation in one spatial dimension under zero boundary conditions on the both ends of the x-domain.

A.1 Matlab program to set initial condition and set the grid system

```
%------------------

clc; clear; close all; myeps = 1e-6; tic
scrsz = get(0,'ScreenSize'); % [ 1 1  1920  1200]

% ----------------------------
A_control = load('z_Wave_engine1a.txt');
istep_CM = A_control(1,1); % 10; % istep_CM to display CM
istep_CM1 = A_control(2,1); % 10; % istep_CM1 to save CM;
% istep_S2 = A_control(3,1); % istep_S2 to save A1;
        istep_S2 = 10 % 0.1/dt; % istep_S2 to save A1;

% ----------------------------
method_eps = 0
method_dis = 1 % 1: 1D-IRBFN

betaG=1;
theta = 0.5;

% Problem's parameters
A=10; B=1.0; C=1.0;
C1=1; C2=0; % Initial condition
```

```
% 1/ Geometry
nx = 201


L = 30;


xA = 0;xB = L;
xC=L/2;
dx = abs(xA-xB)/(nx-1);
x = [xA:dx:xB]';

dt=1e-5

%Tmax=100*dt % 1 % 10*dt % 1.0;

Tmax=1500*dt;




% 2/ Find

%  2a/ Initial condition

%for i_fold = 1
%    u0 = zeros(nx,1);
%    u0(x<=xC+myeps)=C1;
%    u0(x>xC+myeps)=C2;
%    u0i=u0;
%end % for i_fold = 1

    u0 = 7*exp(-1*x.^2);
    u0i=u0;

% 3/ Discretisation
for i_fold = 1
    c1=x;a1 = betaG*dx;
    [D1x,D2x,D3x,D4x,D5x,D6x,...
        D1xB,D2xB,D3xB,D4xB,D5xB,D6xB] = Determine1D6_f3A_both(x,c1,nx,a1);
% Determine E1
    Inx = eye(nx,nx);
    EL = (1/dt*Inx - theta*C*D6x);
end
```

A.2 Matlab program to solve the equation

```
    % for i_fold = 1

% 4/ Solve
A1=[];
t1=0;
istep = 0;
method_load = 0
```

```
if (method_load==1)
    t1 = 0.1
    filename = sprintf('Result_1D\\W1a_dis_%02d_nx_%03d_dt_%2.1f_t_%2.5f_A.mat',...
        method_dis,nx,abs(log(dt)/log(10)),t1)
    %         save(filename,'A1','u0','u_1');
    load(filename);
    istep = A1(end,1);
    t1 = A1(end,2);
end


while (t1<=Tmax+myeps)
    t1=t1+dt;
    istep = istep+1;
    temp1 = A*(D1x*u0).^2;
    [ED1] = Multiply_v_m(temp1,D2x);
    E1 = EL+ED1;
    E1 = sparse(E1);
    [L1,U1,P1,Q1] = lu(E1);
    RHS1 = u0/dt + (1-theta)*C*(D6x*u0) + B*(D1x*u0).^4;
    u1 = Q1*(U1\(L1\(P1*RHS1)));
    CM = norm(u0-u1)/norm(u1);
    temp=[istep t1 CM toc];
    u0=u1;


    if (mod(istep,istep_CM)<myeps)
        A_control = load('z_Wave_engine1a.txt');
        istep_CM = A_control(1,1); % 10; % istep_CM to display CM
        istep_CM1 = A_control(2,1); % 10; % istep_CM1 to save CM;
%         istep_S2 = A_control(3,1); % istep_S2 to save A1;
%                 istep_S2=1; %0.2/dt; % istep_S2 to save A1;

    end

    if (mod(istep,istep_CM)<myeps)
        temp
    end
    if (mod(istep,istep_CM1)<myeps)
        A1=[A1;temp];
    end
    if (mod(istep,istep_S2)<myeps)
        filename = sprintf('Result_1D\\W1a_dis_%02d_nx_%03d_dt_%2.1f_t_%2.5f_A.mat',...
            method_dis,nx,abs(log(dt)/log(10)),t1)
        save(filename,'A1','u0','u1');
    end
end % while (t1<=Tmax+myeps)

filename = sprintf('Result_1D\\W1a_dis_%02d_nx_%03d_dt_%2.1f_t_%2.5f_A.mat',...
    method_dis,nx,abs(log(dt)/log(10)),t1)
save(filename,'A1','u0','u1');
```

```
function [D1x,D2x,D3x,D4x,D5x,D6x,...
    D1xB,D2xB,D3xB,D4xB,D5xB,D6xB] = Determine1D6_f3A_both(x,c1,nx,a1)
% Version Determine1D4_2: rectangular domain
% Version Determine1D4_3: rectangular domain, non-CM
% Version Determine1D4_4: rectangular domain, non-CM, only nip


% Step 1: Determine H0, H1, H2, H3, H4 for direction X
for i_fold = 1
    H0 = zeros(nx,nx+6);
    H1 = zeros(nx,nx+6);
    H2 = zeros(nx,nx+6);
    H3 = zeros(nx,nx+6);
    H4 = zeros(nx,nx+6);
    H5 = zeros(nx,nx+6);
    H6 = zeros(nx,nx+6);

    for i =1:nx
        %Determine  H6 (H6 = G)
        for j=1:nx+6
            if j<=nx
                r=(x(i)-c1(j));
                H6(i,j)=(r^2+a1^2)^0.5;
            else
                H6(i,j)=0;
            end
        end

        %Determine H5
        for j=1:nx+6
            if j<=nx
                r=(x(i)-c1(j));
                A=(r^2+a1^2)^0.5;
                B=log(r+A);
                H5(i,j)=0.5*r*A + 0.5*a1^2*B;
            elseif j==nx+1
                H5(i,j)=1;
            else
                H5(i,j)=0;
            end
        end

        %Determine H4
        for j = 1:nx+6
            if j<=nx
                r=(x(i)-c1(j));
                A=(r^2+a1^2)^0.5;
                B=log(r+A);
                H4(i,j)=(r^2/6-a1^2/3)*A  + 0.5*a1^2*r*B;
            elseif j==nx+1
                H4(i,j)=x(i);
```

```
    elseif j==nx+2
        H4(i,j)=1;
    else
        H4(i,j) = 0;
    end
end

%Determine H3
for j=1:nx+6
    if j<=nx
        r=(x(i)-c1(j));
        A=(r^2+a1^2)^0.5;
        B=log(r+A);
        H3(i,j) = (-13*a1^2*r/48 + r^3/24)*A + (-a1^4/16 + a1^2*r^2/4)*B;
    elseif j==nx+1
        H3(i,j) = x(i)^2/2;
    elseif j==nx+2
        H3(i,j) = x(i);
    elseif j==nx+3
        H3(i,j) = 1;
    else
        H3(i,j) = 0;
    end
end

%Determine H2
for j=1:nx+6
    if j<=nx
        r=(x(i)-c1(j));
        A=(r^2+a1^2)^0.5;
        B=log(r+A);
        H2(i,j) = (a1^4/45 - 83*a1^2*r^2/720 + r^4/120)*A
                    + (-3*a1^4*r/48 + 4*a1^2*r^3/48)*B;
    elseif j==nx+1
        H2(i,j) =  x(i)^3/6;
    elseif j==nx+2
        H2(i,j) = x(i)^2/2;
    elseif j==nx+3
        H2(i,j) =  x(i);
    elseif j==nx+4
        H2(i,j) =  1;
    else
        H2(i,j) =  0;
    end
end

%Determine H1
for j=1:nx+6
    if j<=nx
        r=(x(i)-c1(j));
        A=(r^2+a1^2)^0.5;
        B=log(r+A);
        H1(i,j) = (15*a1^6*B + 60*a1^2*B*r^2*(-3*a1^2 + 2*r^2)
                    + A*r*(113*a1^4 - 194*a1^2*r^2 + 8*r^4))/5760;
    elseif j==nx+1
```

```
                H1(i,j) =  x(i)^4/24;
            elseif j==nx+2
                H1(i,j) = x(i)^3/6;
            elseif j==nx+3
                H1(i,j) =  x(i)^2/2;
            elseif j==nx+4
                H1(i,j) =  x(i);
            elseif j==nx+5
                H1(i,j) =  1;
            else
                H1(i,j) =  0;
            end
        end

        %Determine H0
        for j=1:nx+6
            if j<=nx
                r=(x(i)-c1(j));
                A=(r^2+a1^2)^0.5;
                B=log(r+A);
                H0(i,j) = (3*B*(5*a1^6*r-20*a1^4*r^3+8*a1^2*r^5)
                              +1/35*A*(-128*a1^6+1779*a1^4*r^2-1518*a1^2*r^4+40*r^6))/5760;
            elseif j==nx+1
                H0(i,j) =  x(i)^5/120;
            elseif j==nx+2
                H0(i,j) =  x(i)^4/24;
            elseif j==nx+3
                H0(i,j) = x(i)^3/6;
            elseif j==nx+4
                H0(i,j) =  x(i)^2/2;
            elseif j==nx+5
                H0(i,j) =  x(i);
            elseif j==nx+6
                H0(i,j) =  1;
            else
                H0(i,j) =  0;
            end
        end

    end
end % i_fold - step 1

% Step 2: Add boundary conditions
K = [H1([1 end],:);H2([1 end],:);H3([1 end],:)];
C = [H0;K]; % (nx+3; nx+6)
C_inv = pinv(C);% (nx+6; nx+3)

% Step 3: Determine D41x D42x D43x D44x
D1x = H1*C_inv;% (nx-1,nx+2)
D2x = H2*C_inv;% (nx-1,nx+2)
D3x = H3*C_inv;% (nx-1,nx+2)
D4x = H4*C_inv;% (nx-1,nx+2)
D5x = H5*C_inv;% (nx-1,nx+2)
D6x = H6*C_inv;% (nx-1,nx+2)
```

```
D1xB = D1x(:,nx+1:nx+6);% (nx-1,5)
D2xB = D2x(:,nx+1:nx+6);% (nx-1,5)
D3xB = D3x(:,nx+1:nx+6);% (nx-1,5)
D4xB = D4x(:,nx+1:nx+6);% (nx-1,5)
D5xB = D5x(:,nx+1:nx+6);% (nx-1,5)
D6xB = D6x(:,nx+1:nx+6);% (nx-1,5)

D1x = D1x(:,1:nx);% (nx-1,nx)
D2x = D2x(:,1:nx);% (nx-1,nx)
D3x = D3x(:,1:nx);% (nx-1,nx)
D4x = D4x(:,1:nx);% (nx-1,nx)
D5x = D5x(:,1:nx);% (nx-1,nx)
D6x = D6x(:,1:nx);% (nx-1,nx)


function [ED1] = Multiply_v_m(uy,D1xt)
nX = length(uy);
% Multiply a column vector by a matrix: ED1 = uy(nX,1)*D1xt(nX,nX)
ED1 = D1xt;
for i=1:nX
    ED1(i,:) = uy(i)*ED1(i,:);
end
```

A.3 Matlab program to plot the solution

```
% Plotting
clc; clear; close all; myeps = 1e-6; tic
scrsz = get(0,'ScreenSize'); % [ 1 1  1920  1200]
% ------------------------------
A_control = load('z_Wave_engine1a.txt');
istep_CM = A_control(1,1); % 10; % istep_CM to display CM
istep_CM1 = A_control(2,1); % 10; % istep_CM1 to save CM;
% istep_S2 = A_control(3,1); % istep_S2 to save A1;
        istep_S2 = 10 % 0.1/dt; % istep_S2 to save A1;
% ------------------------------
method_eps = 0
method_dis = 1 % 1: 1D-IRBFN

betaG=1;
theta = 0.5;
% Problem's parameters
A=10; B=1.0; C=1.0;
C1=1; C2=0; % Initial condition
% 1/ Geometry
nx = 201
L = 10;
xA = 0;xB = L;
xC=L/2;
dx = abs(xA-xB)/(nx-1);
x = [xA:dx:xB]';
dt=1e-3
Tmax=100*dt % 1 % 10*dt % 1.0;
```

```
% 2/ Find
%  2a/ Initial condition
for i_fold = 1
    u0 = zeros(nx,1);
    u0(x<=xC+myeps)=C1;
    u0(x>xC+myeps)=C2;
    u0i=u0;
end % for i_fold = 1

% 3/ Discretisation


% 4/ Load filename
t1=0.001
filename = sprintf('Result_1D\\W1a_dis_%02d_nx_%03d_dt_%2.1f_t_%2.5f_A.mat',...
    method_dis,nx,abs(log(dt)/log(10)),t1)
%         save(filename,'A1','u0','u1');
load(filename);


% 5/ Plot
for i_fold = 1
    figure(1)
    pos1 = [1+2*scrsz(3)/4 scrsz(4)*0.1+0*scrsz(4)/3 scrsz(3)/4 1.5*scrsz(4)/3];
    set(1,'OuterPosition',pos1)

%    plot(x,u0i,'.-')
%    hold on
    plot(x,u0,'m--')
    xlabel('\fontsize{18} {\it x(m)}')
    ylabel('\fontsize{18} {\it u_0}')
%    legend('t=0','t')
    title(sprintf('Time t = %2.2f',t1))
    grid on
    NFS = 18.0; % fontsize
    NLW = 0.8; % linewidth
    set(gca,'FontSize',NFS,'LineWidth',NLW);

    filename = sprintf('Result_1D\\W1a_dis_%02d_nx_%03d_dt_%2.1f_t_%2.5f_f1.jpg',...
        method_dis,nx,abs(log(dt)/log(10)),t1)
    print('-f1','-djpeg',filename)

end  % for i_fold = 1
```

A.4 Matlab program to plot the solution as a movie

```
%Plotting Movies
clc; clear; close all; myeps = 1e-6; tic
scrsz = get(0,'ScreenSize'); % [ 1 1  1920  1200]
% ------------------------------
A_control = load('z_Wave_engine1a.txt');
istep_CM = A_control(1,1); % 10; % istep_CM to display CM
```

```
istep_CM1 = A_control(2,1); % 10; % istep_CM1 to save CM;
% istep_S2 = A_control(3,1); % istep_S2 to save A1;
istep_S2 = 100 % 0.1/dt; % istep_S2 to save A1;
% ------------------------------
method_eps = 0
method_dis = 1 % 1: 1D-IRBFN
betaG=1;
theta = 0.5;

% Problem's parameters
A=7; B=1.0; C=1.0;
C1=1; C2=0; % Initial condition

% 1/ Geometry
nx = 401
L = 10;
xA = 0;xB = L;
dx = abs(xA-xB)/(nx-1);
x = [xA:dx:xB]';


dt=2e-4


%Tmax=100*dt % 1 % 10*dt % 1.0;
Tmax2=20000*dt;

% 2/ Find
xC=3;
xD=xC+3;
idiC = find(abs(x-xC)<myeps);
if (isempty(idiC)==1)
    disp('Choose nx again (nx=100*k+1, k integer)')
    stop
end

%  2a/ Initial condition
u0=zeros(nx,1);
kA=18;
for i=1:nx
    if (x(i)<=xC)
        u0(i) = kA;
    elseif (x(i)>=xC & x(i)<=xD)
        u0(i) = kA*exp(-1*(x(i)-xC)^2);
    else
        u0(i) = 0;
    end
end

 %u0 = 7*exp(-1*x.^2);
u0i=u0;

% 3/ Discretisation

% 4/ Load filename
```

```
t1=0.2
n=10
dt0=100*dt % 1e-4
for t1=[dt0:dt0:Tmax2]
    close all;

    filename = sprintf('Result_1D\\W2c_dis_%02d_nx_%03d_dt_%2.1f_t_%2.5f_A.mat',...
        method_dis,nx,abs(log(dt)/log(10)),t1)
    %         save(filename,'A1','Ax_wave','u0','u1');
    load(filename);

    % 5/ Plot
    for i_fold = 1
        figure(1)
        pos1 = [1+2*scrsz(3)/4 scrsz(4)*0.1+0*scrsz(4)/3 scrsz(3)/4 1.5*scrsz(4)/3];
        set(1,'OuterPosition',pos1)

        %        plot(x,u0i,'.-')
        %        hold on
        x_real = x+sum(Ax_wave(:,3));
        plot(x_real,u0,'m-')
        xlabel('\fontsize{18} {\it x}')
        ylabel('\fontsize{18} {\it u}')
        %        legend('t=0','t')
        title(sprintf('t = %2.5f',t1))


        %         axis([xA xB -2.0 10.0])
        axis([min(x_real) min(x_real)+L min(u0)-2 max(u0)+5 ])      % ..change y limits


        grid on
        NFS = 18.0; % fontsize
        NLW = 0.8; % linewidth
        set(gca,'FontSize',NFS,'LineWidth',NLW);

        filename = sprintf('Result_1D\\Fig_W2c_dis_%02d_nx_%03d_dt_%2.1f_t_%2.5f_f1.jpg',...
            method_dis,nx,abs(log(dt)/log(10)),t1)
        print('-f1','-djpeg',filename)

    end  % for i_fold = 1

end % for t1=[0.001:0.001:0.01]


%figure(2)

%pos1 = [1+3*scrsz(3)/4 scrsz(4)*0.1+0*scrsz(4)/3 scrsz(3)/4 1.5*scrsz(4)/3];
%set(2,'OuterPosition',pos1)

%plot(x,u0i,'.-')
%hold on
%plot(x_real,u0,'m-')
%xlabel('\fontsize{18} {\it x}')
%ylabel('\fontsize{18} {\it u}')
```

```
%legend('t=0','t1')
%title(sprintf('Time t = %2.5f',t1))
%axis([xA xB min(min(u0)-1,min(u0i)-1)  max(max(u0)+1,max(u0i)+1) ])
%grid on
%NFS = 18.0; % fontsize
%NLW = 0.8; % linewidth
%set(gca,'FontSize',NFS,'LineWidth',NLW);

function [u_up,u_down,x_wave] = Deter_wave(x,u0)

% Determine u_up,u_down,x_wave
% Determine x_up,x_down
u_up = u0(1);
u_down = u0(end);

idi_up = find(abs(u0-u_up)<0.1*(u_up-u_down));
idi_down = find(abs(u0-u_down)<0.1*(u_up-u_down));
x_up = x(idi_up(end));
x_down = x(idi_down(1));
x_wave = 0.5*(x_up+x_down);

function [x_wave,delta_xs,u0] = Deter_shift_u0(xA,xM,dx,myeps,x,u0)

% Determine u_up,u_down,x_wave
[u_up,u_down,x_wave] = Deter_wave(x,u0);
plot(x,u0)
% Shift the solution (x,u0) back if (delta_xs=x_wave-xM > 0)
% Determine delta_xs,u0
nx = length(x);
delta_xs = x_wave-xM;
if (delta_xs>0)
    k=round(delta_xs/dx);
    delta_xs= k*dx;
    idi = find(x>=xA+delta_xs-myeps);
    u2 = zeros(nx,1) + u_down;
    u2(1:length(idi))=u0(idi);
    u0=u2;
else
    delta_xs = 0;
end
```

Appendix B

Matlab program

The numerical code for chapter 5 is the same as for chapter 4 just Matlab program to discretize the spatial part of the equation is slightly different here as we added the forced function.

B.1 Matlab program to solve the forced NEP equation

```
clear; clc; close all;tic;

% Step 1a: Create a geometry(IRBFN method for 1D case)

nx =100;       % no of nodes
xA = 0;
xB =10;%4*pi;
dx = abs(xB-xA)/(nx-1); %distance between consecutive nodes
x = [xA:dx:xB]';% dx is distance between two consecutive nodes
c = [xA:dx:xB] ;
Tmax =20;   % maximum time period
theta = 0.5;
dt = 1e-3; %time step
t = [0:dt:Tmax]';
nt = length(t) ; %number of time step

[xx,tt]=ndgrid(x,t);
nxnt = nx*nt;
X = reshape(xx,nxnt,1);
T = reshape(tt,nxnt,1);

% Step 2: Determine the exact solution
k1=-1;
uE1 = sin(X+k1*T);
uEm = reshape(uE1,nx,nt);
% Derivatives
uE =    @(x,t)  sin(x+k1*t);
```

```
du =    @(x,t)  cos(x+k1*t);
ddu =   @(x,t) -sin(x+k1*t);
dddu =  @(x,t) -cos(x+k1*t);

uE2m = reshape(uE(X,T),nx,nt);
% Determine fxt
fxt = @(x,t) k1*cos(x+k1*t) - 1*(sin(x+k1*t)).*(cos(x+k1*t)).^2
          - (sin(x+k1*t)).^4 + (sin(x+k1*t));

% Step 3: Discretisation using 1D-IRBFNs method ...........
[H0,H1,H2,H3,H4,H5,H6] = Deter_IRBF_H0_H6(x,c,dx);
C_inv = pinv(H0);

%   Initial condition
u0=uE(x,0);

%----------------------------
U = [];
CM = 1;
W=[];
for k=1:nt
    tk = t(k)
    % Determine w0
    w0=C_inv*u0;
    L=(H1*w0).*(H1*w0);

    P=zeros(nx,nx+6);

    for i=1:nx
        P(i,:)= L(i,:)*H2(i,:);
    end

    M=(H1*w0).*(H1*w0).*(H1*w0);

    Q=zeros(nx,nx+6);

    for i=1:nx
        Q(i,:)= M(i,:)*H1(i,:);
    end
    % Determine E
    E = H6-1*P+Q;
    E1 = 1/dt*H0 - theta*E;
    % Determine fxt
    f = fxt(x,tk);
    b1 = H0/dt*w0 + (1-theta)*E*w0 + f;

    % Determine boundary conditions
    E2=H1(1,:);
    E3=H1(nx,:);
    E4=H2(1,:);
    E5=H2(nx,:);
    E6=H0(1,:);
    E7=H0(nx,:);
    E=[E1;E2;E3;E4;E5;E6;E7];
```

```
    b2=du(x(1),tk);
    b3=du(x(nx),tk);
    b4=ddu(x(1),tk);
    b5=ddu(x(nx),tk);
    b6=uE(x(1),tk);
    b7=uE(x(nx),tk);

    b=[b1;b2;b3;b4;b5;b6;b7];

    w1=E\b;
    u1=H0*w1;

    U(:,k) = u1;
    u0 = u1;
    W(:,k)=w1;
    w0=w1;
end

Ne= norm(U-uE2m)/norm(uE2m)


% 5/ Plot
figure(1)
%subplot(2,1,1)
surf(xx,tt,uEm,'EdgeColor','none');
%contour(xx,tt,uEm);
xlabel('x')
ylabel('t')
grid on
title(sprintf('Exact solution uE(x,t), k1=%2.2f',k1))
%uEm(:,1)

figure(2)
%subplot(2,1,2)
surf(xx,tt,U,'EdgeColor','none');
%contourf(xx,tt,U);
xlabel('x')
ylabel('t')
grid on
title(sprintf('IRBF solution u(x,t), k1=%2.2f',k1))




%axis([0 4*pi -4 12])


NFS = 18.0; % fontsize
NLW = 0.8; % linewidth
set(gca,'FontSize',NFS,'LineWidth',NLW);

toc;


function [H0,H1,H2,H3,H4,H5,H6] = Deter_IRBF_H0_H6(x,c,dx)
```

```
nx=length(x);
%IRBFNs ...........
H6 = zeros(nx,nx+6);

% dx=a

for i = 1:nx


    for j = 1:nx+6
        if ( j <= nx)
            r = (x(i)-c(j));
            A = sqrt(dx^2+r^2);
            B=log(r + A);
            H6(i,j)= sqrt(dx^2+ r^2);


        elseif(j == nx+1)

            H6(i,j) =0 ;



        elseif(j== nx+2)


            H6(i,j) =0 ;
        elseif(j== nx+3)
            H6(i,j) = 0;

        elseif(j== nx+4)

            H6(i,j) = 0;

        elseif(j== nx+5)

            H6(i,j) = 0;

        elseif(j== nx+6)

            H6(i,j) = 0;
        end

    end
end

 %Determine H5

 H5 = zeros(nx,nx+6);

for i = 1:nx


    for j = 1:nx+6
        if ( j <= nx)
```

```
            r = (x(i)-c(j));
            A = sqrt(dx^2+r^2);
            B=log(r + A);
            H5(i,j)= 0.5*A*r+0.5*B*dx^2;


        elseif(j == nx+1)

            H5(i,j) = 1 ;



        elseif(j== nx+2)


            H5(i,j) =0 ;
        elseif(j== nx+3)
            H5(i,j) = 0;

        elseif(j== nx+4)

            H5(i,j) = 0;

        elseif(j== nx+5)

            H5(i,j) = 0;

        elseif(j== nx+6)

            H5(i,j) = 0;
        end

    end
end
H4 = zeros(nx,nx+6);

for i = 1:nx


    for j = 1:nx+6
        if ( j <= nx)
            r = (x(i)-c(j));
            A = sqrt(dx^2+r^2);
            B=log(r + A);
            H4(i,j)=  1/6*(3*dx^2*B*r+A*(-2*dx^2+r^2));


        elseif(j == nx+1)

            H4(i,j) =x(i) ;



        elseif(j== nx+2)
```

```
            H4(i,j) =1 ;
        elseif(j== nx+3)
            H4(i,j) = 0;

        elseif(j== nx+4)

            H4(i,j) = 0;

        elseif(j== nx+5)

            H4(i,j) = 0;

        elseif(j== nx+6)

            H4(i,j) = 0;
        end

    end
end

H3 = zeros(nx,nx+6);

for i = 1:nx


    for j = 1:nx+6
        if ( j <= nx)
            r = (x(i)-c(j));
            A = sqrt(dx^2+r^2);
            B=log(r + A);
            H3(i,j)=  1/48*(-3*dx^4*B+12*dx^2*B*r^2+A*r*(-13*dx^2+2*r^2));


        elseif(j == nx+1)

            H3(i,j) =1/2*( x(i)*x(i)) ;



        elseif(j== nx+2)


            H3(i,j) =x(i) ;
        elseif(j== nx+3)
            H3(i,j) = 1;

        elseif(j== nx+4)

            H3(i,j) = 0;

        elseif(j== nx+5)

            H3(i,j) = 0;
```

```
        elseif(j== nx+6)

            H3(i,j) = 0;
        end

    end
end



H2 = zeros(nx,nx+6);

for i = 1:nx


    for j = 1:nx+6
        if ( j <= nx)
            r = (x(i)-c(j));
            A = sqrt(dx^2+r^2);
            B=log(r + A);
            H2(i,j)=  1/720*(B*(-45*dx^4*r+60*dx^2*r^3)
                        +A*(16*dx^4-83*dx^2*r^2+6*r^4));


        elseif(j == nx+1)

            H2(i,j) =1/6*( x(i)*x(i)*x(i)) ;



        elseif(j== nx+2)


            H2(i,j) =1/2*( x(i)*x(i)) ;
        elseif(j== nx+3)
            H2(i,j) = x(i);

        elseif(j== nx+4)

            H2(i,j) = 1;

        elseif(j== nx+5)

            H2(i,j) = 0;

        elseif(j== nx+6)

            H2(i,j) = 0;
        end

    end
end

H1 = zeros(nx,nx+6);
```

```
for i = 1:nx


    for j = 1:nx+6
        if ( j <= nx)
            r = (x(i)-c(j));
            A = sqrt(dx^2+r^2);
            B=log(r + A);
            H1(i,j)=  1/5760*(15*dx^6*B+60*dx^2*B*r^2*(-3*dx^2+2*r^2)
                          +A*r*(113*dx^4-194*dx^2*r^2+8*r^4));


        elseif(j == nx+1)

            H1(i,j) =1/24*( x(i)*x(i)*x(i)*x(i)) ;



        elseif(j== nx+2)


            H1(i,j) = 1/6*( x(i)*x(i)*x(i));
        elseif(j== nx+3)
            H1(i,j) =1/2*( x(i)*x(i)) ;

        elseif(j== nx+4)

            H1(i,j) = x(i);

        elseif(j== nx+5)

            H1(i,j) = 1;

        elseif(j== nx+6)

            H1(i,j) = 0;
        end

    end
end



H0=zeros(nx,nx+6);
% i= Row number j=column number

for i = 1:nx


    for j = 1:nx+6
        if ( j <= nx)
            r = (x(i)-c(j));
            A = sqrt(dx^2+r^2);
            B=log(r + A);
            H0(i,j)=  1/5760*(3*B*(5*dx^6*r-20*dx^4*r^3+8*dx^2*r^5)
```

```
                        +(1/35)*A*(-128*dx^6+1779*dx^4*r^2-1518*dx^2*r^4+40*r^6));


        elseif(j == nx+1)

            H0(i,j) = 1/120*( x(i)*x(i)*x(i)*x(i)*x(i)) ;



        elseif(j== nx+2)


            H0(i,j) = 1/24*( x(i)*x(i)*x(i)*x(i)) ;
        elseif(j== nx+3)
            H0(i,j) = 1/6*( x(i)*x(i)*x(i)) ;

        elseif(j== nx+4)

            H0(i,j) = 1/2*( x(i)^2);

        elseif(j== nx+5)

            H0(i,j) = x(i);

        elseif(j== nx+6)

            H0(i,j) = 1;
        end

    end
end
```